(1)

DEPARTMENT OF THE AIR FORCE

AIR UNIVERSITY

AIR FORCE INSTITUTE OF TECHNOLOGY

Wright-Patterson Air Force Base, Ohio

AFIT/GE/AA/86J-1

CORONA WIND COOLING COMPARISONS

FOR HORIZONTAL CYLINDERS

THESIS

Pamela R. C. Hodge
Captain, USAF

AFIT/GE/AA/86J-1

Approved for public release; distribution unlimited

AFIT/GE/AA/86J-1

CORONA WIND COOLING COMPARISONS FOR HORIZONTAL CYLINDERS

THESIS

Presented to the Faculty of the School of Engineering

of the Air Force Institute of Technology

Air University

In Partial Fulfillment of the

Requirements of the Degree of

Master of Science in Electrical Engineering

Pamela R. C. Hodge

Captain, USAF

September 1988

Preface

The purpose of this study was to examine the effects of corona wind on the heat transfer rate from horizontally suspended heated cylinders and compare the results for variations in cylinder diameter, emitter device, and emitter-to-cylinder distance.

The cooling capacity of corona wind has already been harnessed, and used for consumer applications. I found the phenomenon particularly interesting because of the possibilities for application in weld processes.

Thanks go out to my thesis advisor, Dr. Milton Franke, who kept me on the straight and narrow, and to Professor James Hitchcock for impromptu aid. A debt of gratitude is owed to Mr. Nick Yardich, Mr. Leroy Cannon, and especially to Mr. Jay Anderson. They procured the equipment I needed to get the experiment started, and kept it going when the going got tough.

Personal message to my husband, [redacted] and to my [redacted] son, [redacted]

"Thanks guys! I couldn't have done it without you."

Table of Contents

List of Figures

List of Tables

List of Symbols

Symbol	Definition	Units
A	Area	ft^2
a	Current	amp
c_p	Specific heat of fluid	Btu/lbm-^oF
D	Cylinder diameter	in
d_e	Emitter to cylinder distance	in
E	Electric potential, AC	volt
g	Acceleration due to gravity, 32.2	ft/sec^2
h	Convection heat transfer coefficient	Btu/hr-ft^2-^oF
I	Current, AC	amp
k	Thermal conductivity	Btu/hr-ft-^oF
L	Cylinder length	in
P	Barometric Pressure	in-mercury
P_f	Electric field power	watt
P_h	Input power to cylinder heating coil	watt
Q	Heat transfer rate	Btu/hr
R	Electric Resistance	ohm
T,t	Temperature	^oF,^oR
ΔT	Temperature difference, T_s-T_a	^oF
V	Electric potential, DC	kilovolt (kV)
β	Thermal coefficient of volume expansion	1/^oF
ϵ	Emissivity for radiation	--
μ	Dynamic viscosity	lbm/ft-hr

ν	Kinematic viscosity	ft^2/hr
ρ	Fluid density	lbm/ft^3
σ	Stefan-Boltzmann constant, 0.1714×10^{-8}	$Btu/hr\text{-}ft^2\text{-}^oR^4$

Subscripts

a	Ambient
c	Convection or convective
c1	Convection from horizontal cylindrical surface
c2	Convection from horizontal cylinder end surface
cd	Conduction or conductive
f	Evaluated at film temperature
o	No field applied
r	Radiation or radiative
s	Surface of cylinder
t	Total
to	Total for no field applied

Abstract

Experiments were conducted to determine the effect of the corona wind on the convective heat transfer rate from each of three horizontally mounted, heated aluminum cylinders. The cylinder was maintained at ground potential and an emitter was connected to a high voltage source. Stretched wire and multipoint emitter devices were used. Emitter-to-cylinder spacing and field voltage were parameters. Blown air was also used to simulate the corona wind generated from the stretched wire emitter.

An energy balance method was used for data analysis. Free convection heat transfer rates were used as a baseline. The results of all experiments were compared and contrasted. The multipoint emitter was a more efficient emitter device than the stretched wire emitter. The convection heat transfer rate due to the corona wind with an applied high voltage field of 15kV was as much as 6.5 times the free convection heat transfer rate.

I. Introduction

An experimental study of the effects of corona wind on the cooling of a horizontal cylinder was accomplished at the Air Force Institute of Technology recently by Hogue (5). Interest in the corona wind phenomenon has been renewed after a period of relative neglect. Within the last ten years, Franke and Hutson (4), Hrycak (6), Hogue(5), Stefkovich (14), Didkovsky and Bologa (3), Velkoff and Godfrey (16), Cross (2), and Mitchell (9), have all published papers or theses on cooling augmentation with corona wind.

This revived interest, by academia and industry, can be attributed to better equipment and analytical techniques for studying the corona wind phenomena, and to the identification of special heat transfer problems which may be solved by applying the unique properties of electrostatic cooling (1:1).

Background

Corona wind ~~(11:143)~~ refers to the movement of gas induced by the repulsion of ions from the vicinity of a high voltage discharge electrode. A typical corona test configuration (13:4) is illustrated in Figure 1. Free charges are produced in the ionized region surrounding the high field active electrode. These charged particles migrate and collide with neutral air particles in the drift

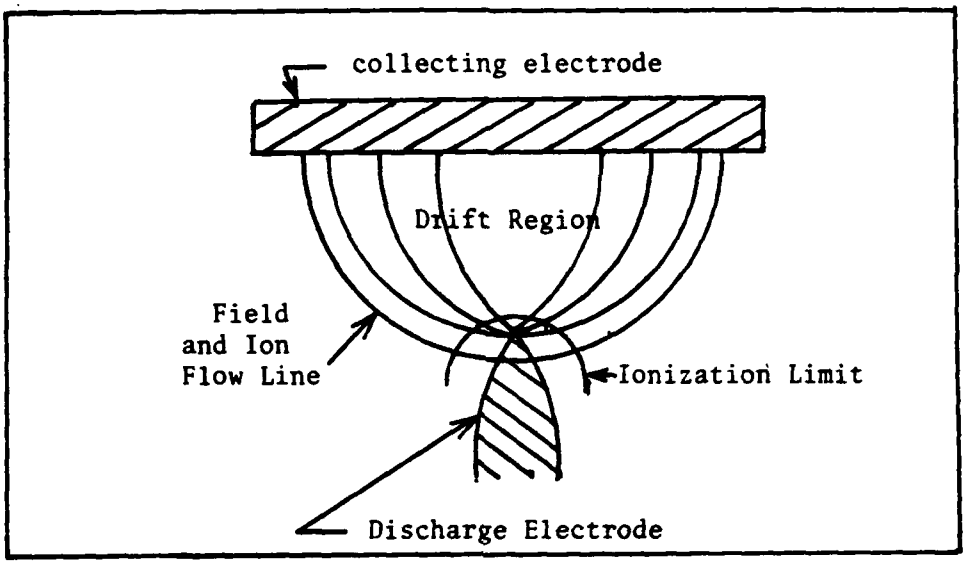

Figure 1. Diagram of a Typical Corona Wind Generation System (13:4)

region. The collisions transfer momentum to the neutral gas, the result of which is an electric wind directed away from the active electrode. These ions are then collected by the low field passive electrode.

A temperature gradient forms around a heated surface which is surrounded by a cooler fluid. The heated surface heats the adjacent fluid, which lowers the density of that fluid and thus causes it to rise. The fluid motion cools the heated surface. This cooling is termed free convection. The corona wind induces an artificial air flow which increases convection heat transfer away from the heated surface. Recent experimenters have achieved convection heat transfer rates of from two to six times the free convection rate (5, 14 and 17).

Until recently the wind had primarily been used to

blow out candles and drive windmills in demonstration experiments (13:8). However, as noted earlier, more practical applications are now being considered. Inter-Probe (17) has done extensive work with corona wind. This company holds many patents in the field of electrostatically accelerated heat transfer technology. They also have products called Modular Energy Transfer Catalyzers, which use corona wind for heating and cooling. These units can generate corona wind velocities of up to 1000 feet per minute and operate in temperature environments ranging from -100°F to +500°F. Many applications are advertised. The units may be mounted over, under or beside stationary processing equipment or moving conveyors. Application examples cited included heating or cooling of paper, food, metal, ceramic and glass products.

There has also been recent interest in corona wind for cooling applications in the aerospace industry. Martin Marietta Aerospace (1) recently published results of their investigation into the control of heat transfer in welding processes through the use of corona wind.

Welding heat effects cause problems with product integrity and reproducibility. Controlled solidification of welds can reduce the heat-affected-zone and subsequently the number of flaws. It was toward this end that Martin Marietta Aerospace developed and tested a proprietary electrostatic cooling system. Beal (1) reported that the overall test results indicated improved weld quality with a

more refined weld micro structure. Selective spot cooling applications around weld puddles decreased detrimental stresses during and after the welding process.

AFIT thesis and staff work, investigating numerous geometries and test configurations, has also stepped up in the last few years (4, 5, and 14). Hogue (5) compared corona augmented convection from a cylindrical surface to baseline free convective heat transfer and to non-ionized forced air cooling. He used a 1-in-diameter solid aluminum cylinder and studied the results produced by varying discharge electrode (emitter) geometry, electrostatic field voltage, and emitter-to-cylinder spacing. Hogue also used a grid and/or shroud in his study in an attempt to direct and/or accelerate the corona wind. He found that the grid and shroud configurations tested did not improve and, indeed, in some cases, actually reduced the amount of cooling achievable with the emitter alone.

Objective

The objective of this study was to determine the effects of corona induced forced convection on the heat transfer rates from 2, 1, and 1/4-in-diameter horizontally suspended aluminum cylinders. Experimental test runs were to be accomplished with stretched wire and multipoint corona emitter devices and with a jet of uncharged air configured to simulate the corona discharge from the stretched wire emitter device.

The free convection heat transfer coefficient was to be determined from an empirical model and used as a baseline for the analysis of the experimental data. The adequacy of this model was to be validated by incorporating the modelled free convection heat transfer coefficient into a well developed definition of the total heat transfer rate, and then comparing the value for total heat transfer rate calculated with the definition to the value measured during the experiment.

Approach

The investigation was divided into the following parts, for each of the three cylinders.

1. Measurement of the total heat transfer rate with no forced convective cooling. Comparison of this rate with the rate calculated from the mathematical model. Extraction of the baseline free convection rate.

2. Measurement of the change in the convection heat transfer rate when (a) a multipoint emitter and (b) a stretched wire emitter were employed to generate a corona wind.

3. Measurement of the change in the heat transfer rate when a jet of uncharged air was used to simulate the corona wind.

4. Comparison of the measured changes in the heat transfer rates for (a) baseline free convection, (b) corona induced forced convection, and (c) forced air convection.

The cylinder surface was maintained at a temperature 50°F above the temperature of the ambient air. Source to test cylinder spacing and field voltage were the parameters varied for each of the noted test.

The Energy Balance Method, developed by Franke (4) and modified by Stefkovich (14), was used to determine the ratio of the forced convection heat transfer coefficient to the free convection heat transfer coefficient. This ratio was used for the analysis and comparison of the test results. This Energy Balance Method is described in Appendix A.

II. Equipment

The equipment used in this experiment was divided into five basic groups according to task. The equipment used for cylinder heating, temperature measurement, corona wind generation, blown air generation, and visualization are depicted and described below. The test cylinders and test stand are also described. The monitoring and control station is shown in Figure 2.

Test Cylinders

There were three right circular 10-in-long test cylinders with diameters of 2, 1, and 1/4 in. The cylinders were fabricated from 2219-T87 aluminum alloy which was selected for evaluation because of its many aerospace applications. The 1-in-diameter cylinder, designed by Hogue (5), was constructed in two horizontal halves to allow for installation of thermocouples and for a heater coil in a 3/8-in-diameter longitudinal cavity. Flush fitting ring collars were used to assemble the two halves. Figure 3 is a schematic of this cylinder. There were 12 thermocouples which were located 0.025 inch below the outside surface.

The 1/4-in-diameter cylinder is depicted in the schematic in Figure 4. This cylinder was fabricated with two tubes. Eight axial slots for the thermocouples were cut into the surface of the smaller tube. After insertion of

(1) HP 3495A Scanner
(2) HP 3455A Digital Voltmeter
(3) HP 3466A Digital Multimeter
(4) Amp Meter
(5) HP 3466A Digital Multimeter
(6) HP 6205B Dual Power Supply
(7) Electrical Bridge
(8) HP 9835B System Controller
(9) Variable AC Transformer
(10) Variable Resistor
(11) Field Voltage Volt Meter
(12) Amp Meter
(13) Field Voltage Volt Meter
(14) Thermocouple Leads

Figure 2. Photograph of the Monitoring and Control Station

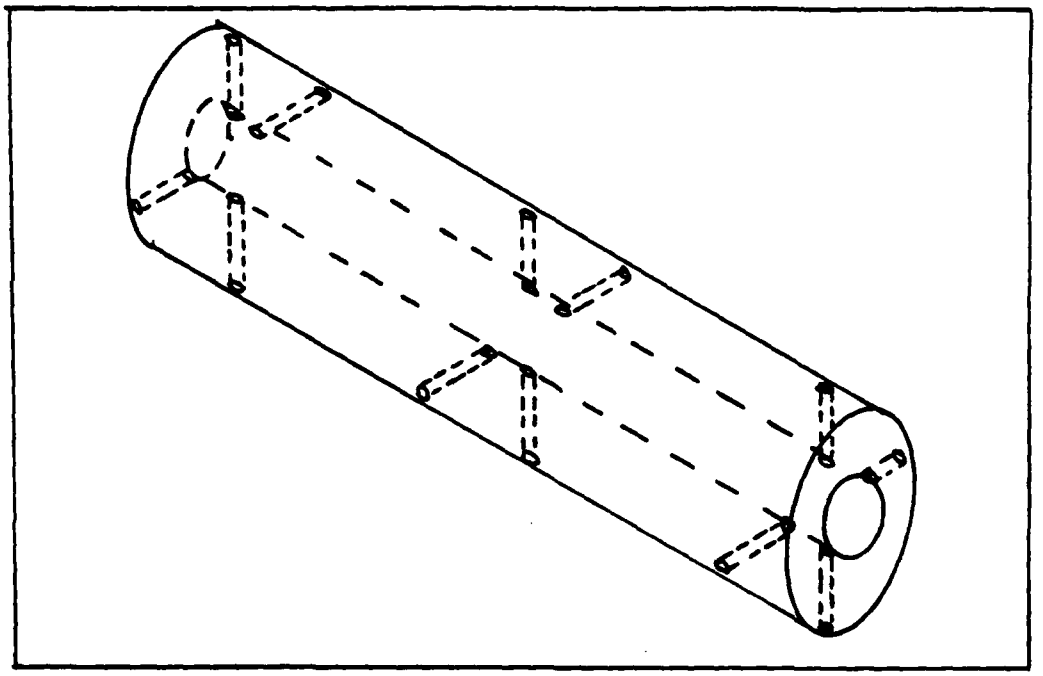

Figure 3. Diagram of the One-Inch-Diameter Test Cylinder

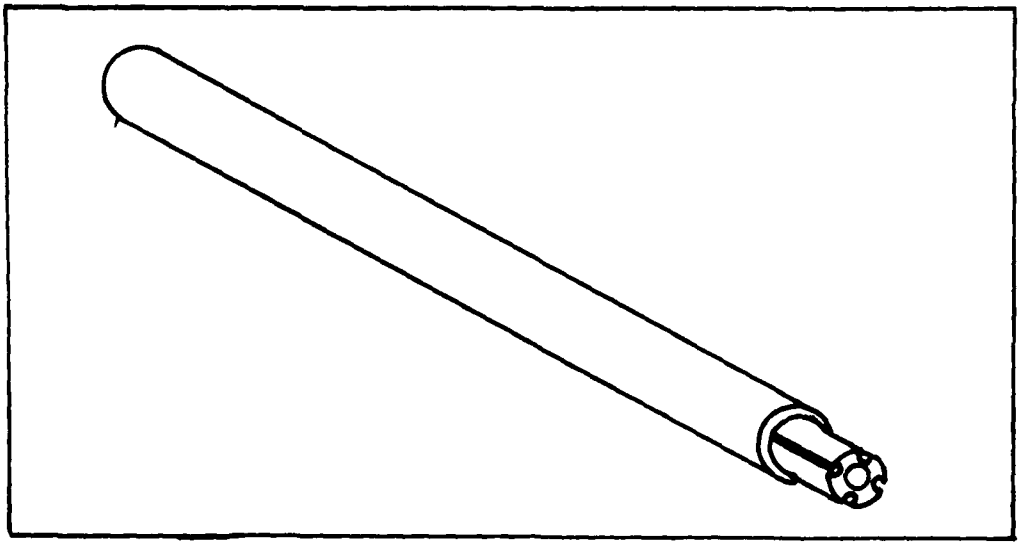

Figure 4. Diagram of the 1/4-Inch-Diameter Test Cylinder

the thermocouples, the smaller tube was pressed into the larger tube. The heater wire was inserted in the center channel of the smaller tube.

The configuration of the 2-in-diameter cylinder was very similar to that of the 1-in-diameter cylinder. This cylinder had five rings of thermocouples, for a total of twenty. The thermocouple wires were recessed into channels away from the heater coil. A schematic diagram of the 2-in-diameter cylinder is shown in Figure 5.

Heater Circuit

The heater circuit was composed of a heater coil or strand, a variable voltage transformer, and a digital multimeter. A schematic of the circuit is shown in Figure 6. A bridge was used to connect each of the three components in series. This system was employed to maintain the cylinder at a equilibrium temperature $50^{\circ}F \pm 1^{\circ}F$ above the atmospheric temperature.

The heaters for the 1 and 2-in-diameter cylinders were helical coils of 0.0125-in-diameter nichrome wire sheathed in teflon tubing. The heater for the 1/4-in-diameter cylinder was a single strand of the same wire. Nichrome was chosen because of its high resistivity. The variable voltage transformer was used to scale the 110 volt AC input to any output level between 0 and 110 volts AC. This voltage was adjusted to the level required to maintain the test cylinder at a temperature $50^{\circ}F$ above the ambient room

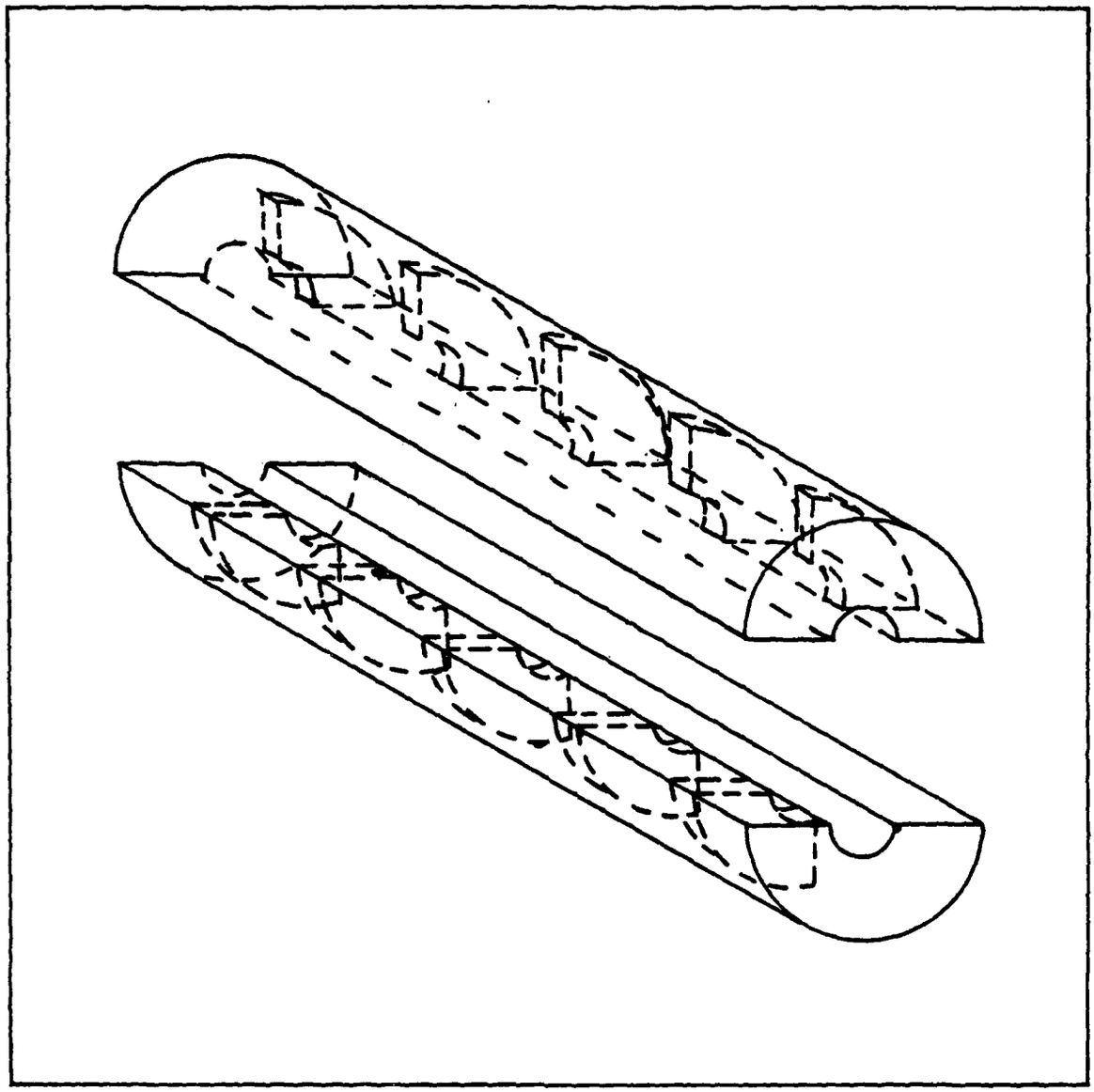

Figure 5. Diagram of the Two-Inch-Diameter Test Cylinder

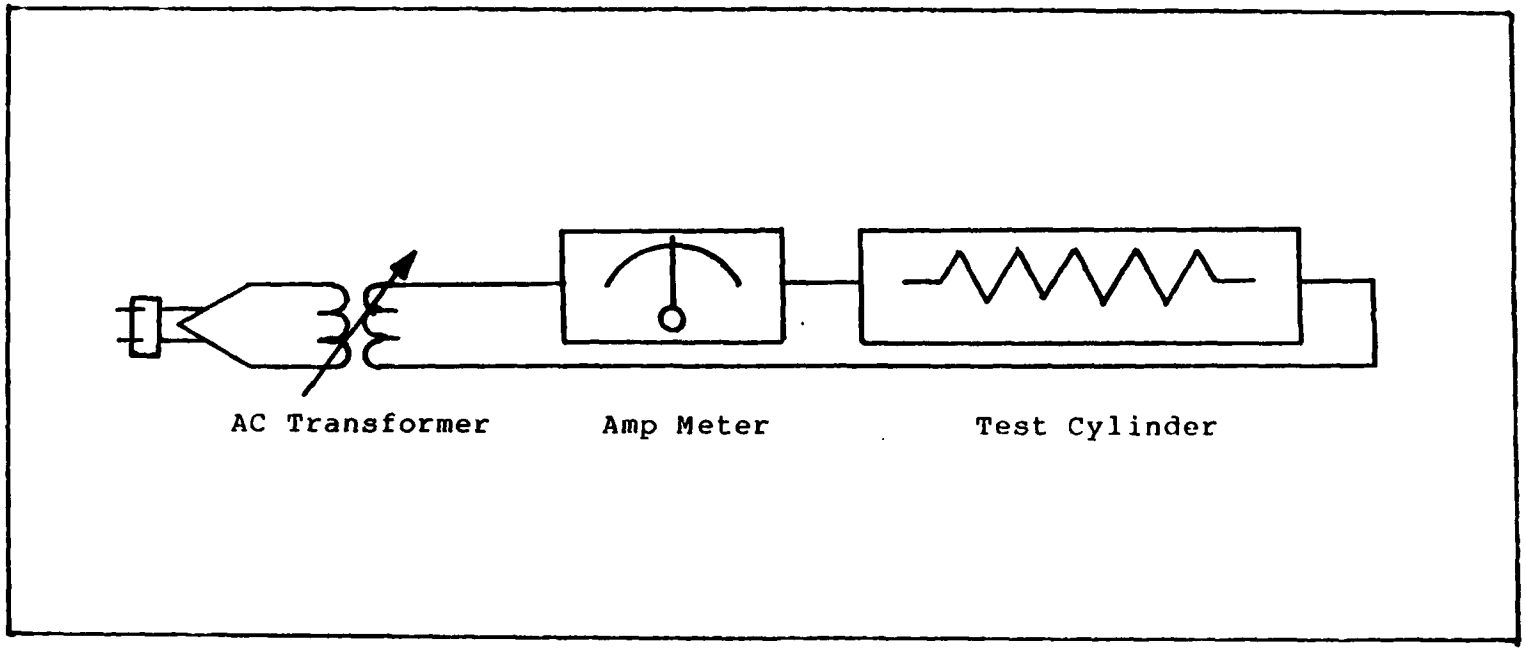

Figure 6. Schematic Diagram of the Heater Circuit

temperature.

Once an equilibrium temperature was achieved, an RMS reading of the AC current was recorded from a digital multimeter reading. The multimeter range was 0 to 2000 mA. A 0 to 5 amp AC ammeter was substituted when higher current flows were required during testing of the 1/4-in-diameter cylinder. The current readings and the heater coil resistance were used later to compute the power required to maintain the test cylinder at an equilibrium temperature $50^{\circ}F$ above the ambient temperature.

A variable resistor was added to this system when the 1/4-in-diameter cylinder was tested. The less voluminous 1/4-in-diameter cylinder had a much smaller heater and subsequently added very little resistance to the overall test circuit. From Ohm's law, a given current level can be maintained if the voltage is lowered in response to lowering the resistance. The variable transformer voltage output was unstable at low settings and caused erratic current readings. The multimeter current readings stabilized when the additional resistance was added to the circuit. Higher voltage settings were required to maintain the desired current flow through the cylinder heater.

Temperature Measurement

In order to maintain a constant ΔT of $50^{\circ}F$, it was first necessary to monitor the test cylinder and ambient temperatures. Thermocouples were embedded in the cylinder

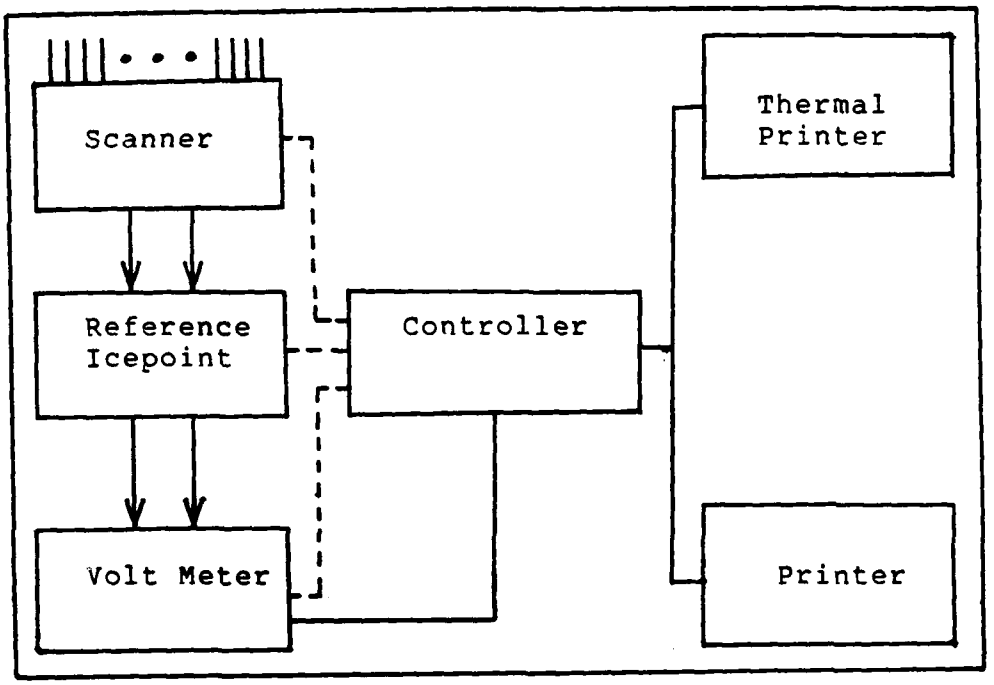

Figure 7. Schematic Diagram of the Temperature Measurement Equipment

and attached to the inside of the lower horizontal test stand member.

The thermocouples were fabricated by arc welding from Type T 30 gage copper (high junction) and constantan (low junction) teflon coated thermocouple wire. "Omegabond 101" adhesive was used to install the thermocouples in the cylinder and to coat the two thermocouples mounted in the test stand. This adhesive was a thermally conductive, electrically insulating epoxy.

The automatic data system shown in Figure 7 was composed of a HP 9835B System Controller, a HP 3455A Digital Voltmeter, and a HP 3495A Scanner. The scanner has multiple input channels and a single output. The thermo-

couple leads were connected directly to the scanner and the scanner output was connected to the electronic icepoint. This arrangement of scanner before reference junction is an application of the second thermocouple law (20). The Law of Intermediate Metals states that the introduction of a third metal has no effect, as long as the junctions of the third metal with the two thermocouple wires are at the same temperature.

The voltmeter measured the emf of the thermocouples and displayed the voltage readings. The system controller used the computer program shown in Appendix B to drive the scanner and voltmeter. The controller then used a HP conversion algorithm to convert each voltage reading to a temperature in both Celsius and Fahrenheit, and computed the average test cylinder temperature and the ΔT between this temperature and the ambient temperature.

Corona Wind Generation

The corona wind generation system consisted of a direct current (DC) power supply (0 to 30 kV), emitter devices, an in-line DC micrometer, and an electrostatic voltmeter (0 to 15kV). A schematic of the system is shown in Figure 8. Beldon type 8866 high voltage wire was used to interconnect these elements.

The 0-15 kV voltmeter was used in lieu of the voltmeter on the DC power supply to gain greater accuracy on the voltage readings. Use of the 0-15 kV voltmeter limited

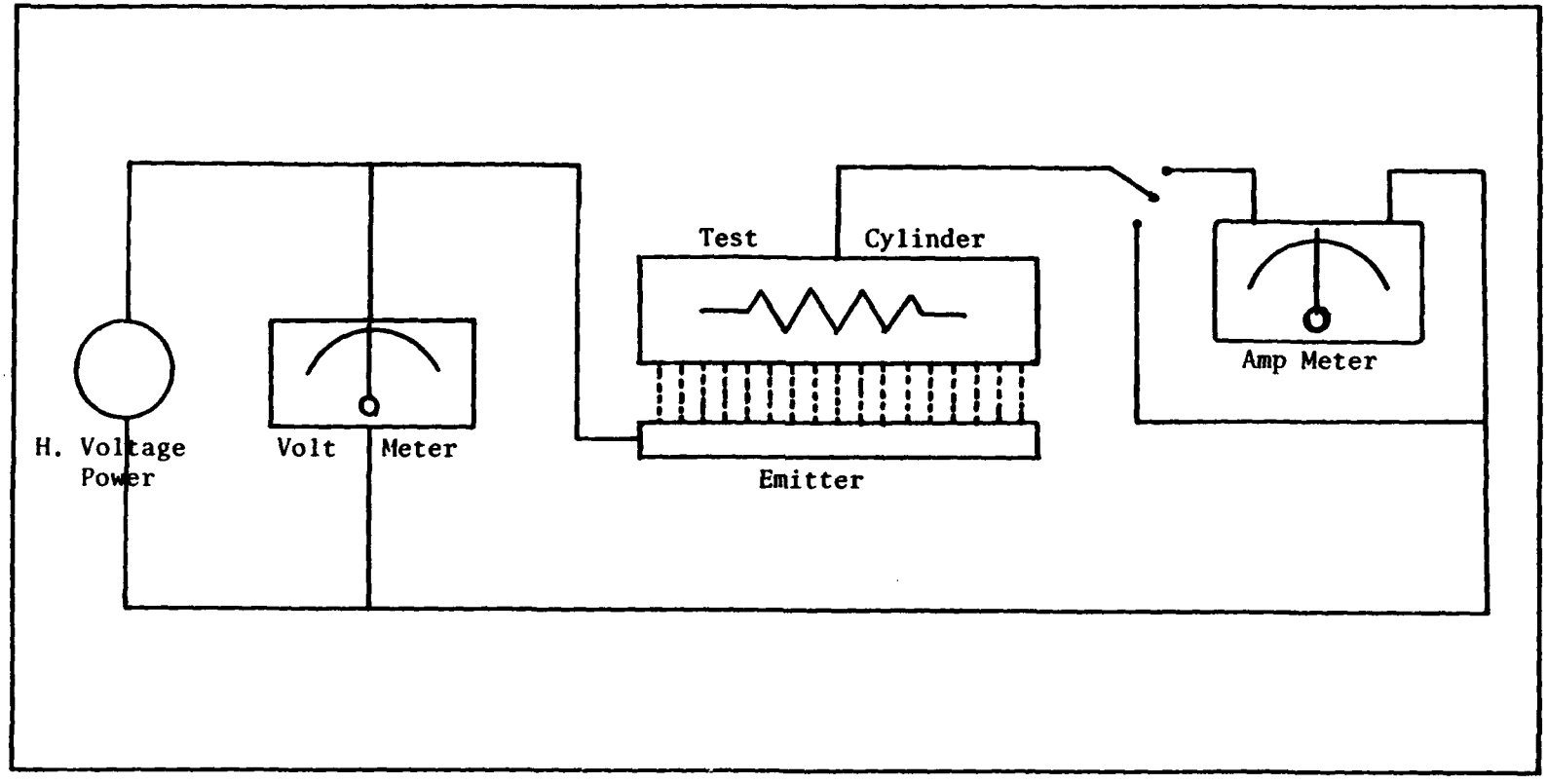

Figure 8. Schematic Diagram of the Corona Wind Generation Equipment

the experiment to a 15 kV maximum applied voltage to the emitter device.

The micrometer measured the current resultant from the ion flow between the emitter and the grounded test cylinder.

Two types of emitters were used during testing, both are depicted in Figure 9. The stretched wire emitter was a strand of 40 gage (0.0031-in diameter) Chromel wire mounted taunt between two copper rods. These rods were screwed into brackets on each side of the test stand and connected to the high voltage power supply. The stretched wire was mounted directly beneath, and parallel to the longitudinal axis of the test specimen. Figure 10 shows this emitter device mounted in the test section.

The multipoint emitter had nineteen 1/4-in-lengths of the 40 gage Chromel wire mounted perpendicular to the longitudinal axis of the cylinder (see Figure 9). The Chromel emitters were mounted in 4-in-long, 1/4-in-diameter copper rods. These rods were screwed into a copper bus bar embedded in a Plexiglas holder. The copper bus bar had threaded ends which extended through the mounting brackets. The high voltage source was connected to the two threaded bus bar end segments. This emitter is shown mounted in the test section in Figure 11.

Blown Air Generation

The blown air system consisted of a wedge shaped

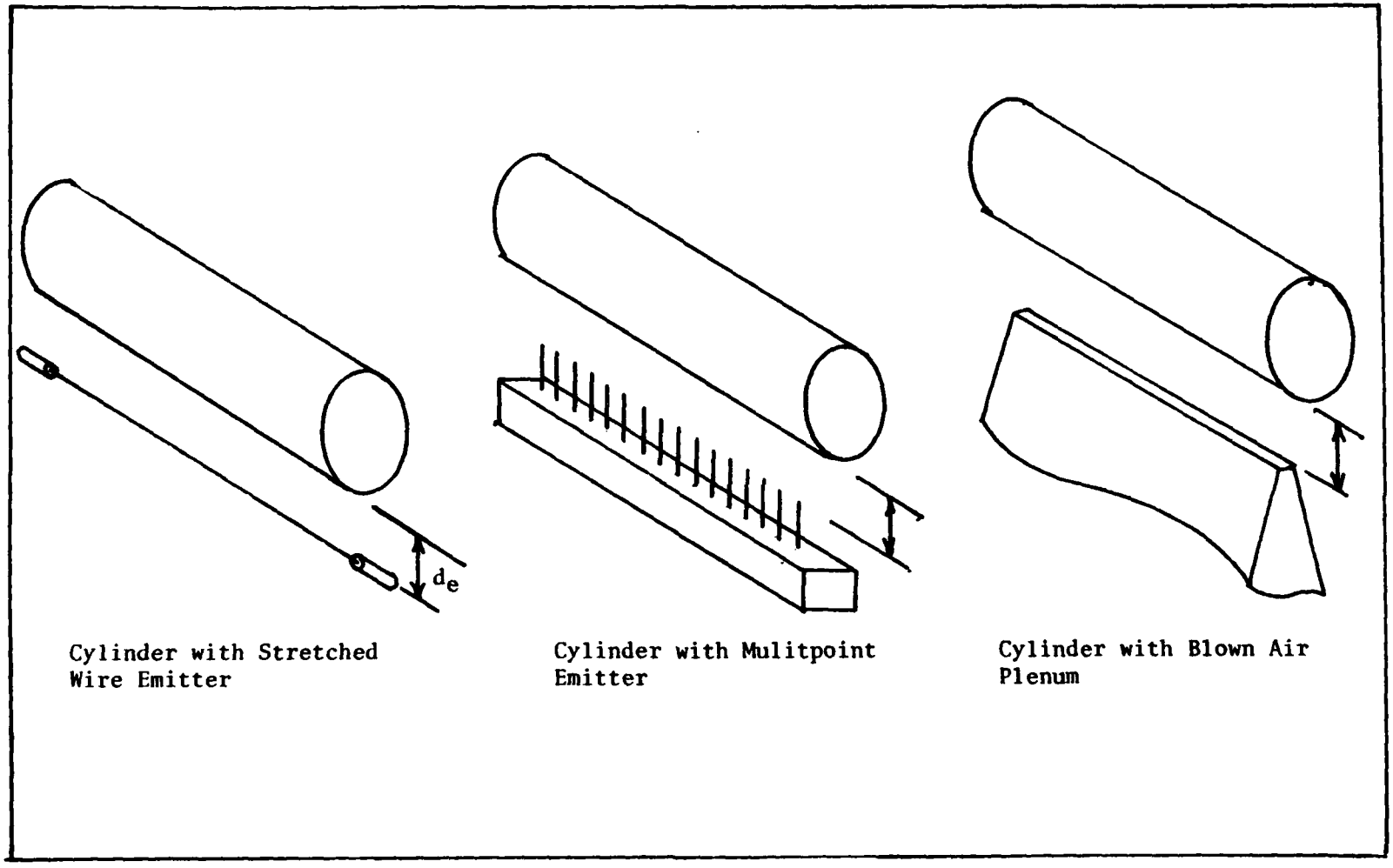

Figure 9. Diagrams of the Emitter Devices and Plenum Chamber Configurations

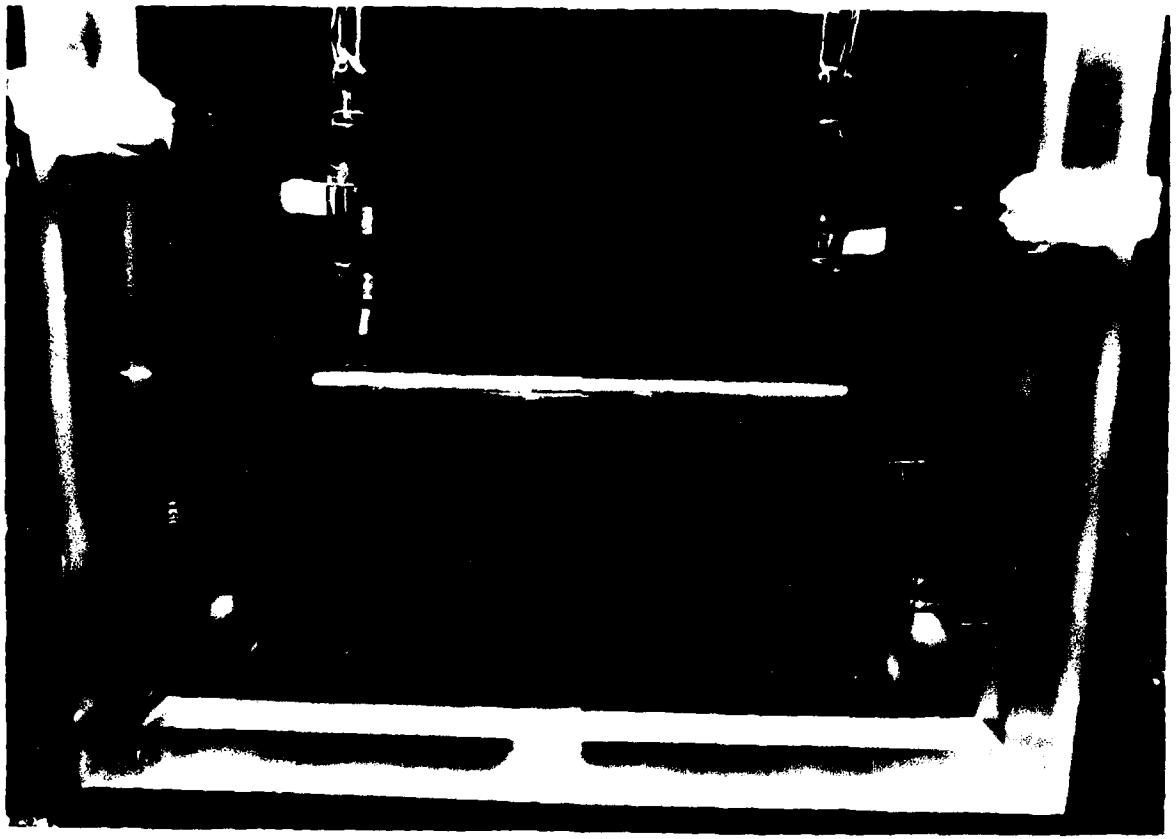

Figure 10. Photograph of the One-Inch-Diameter Test Cylinder with Stretched Wire Emitter in the Test Section

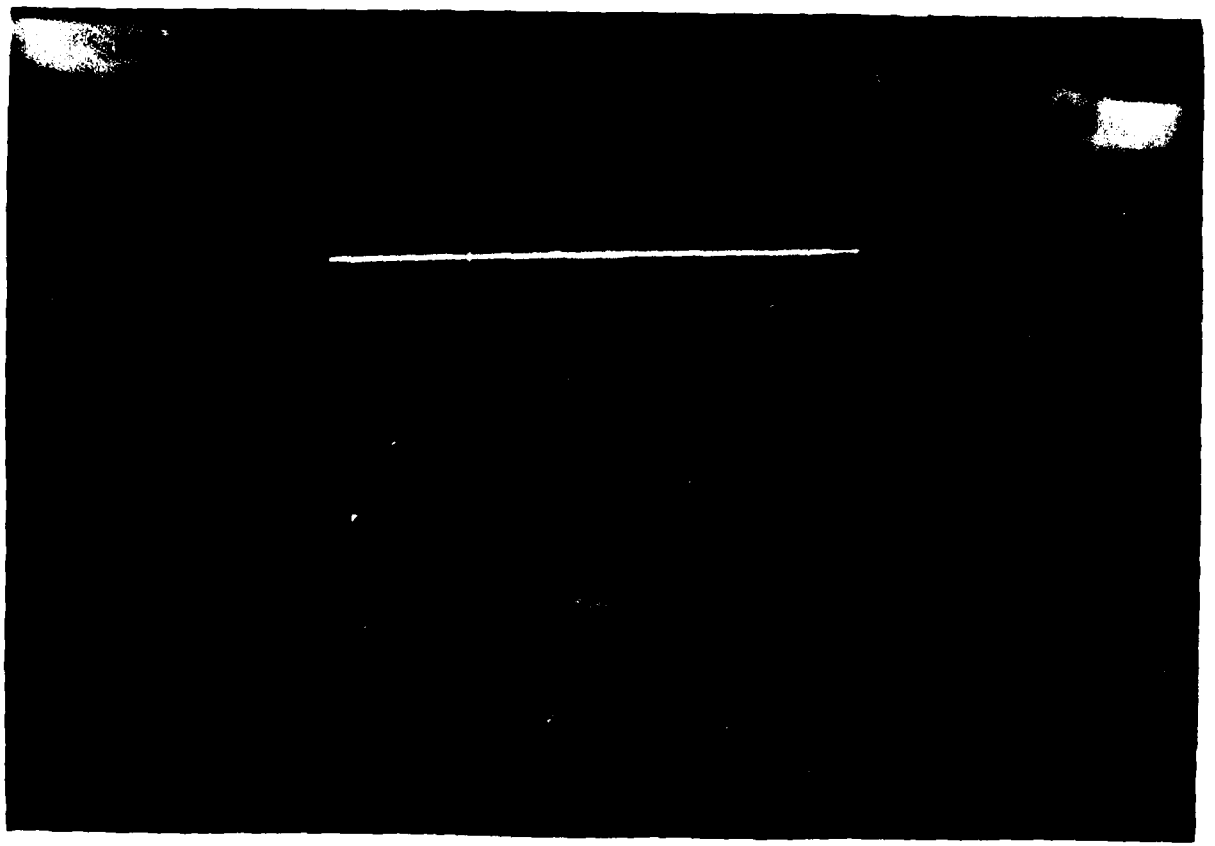

Figure 11. Photograph of the One-Inch-Diameter Test Cylinder with Multipoint Emitter in the Test Section

plenum chamber,a Bell and Howell pressure transducer, a HP 6205B DC power supply, a HP 3466A digital voltmeter, a pressure gauge, and a supply of compressed air. The system is depicted in Figure 12 and shown mounted in the test section in Figure 13. The plenum chamber had a 12-in-long by 1/64-in-wide slot in its top edge, and two quick connect inlets near its bottom. Compressed air from the AFIT laboratory supply line was introduced into the plenum to produce an air flow from the slot. The pressure transducer was used to measure the stagnation pressure in the plenum before and during testing. The pressure transducer was excited with 10 volts DC from the power supply. The transducer output a DC voltage which was read by the digital multimeter.

Visualization

A Mach-Zehnder type interferometer, depicted in Figure 14, was used for visualization of the thermal gradients around the cylinder. Photographs of the interferometer images of the fringe patterns were taken with a Polaroid Graflex camera and Polaroid type 42 film.

Test Stand

The test stand is depicted in Figure 15. The main structure was made entirely of Plexiglas. The runners used to hang the test stand in the test section of the interferometer were wooden.

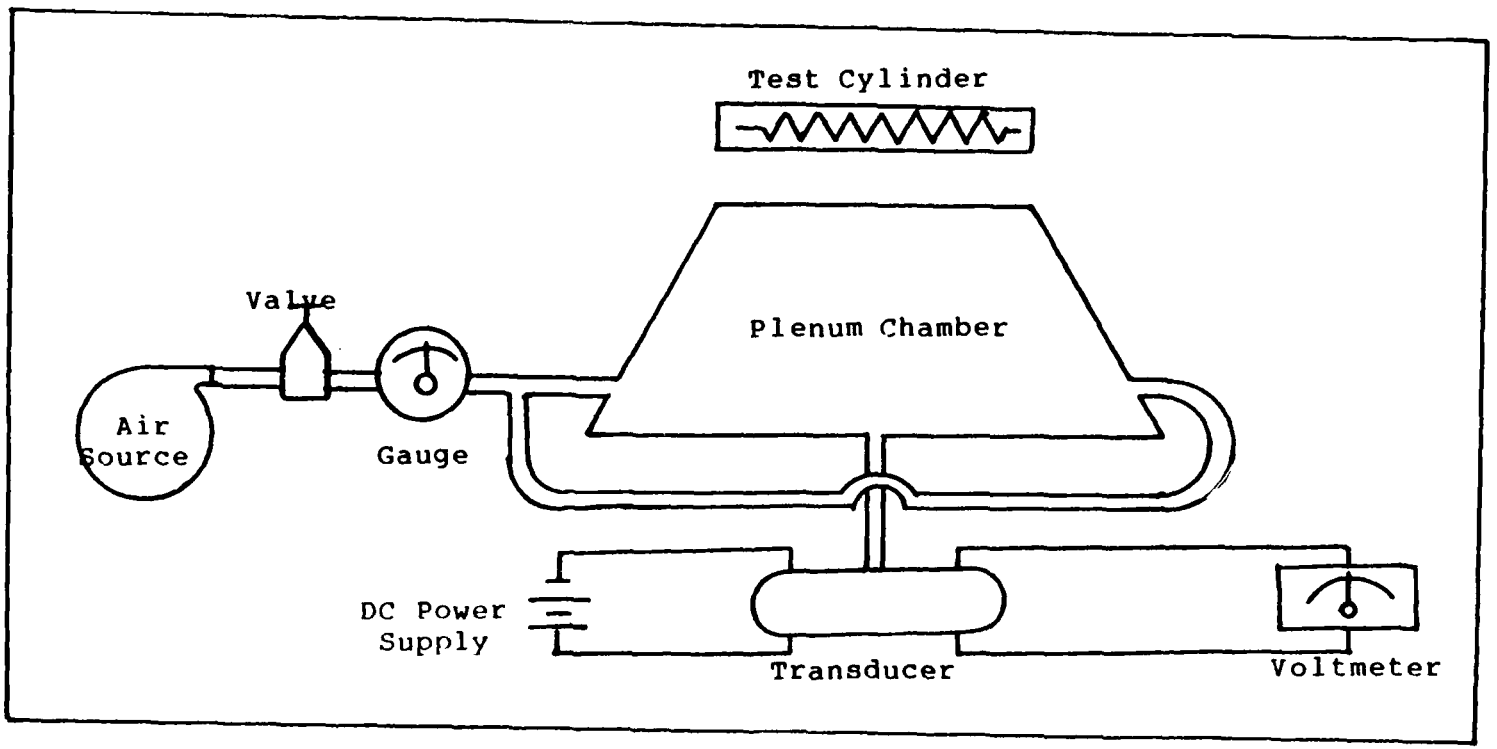

Figure 12. Schematic Diagram of the Blown Air Generation Equipment

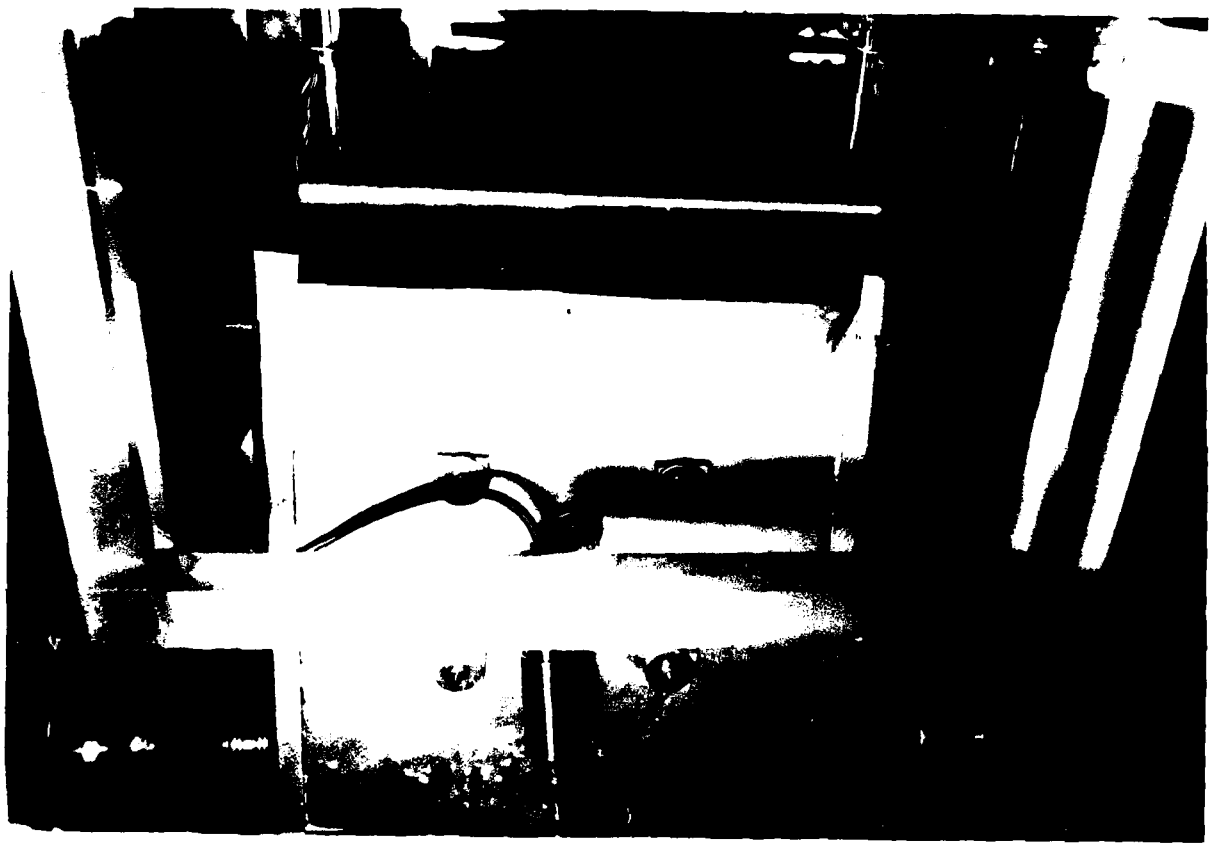

Figure 13. Photograph of the One-Inch-Diameter Test Cylinder with Blown Air Plenum in the Test Section

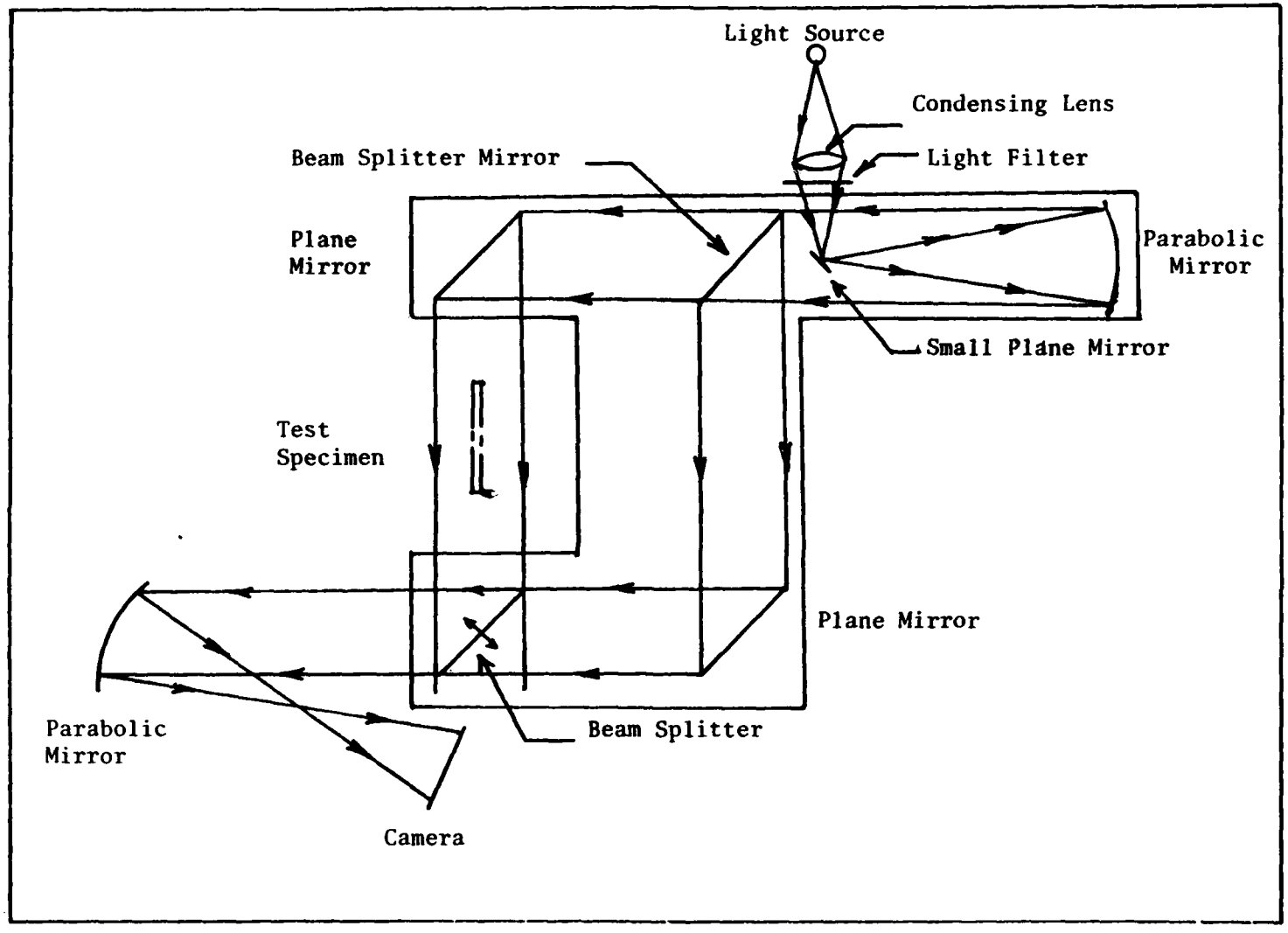

Figure 14. Schematic Diagram of the Interferometer

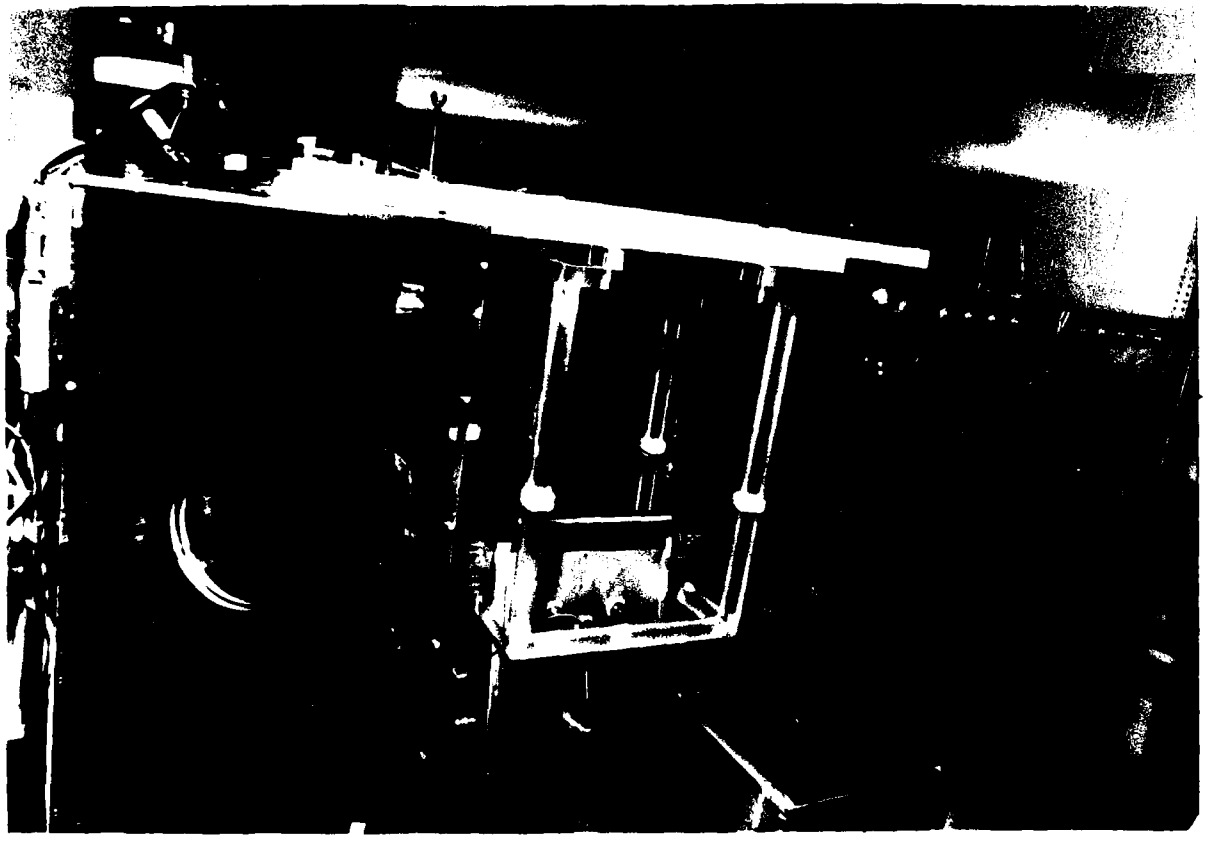

Figure 15. Photograph of the Interferometer Test Section with One-Inch-Diameter Cylinder and Blown Air Plenum Mounted

III. Experimental Procedure

The experiment was divided into three basic categories: set-up and calibration, data collection, and data reduction.

Set-up and Calibration

Set-up and calibration encompassed calibrating the thermocouples and meters, determining heater coil resistances, adjusting the interferometer, aligning the cylinder and emitter devices, and measuring corona wind and blown air velocities.

All of the mechanical meters were checked and zeroed with the set-screw. The electrical meters were calibrated by the Wright-Patterson AFB Precision Measurement Equipment Laboratory as required.

The thermocouples for each cylinder were calibrated against a Fisher Scientific mercury thermometer before being mounted. The thermocouples were connected to the HP Automatic Data Acquisition System and electronic icepoint. Temperature measurements were taken with the measurement junctions exposed to the ambient air, submerged in a distilled water icebath, and submerged in a heated bath of distilled water. All thermocouple measurements were within $\pm 1^{\circ}F$ of the mercury thermometer readings at each test condition.

Periodically during testing, an additional calibration

was performed. The measurement junction of a thermocouple was submerged in a distilled water ice bath to verify the accuracy of the electronic icepoint. The readings were always between 0.0 and 0.1°C.

The resistance of each cylinder heater coil was measured with a HP 3466A digital multimeter.

One heater coil was used to determine the resistance vs. temperature properties of nichrome. The measured resistance was a weak function of temperature, exhibiting a temperature coefficient of 0.014 percent/°C. This value is well within the 0.012 to 0.017 percent/°C commercial minimum/maximum temperature coefficient ratings (21). The value of heater resistance measured at ambient temperature were therefore used for all power calculations.

During the initial apparatus set-up, the interferometer was focused and aligned to yield the fringe pattern. The interferometer was then adjusted to the infinite fringe setting. This last adjustment was checked before each test run and repeated as necessary.

Before each test run, the cylinder was first adjusted to the proper height above the emitter and then aligned in the interferometer test section. The image projected to the camera after proper alignment was one of a solid circle.

Prior to each test, the ambient temperature, relative humidity, and barometric pressure were recorded. A sling psychrometer was used to determine the dry-bulb and wet-

bulb temperatures. These temperatures were used to determine the percent relative humidity.

Corona wind and blown air velocities were measured with a Velometer. A velocity probe was mounted above the stretched wire corona wind emitter at each of three emitter-to-cylinder distances. Velocity measurements were recorded for discrete high field voltages. These measurements were repeated with low velocity (0 - 300 ft/min) and high velocity (0 - 1250 ft/min) Velometer probes. The data was used to plot transform curves between high field voltage and velocity (see Figure 16). These transforms were needed to facilitate comparisons of corona and blown air experimental data.

Blown air velocities were measured with a Velometer probe mounted above the plenum chamber in place of a test cylinder. Velocity was measured at three plenum-to-cylinder distances for various line pressures. These measurements were also repeated for low and high velocity Velometer probes. Blown air cooling data were recorded versus compressed air line pressure gauge readings, and later transformed to a velocity baseline (see Figure 17).

Data Collection

The procedure was the same for each experimental configuration. Each experimental test run began by establishing a stable 50°F ΔT between cylinder surface and ambient room temperatures. This was accomplished by ad-

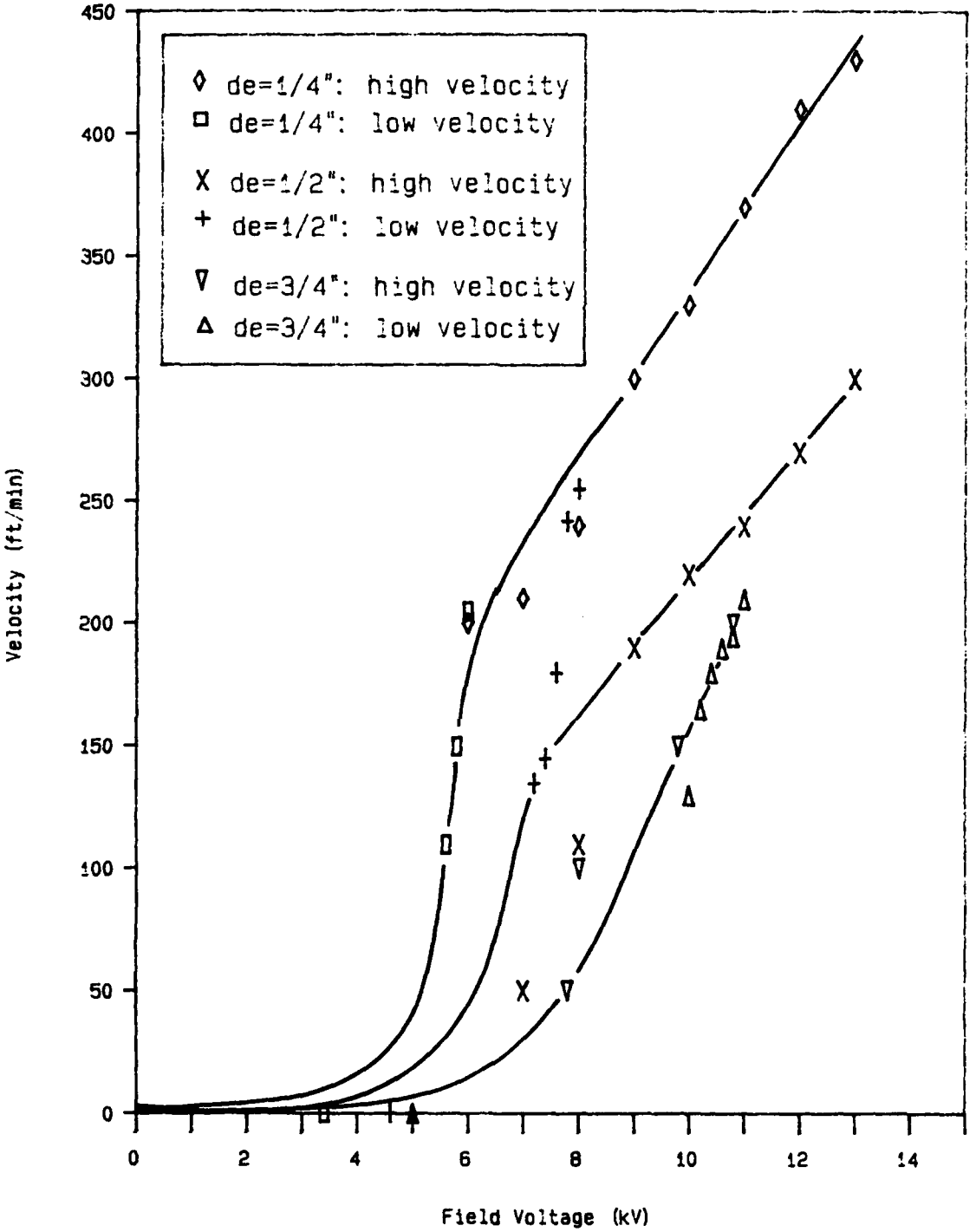

Figure 16. Measured Transform Between Corona Wind Field Voltage and Corona Wind Velocity using High and Low Velocity Probes

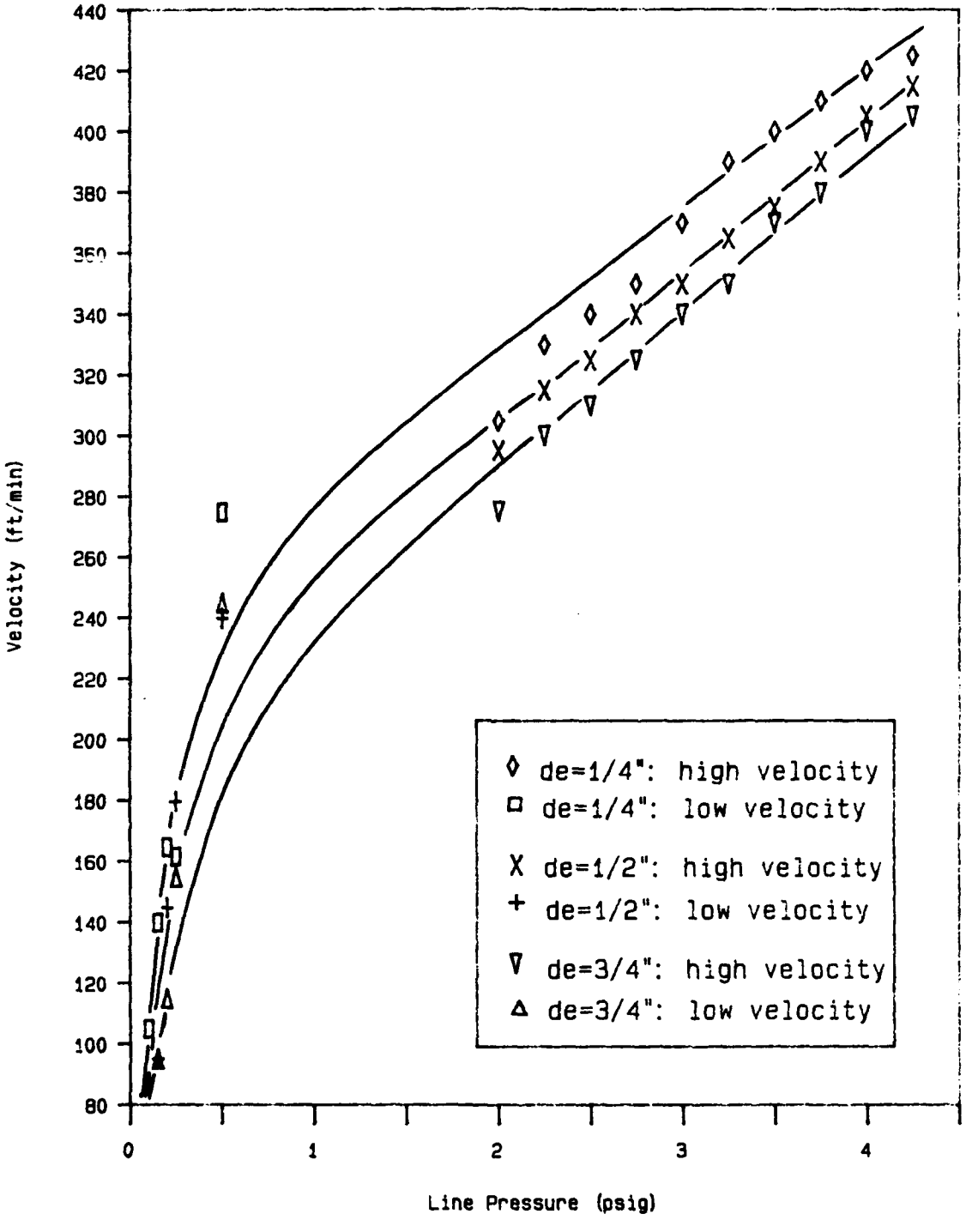

Figure 17. Measured Transform Between Blown Air Line Pressure and Blown Air Velocity using High and Low Velocity Probes

justing the voltage transformer output to the cylinder heater while monitoring average cylinder surface temperature readings. After stabilization, the heater current and average cylinder surface temperature were recorded.

After this initial step, DC high voltage was applied to the emitter to induce the corona wind. The cylinder heater current was then adjusted to reestablish the stable $50^{\circ}F$ ΔT. After stabilization, the heater current, temperature data, and current induced between the emitter and grounded cylinder were recorded. At this point, a photograph was taken of the interferometer image, and the process was repeated for a different high voltage setting.

This data collection process was modified slightly for the blown air experimental test runs. The corona emitter device was replaced with the blown air plenum chamber. The voltage transformer output was then adjusted to achieve the $50^{\circ}F$ ΔT, and the cylinder heater current and temperature data were recorded. Next the compressed air line pressure was adjusted to the desired level and the heater current was adjusted to reestablish the $50^{\circ}F$ ΔT. After stabilization, the heater current, temperature data and plenum chamber stagnation pressure were recorded and a photograph was taken of the interferometer image. The process was repeated for all blown air test runs.

Data Reduction

Newton's (7:13) equation defining the convection heat

transfer rate is

$$Q_c = hA\Delta T \tag{1}$$

For constant A and ΔT, equation (1) can be used to demonstrate that the ratio of h/h_o is equivalent to a like ratio of the convection heat transfer rates.

The equation for h/h_o developed in the energy balance data reduction technique described in Appendix A is

$$h/h_o = 1 + \Delta P_h/Q_{oc} \tag{2}$$

ΔP_h is the difference between the power required to maintain a 50^oF ΔT for forced convection and the power required to maintain the 50^oF ΔT for free convection. P_h for each condition was calculated using equation (3).

$$P_h = I^2R \tag{3}$$

Cylinder heater currents recorded during experimental test runs and heater coil resistances determined during set-up and calibration were used to evaluate equation (3).

The ratio h/h_o was plotted and used to compare the test results.

IV. Empirical Model

Experimental results were validated via a comparison of the free convection experimental test results to a well developed definition of heat transfer.

$$Q_t = Q_c + Q_r + Q_{cd} \tag{4}$$

The models of convection and radiation heat transfer are repeated from references below. Conduction away from the cylinder was negligible.

The test cylinder has convection heat transfer from the horizontal cylindrical surface and from the vertical end sections.

$$Q_c = Q_{c1} + Q_{c2} \tag{5}$$

The heat transfer coefficient needed to calculate Q_{c1} for the horizontal cylindrical surface was determined using the following equation (8:172).

$$h_{c1} = \frac{0.53k_f}{D_o}\left[\frac{D_o^3 \rho_f^2 g \beta_f \Delta T}{\mu_f^2}\left(\frac{c_p \mu}{k}\right)_f\right]^{1/4} \tag{6}$$

The physical properties, c_p, k, ρ, β, and μ were evaluated at a film temperature midway between the average cylinder surface temperature and the ambient fluid temperature.

The value of Q_{c1} calculated for the 1-in-diameter cylinder was 4.34 watt for the atmospheric conditions listed in Table I.

The convection heat transfer coefficient for convection from the vertical ends of the cylinder was calculated

TABLE I

Air Properties and Ambient Conditions

T_s	130.8°F
T_a	80.7°F
ΔT	50°F
p	29.076 in-Hg
D_0	0.0833 ft
g	4.17(10E08) ft/hr^2
k_f	0.015804 Btu/hr-ft^2-F
β_f	9.4563(10^{-3}) (°F)$^{-1}$
ρ_f	0.069 lbm/ft^3
μ_f	0.04626 lbm/ft-hr
c_{pf}	0.214 Btu/lbm-°F

using the following equation (8:172).

$$h_{c2} = \frac{0.59k_f}{D_o}\left[\frac{D_o^3 \rho_f^2 g \beta_f \Delta T \left(\frac{c_p \mu}{k}\right)}{\mu_f^2}\right]_f^{1/4} \qquad (7)$$

The h_{c2} calculated with equation (7) for the 1-in-diameter cylinder was used in equation (1) to yield a Q_{c2} of 0.42 watt.

Q_{c1} and Q_{c2} sum for a total convection heat transfer rate Q_c of 4.77 watt.

The Stefan-Boltzmann law (15:5-10) states that the radiation from a black body to another body is proportional

to the difference between the fourth power of the absolute temperatures of the two bodies. When the radiating body is not a perfect black body, as in the case of the aluminum cylinder,

$$Q_r = (0.174 \times 10^{-8}) A \epsilon (T_s^4 - T_a^4) \quad (8)$$

Emissivity for polished aluminum is 0.095 (8:472). The Q_r calculated for the 1-in-diameter cylinder was 0.39 watt.

The test stand was configured to preclude any significant means of conduction heat transfer away from the test cylinder. The cylinder was mounted to Plexiglas (polymethyl methacrylate) which has a thermal conductivity of 0.0833 Btu/hr-ft-^{o}F (19:515.23.5). The thermocouple leads were the only other conduction path. Their contribution to the total heat transfer away from the test cylinder was negligible.

The total heat transfer rate Q_t calculated with the empirical model was 5.16 watt.

The power, P_h, required to maintain a ΔT of 50^{o}F is equivalent to the total heat transfer rate Q_t. P_h was 5.24 watt for the free convection test run model above.

V. Results and Discussion

TABLE II

Free Convection Heat Transfer Rates

Cylinder Diameter (in)	Q_{oc} (watt)
1/4	1.52
1	4.34
2	7.31

Baseline Free Convection Heat Transfer

Empirical Model. An empirical model of the total heat transfer rate was developed in Chapter IV for the 1-in-diameter test cylinder with the typical set of actual experiment atmospheric conditions listed in Table I. The Q_t calculated with the mathematical model was 5.16 watt. The power required to maintain the ΔT of 50°F during the test run at the ambient conditions in Table I was 5.24 watt. The experimental value was 1.6% above the empirical value. There was very good correlation between the two values. This correlation validated the experimental data reduction procedures.

Values of h_o from the empirical model were used to calculate the values of Q_{oc} in Table II. These Q_{oc}'s were used in the energy balance data reduction technique to evaluate h/h_o.

Effects of ΔT Variations. The energy balance method used for data reduction assumes a ΔT of 50°F for each data point collected. Actual measurements were at ΔT's between 49 and 51°F. For nonconstant ΔT, the equation of h/ho must be multiplied by the ratio of $\Delta T/\Delta T_o$. The calculated values of h/h_o may include a maximum error of $\pm$ 4%.

Humidity Effects. Evaluation of the air properties used in Chapter IV illuminated the possible impact of humidity on the overall heat transfer rate. The potential for humidity impacts was checked by comparing the h_o's recorded when humidity levels were at the maximum and minimum levels observed during testing of the 1-in cylinder. The high and low relative humidity levels recorded were 28% and 40%, with barometric pressure readings of 29.050 and 29.027 in-Hg, respectively. The corresponding readings for h_o were 1.56 and 1.59 Btu/hr-ft^2-°F. The h_o increased 1.6% for a 42.9% increase in relative humidity. The increase in the h_o was as expected; as the relative humidity of ambient air increases, so too does the thermal conductivity. Humidity remained relatively constant for the time required to collect a complete test run. The thermal conductivity of the ambient air was therefore also constant, and thus the ratio of h/h_o used for data analysis was unaffected by humidity.

Experimental Results

One Inch Diameter Test Cylinder

A total of nine experimental test configurations were

run on the 1-in test cylinder. Emitter to cylinder spacing d_e was set at 1/4, 1/2, and 3/4 in for test runs with the stretched wire emitter, the multipoint emitter, and the blown air plenum.

Stretched Wire Emitter. The results of the test runs with the stretched wire emitter are plotted in Figure 18. This plot illustrates the breakdown voltage phenomenology and the effect of d_e variation. The interferometer photograph (Figure 19) shows the effect of increasing field voltage on the boundary layer. As Hogue (5) observed, the boundary layer separated at about 90° from the bottom of the cylinder.

The initial application of field voltage to the emitter produced no corona wind and thus no corresponding change in the h/h_o ratio. This lack of forced convective cooling was due to the absence of ion flow, current, from the emitter to the cylinder. The field voltage level at which ion flow began was termed the breakdown voltage. The field voltage level required to achieve breakdown voltage increased from 3.4 kV to 5.2 kV as emitter to cylinder spacing increased.

Emitter to cylinder spacing also affected cooling effectiveness of the corona wind. The h/h_o ratio decreased as d_e increased for constant field voltage. This trend was evident even when the plots were shifted along the x-axis to align the breakdown voltages. This functional relationship between h/h_o and d_e was not present in the Figure 20

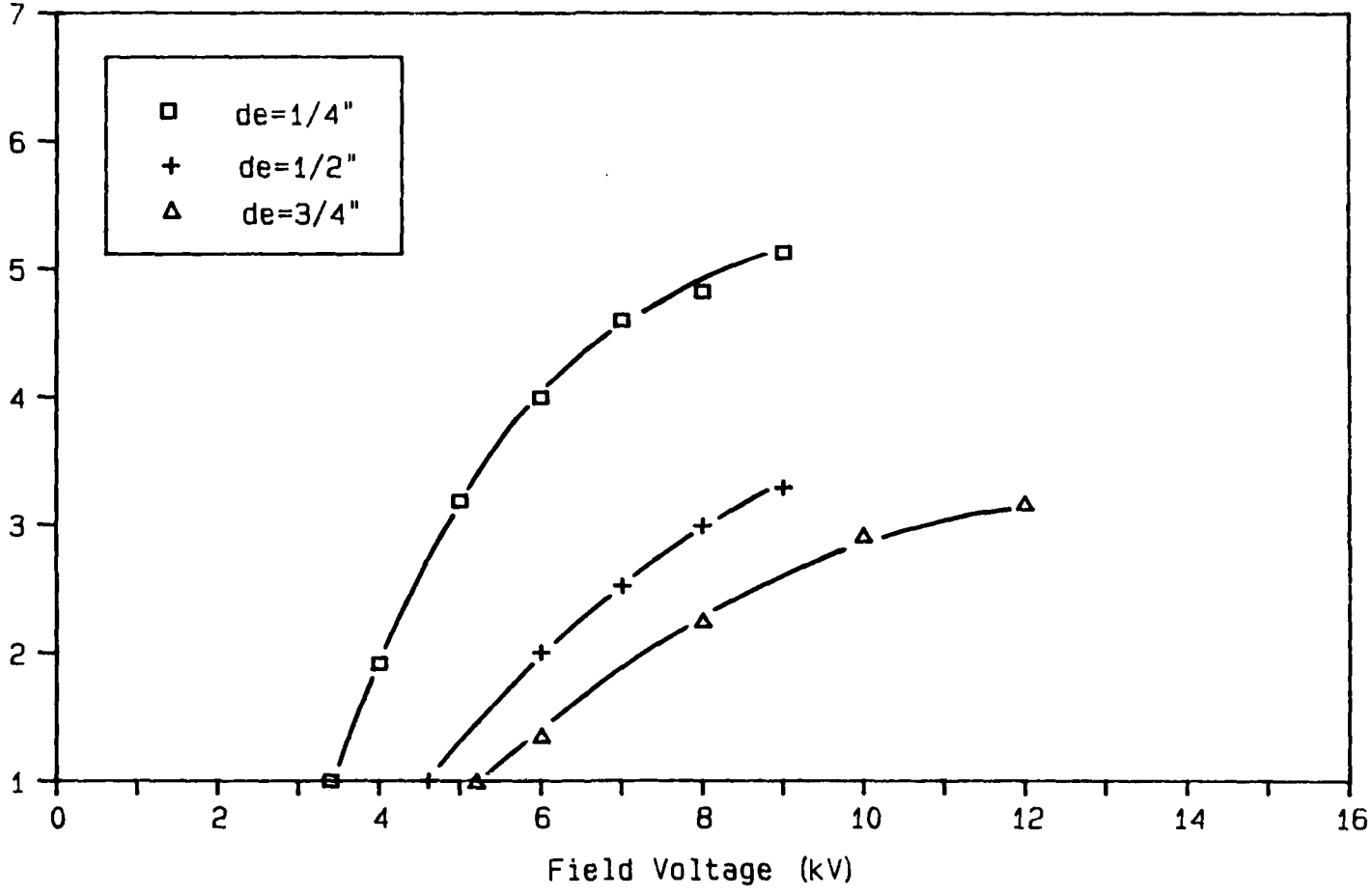

Figure 18. Effect of Corona Wind on the Ratio h/h0 for the 1-in Diameter Test Cylinder at Various Source to Receiver Distances with a Stretched Wire Emitter

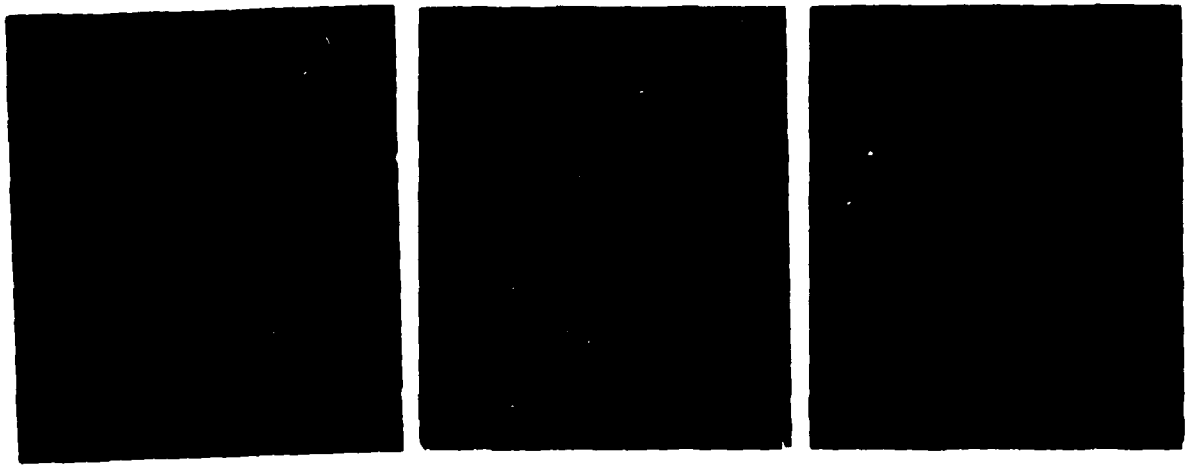

Field Voltage

0 kV 7 kV 10 kV

Figure 19. Interferometer Photograph Showing the Effect of the Corona Wind on the Thermal Boundary Layer of the One-Inch-Diameter Test Cylinder with the Stretched Wire Emitter at 1/2-Inch Source to Receiver Distance

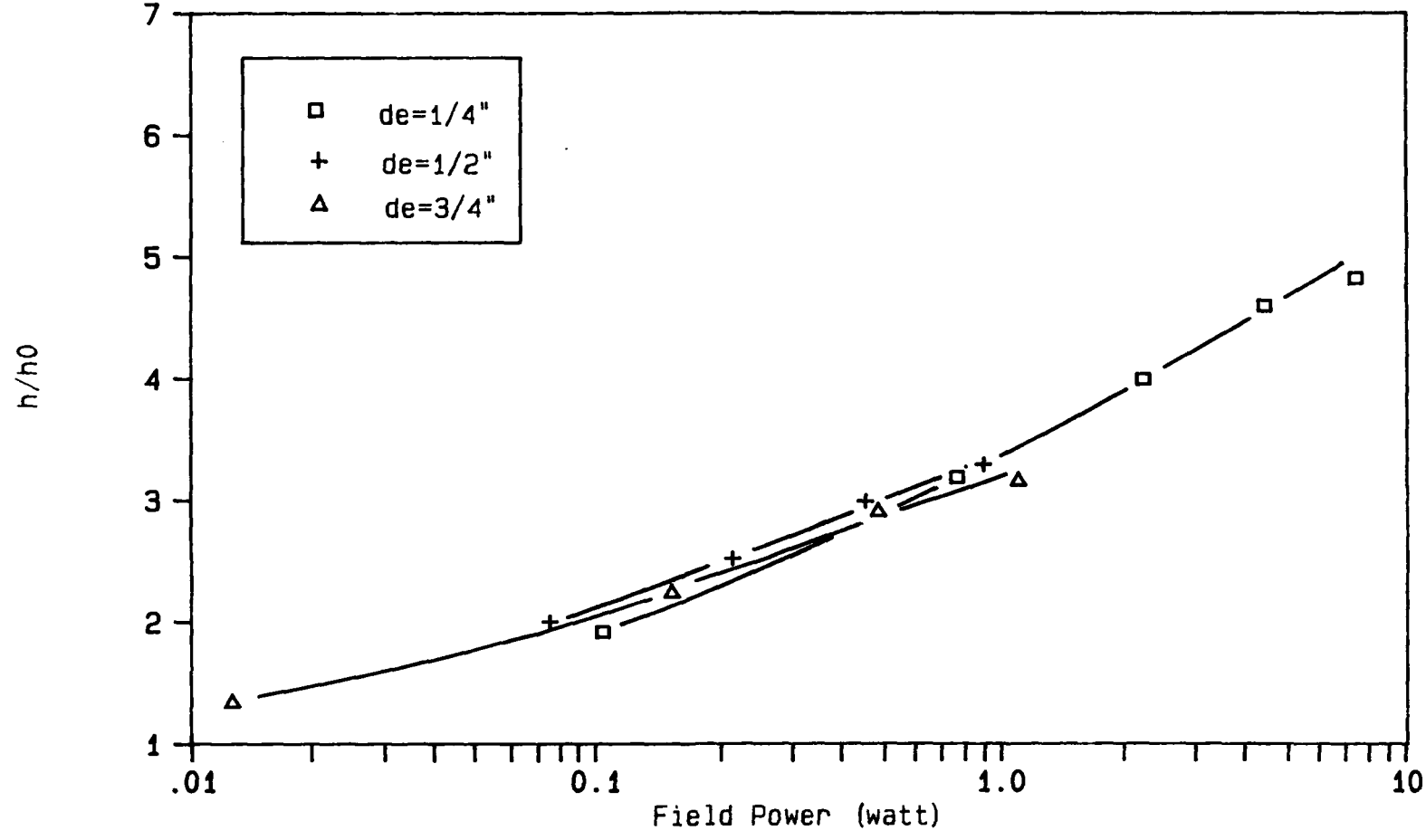

Figure 20. Effect of Field Power on the Ratio h/h0 for the 1-in Diameter Test Cylinder at Various Source to Receiver Distances with a Stretched Wire Emitter

plots of h/ho versus field power.

There was very good correlation between the stretched wire data collect in this experiment and Hogue's (5) data. The shapes of the h/h_0 versus field voltage curves were generally analogous. Hogue's breakdown voltages were higher because he used larger diameter wire (0.004 in versus 0.0031 in) in the emitter. His emitter device, with more total surface area, required higher field power levels to reach the electrostatic field intensity per unit area necessary to produce breakdown. The plots of h/h_0 versus field power in Figures 21 and 22 show excellent correlation between the two sets of data.

Multipoint Emitter. Plots of the data collected for test runs with the multipoint emitter are shown in Figures 23 and 24 for field voltage and field power ordinate axes, respectively. The multipoint emitter had lower breakdown voltages and more turbulent ion flow.

The multipoint emitter was also more efficient than the stretched wire device. Figures 25, 26, and 27 show that for a given field power input, the h/h_0 ratio was higher for the multipoint emitter than for the stretched wire emitter.

Comparison plots of the multipoint and stretched wire data versus field voltage are in Figures 28, 29, and 30. At d_e's of 3/4 and 1/2 in the multipoint emitter produced h/h_o ratios at least 40% higher than those produced with the stretched wire emitter. The two sets of data have

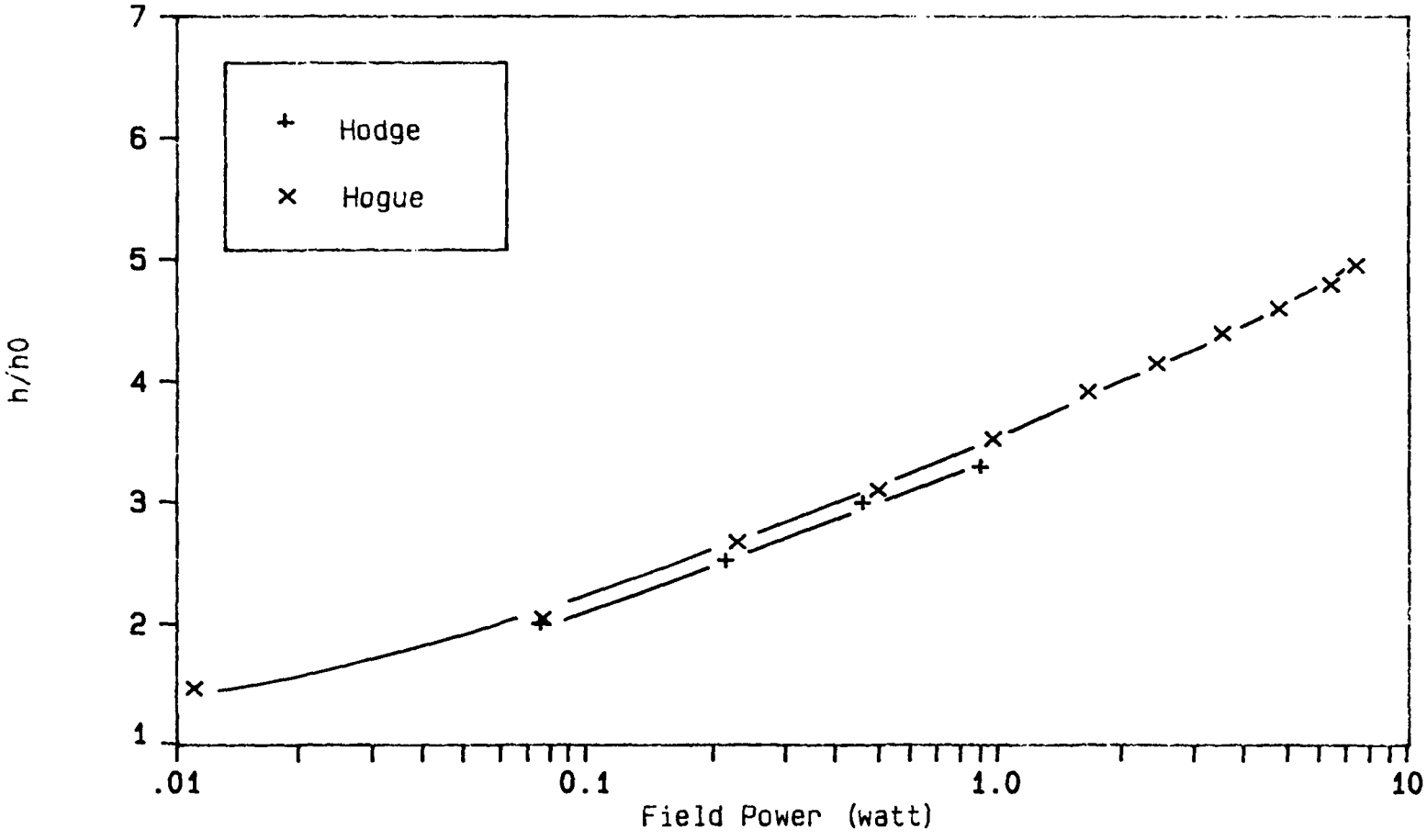

Figure 21. A Comparison of the h/h0 Data Collected in this Experiment To Data Collected by Hogue (5) for the One-Inch-Diameter Test Cylinder at 1/2-in Source to Receiver Distance with a Stretched Wire Emitter

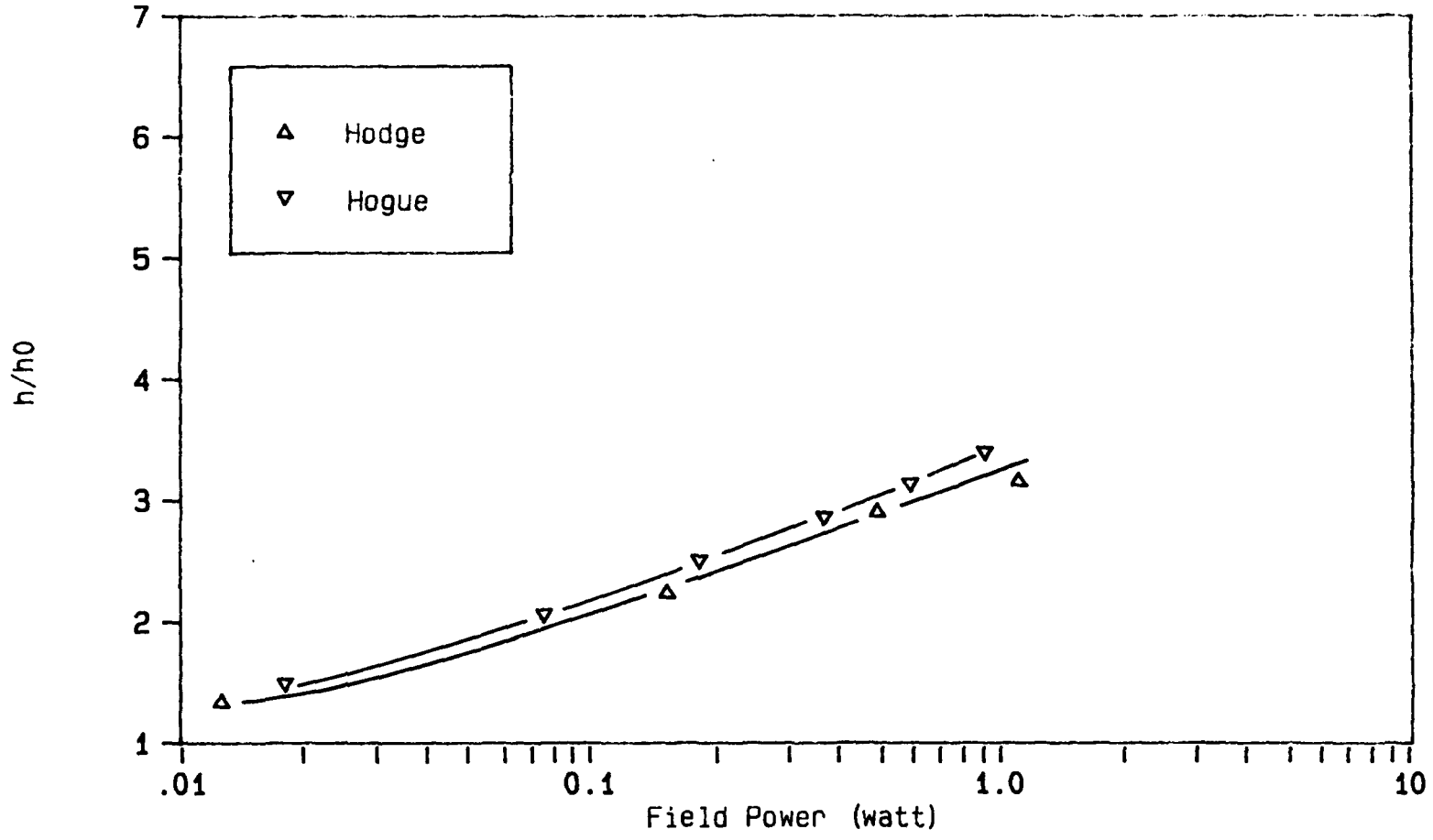

Figure 22. A Comparison of the h/h0 Data Collected in this Experiment To Data Collected by Hogue (5) for the One-Inch-Diameter Test Cylinder at 3/4-in Source to Receiver Distance with a Stretched Wire Emitter

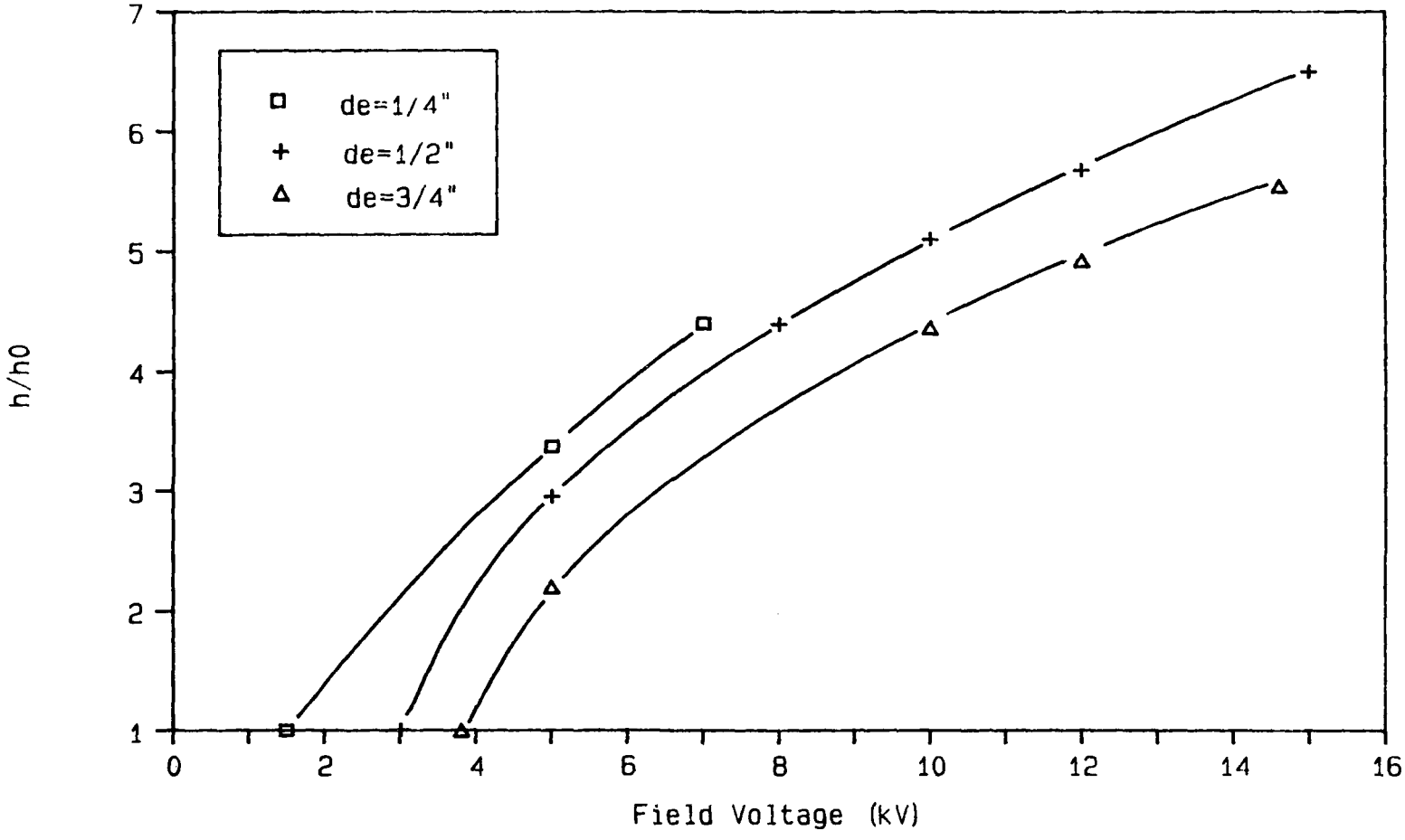

Figure 23. Effect of Corona Wind on the Ratio h/h0 for the 1-in Diameter Test Cylinder at Various Source to Receiver Distances with a Multipoint Emitter

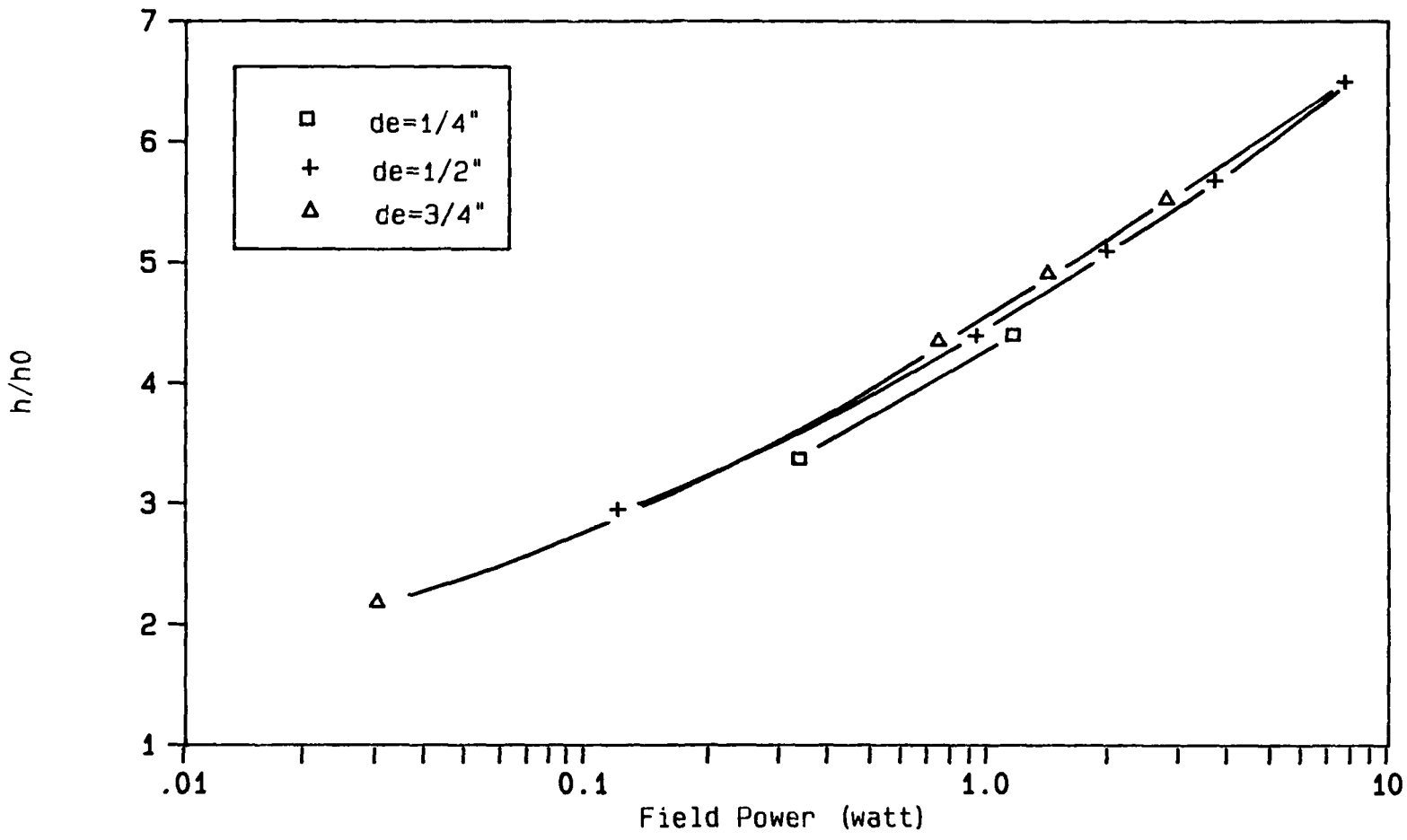

Figure 24. Effect of Field Power on the Ratio h/h0 for the 1-in Diameter Test Cylinder at Various Source to Receiver Distances with a Multipoint Emitter

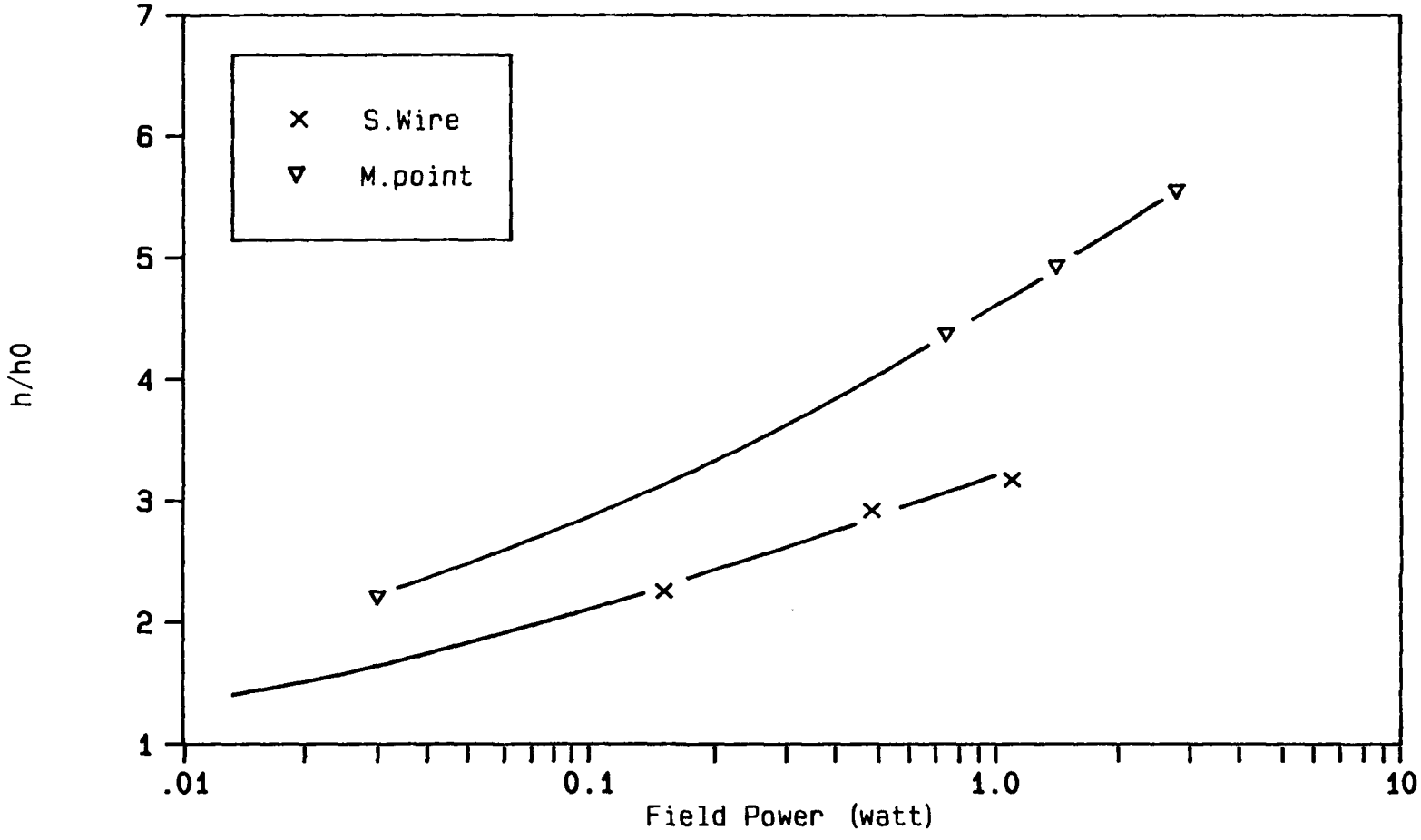

Figure 25. A Comparison of the Effect of Field Power on h/h0 for the 1-in Diameter Cylinder at 3/4-in Source to Receiver Distance with Stretched Wire and Multipoint Emitters

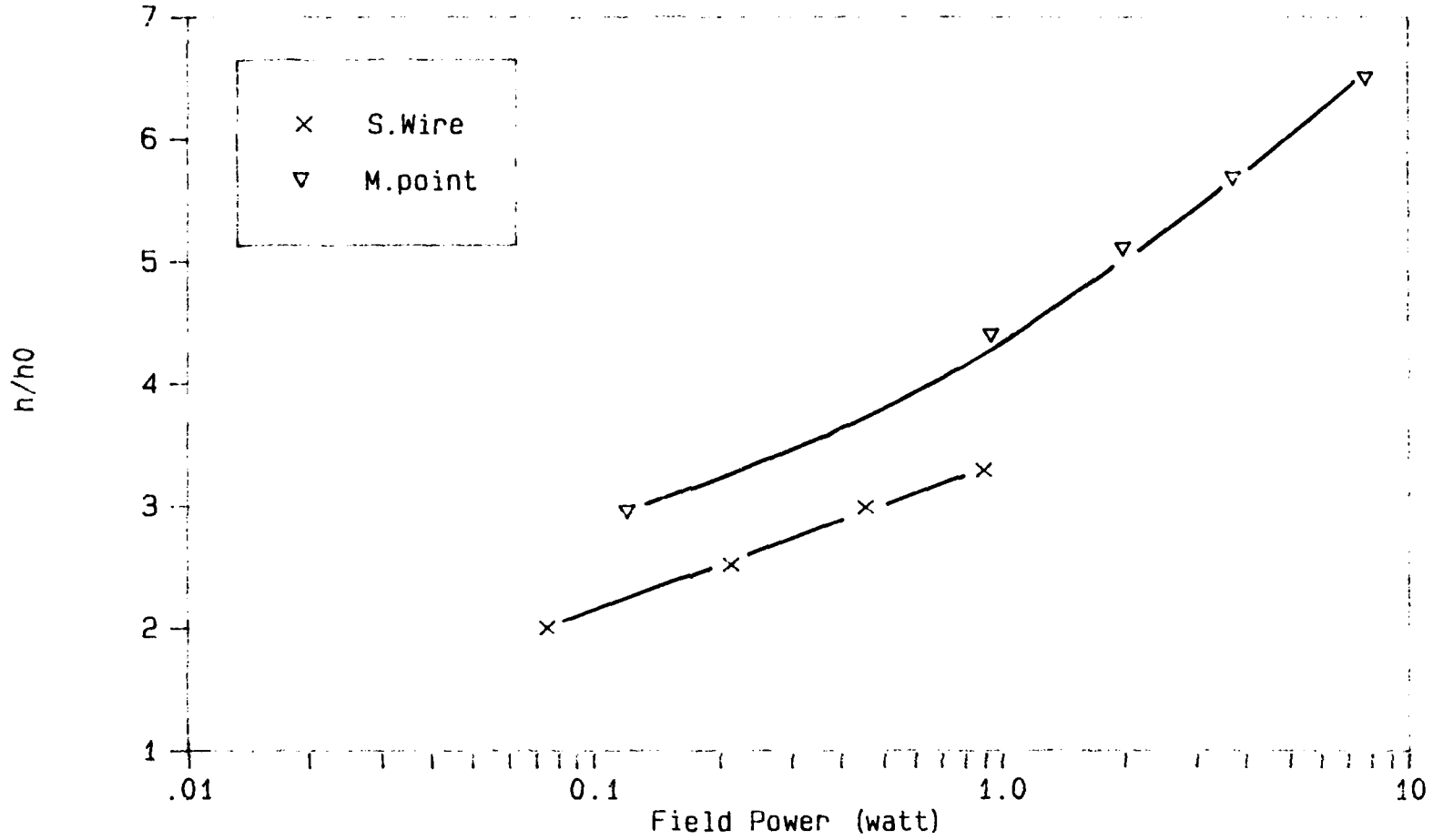

Figure 26. A Comparison of the Effect of Field Power on h/h0 for the 1-in Diameter Cylinder at 1/2-in Source to Receiver Distance with Stretched Wire and Multipoint Emitters

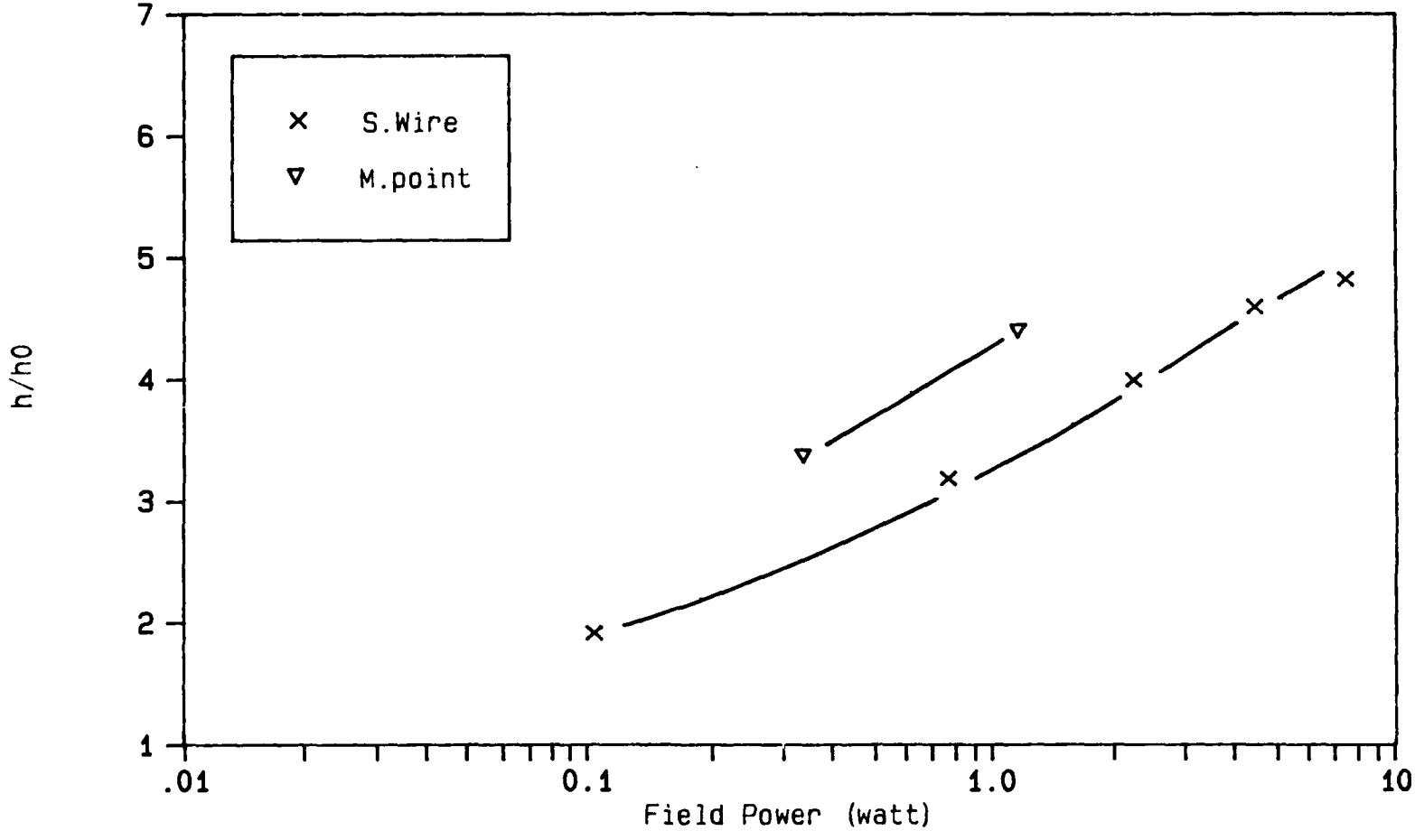

Figure 27. A Comparison of the Effect of Field Power on h/h0 for the 1-in Diameter Cylinder at 1/4-in Source to Receiver Distance with Stretched Wire and Multipoint Emitters

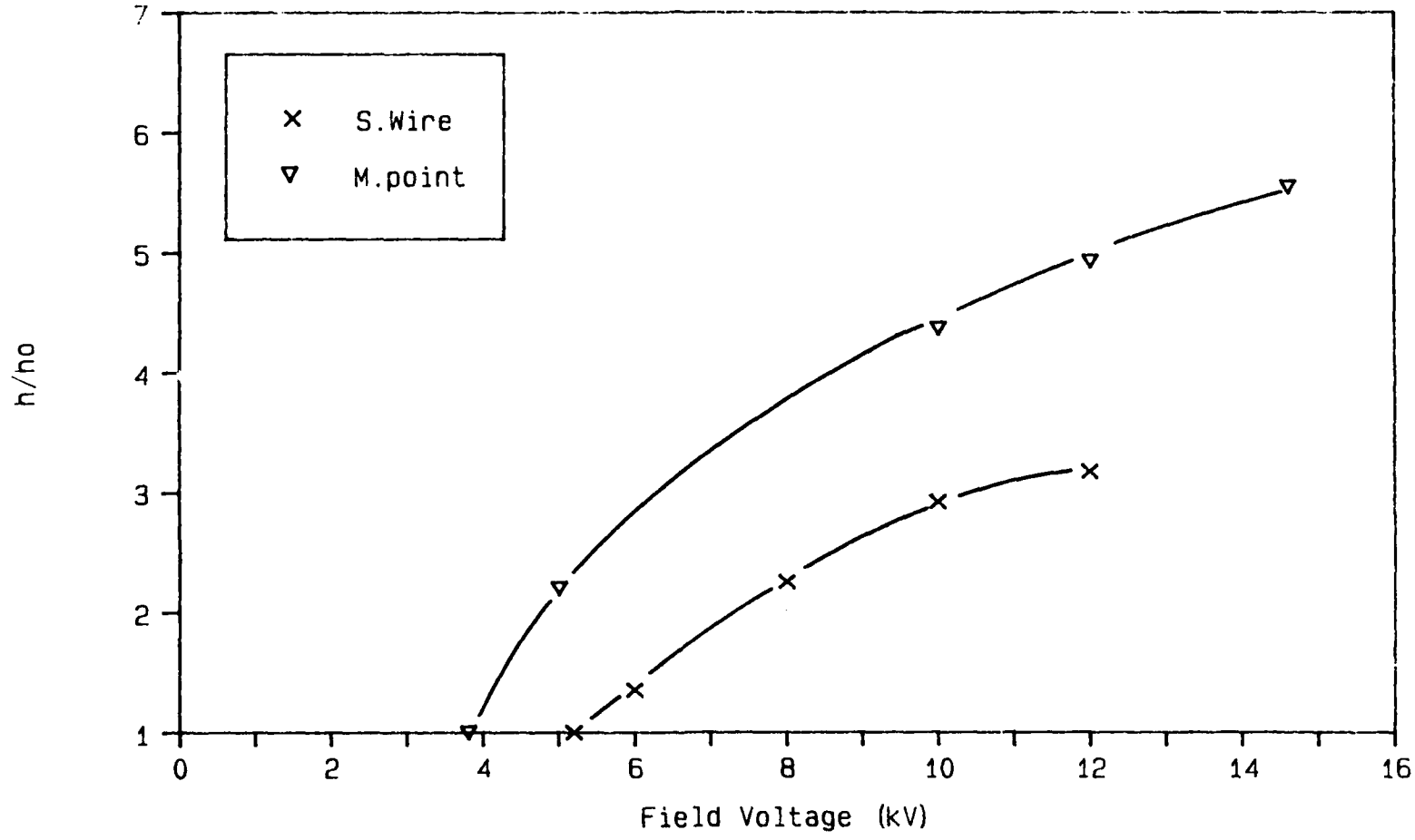

Figure 28. A Comparison of the Stretched Wire and Multipoint Emitter Ratios of h/h0 for the 1-in Diameter Cylinder at 3/4-in Source to Receiver Distance

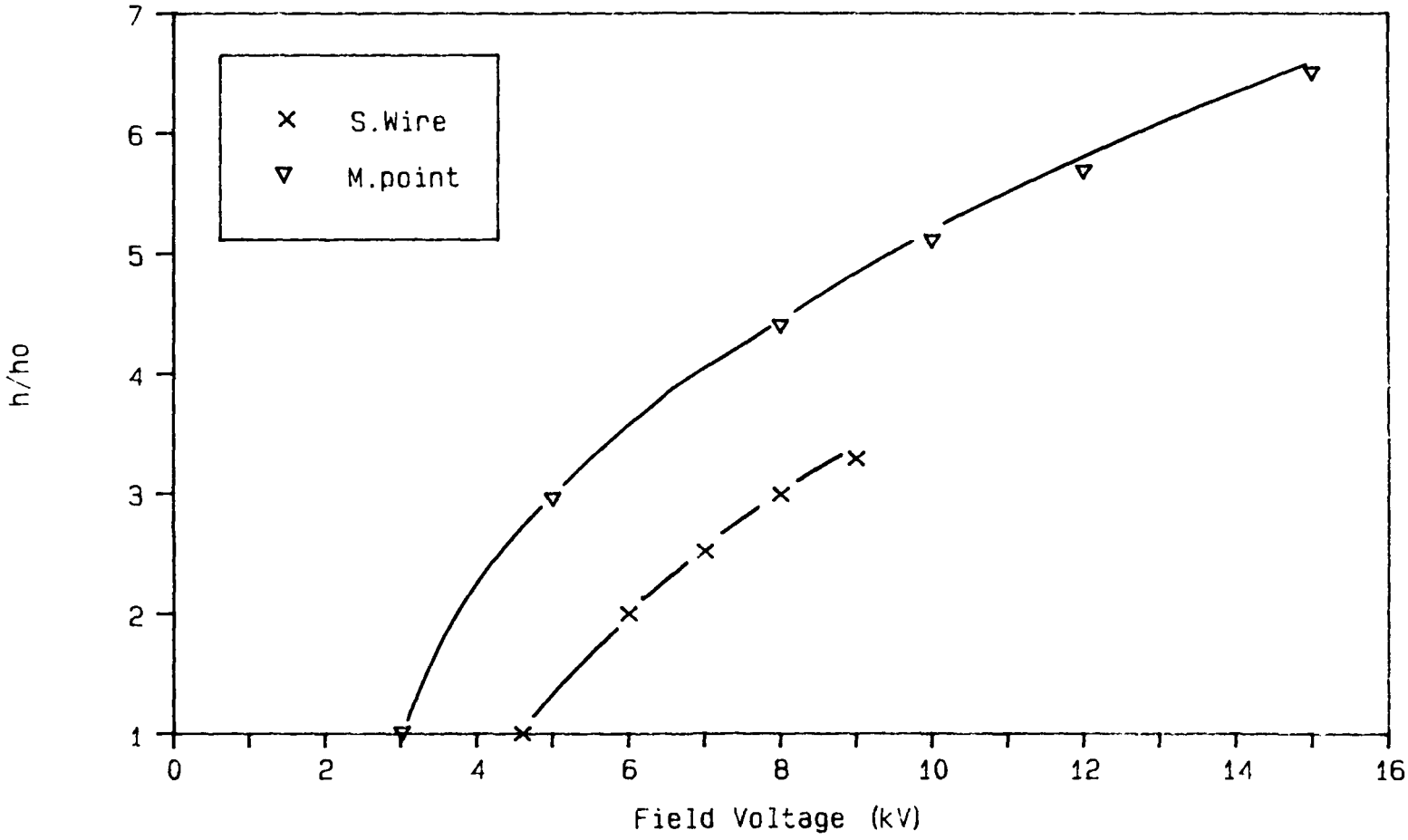

Figure 29. A Comparison of the Stretched Wire and Multipoint Emitter Ratios of h/h0 for the 1-in Diameter Cylinder at 1/2-in Source to Receiver Distance

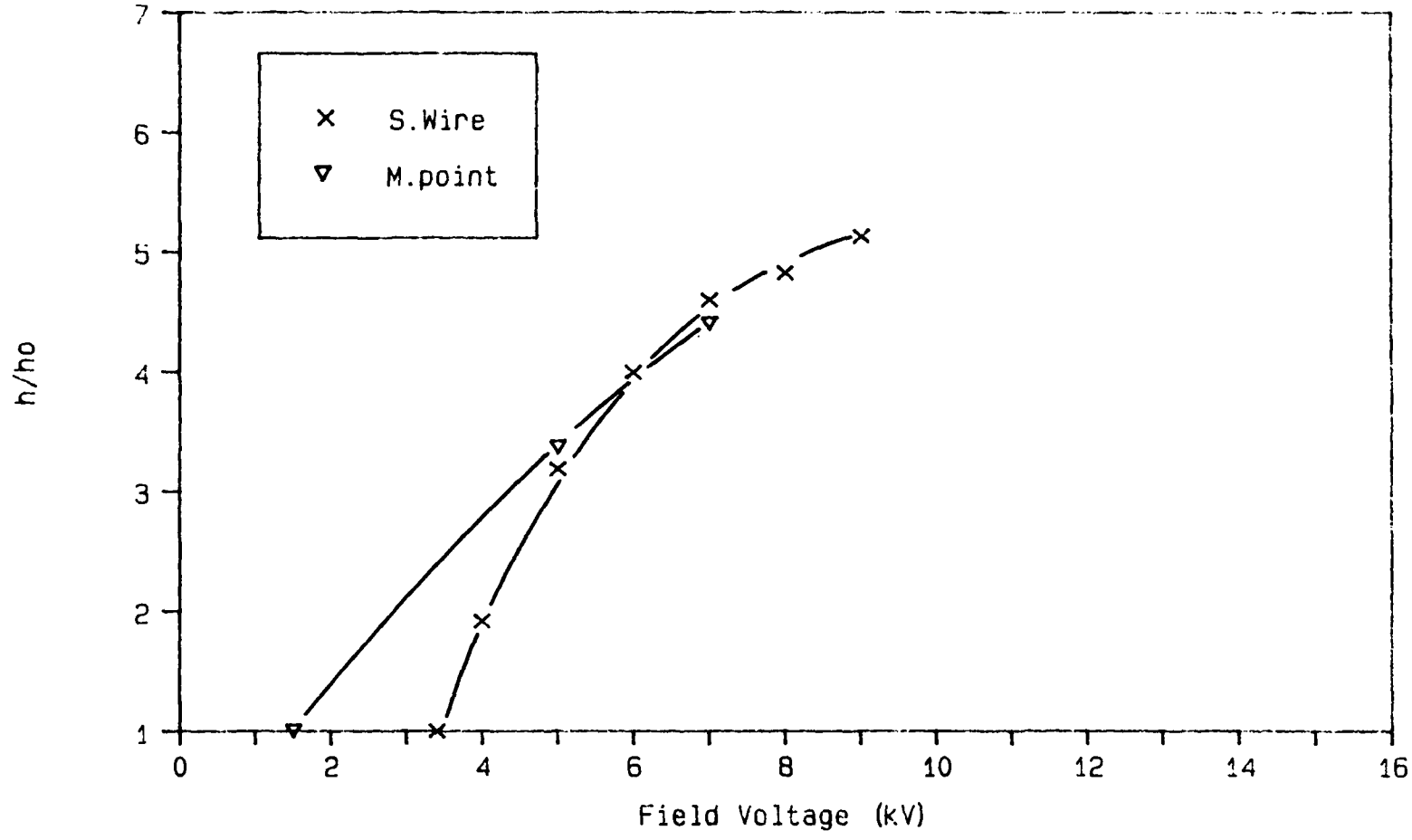

Figure 30. A Comparison of the Stretched Wire and Multipoint Emitter Ratios of h/h0 for the 1-in Diameter Cylinder at 1/4-in Source to Receiver Distance

equal slopes and plot into a single curve when the breakdown voltage affects are nulled by shifting the curves along the x-axis. At 1/4-in d_e the slope of the stretched wire curve is greater than the slope of the multipoint curve.

Blown Air Plenum. The data collected for test runs with the blown air plenum are plotted in Figure 31. The plenum was designed by Hogue (5) to simulate the stretched wire emitter device. A field voltage to corona wind velocity transform was compiled experimentally to facilitate comparison of the cooling data collected with the two devices (see Figure 16). The h/h_o ratio versus velocity data for the stretched wire and blown air configurations are plotted in Figures 32, 33, and 34 for each of the three d_e settings, respectively.

The h/h_o ratio increased almost linearly with velocity for the range of blown air data collected. The corona h/h_o ratio exhibited a more exponential increase with increasing velocity. At low velocities, the blown air had higher h/h_o ratios than the corona wind. At higher velocities, the corona wind ratios were greatest. The two plots crossed at velocities between 150 and 200 ft/min. The crossover velocity point was higher for each increase in the d_e setting.

Hogue plotted similar data for the 1-in-diameter cylinder with d_e settings of 1/2 in and 3/4 in. His data

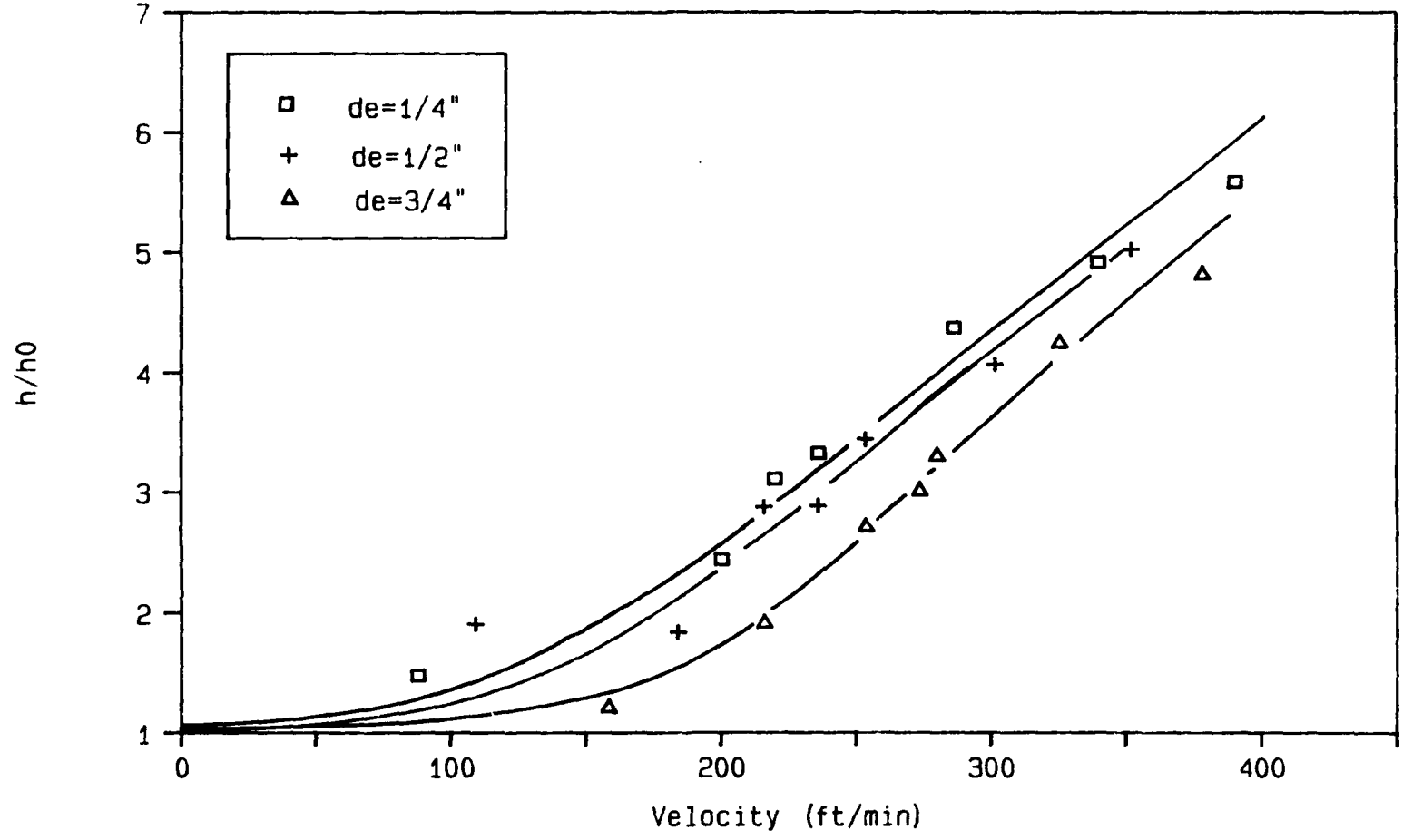

Figure 31. Effect of Blown Air on the Ratio h/h0 for the 1-in Diameter Test Cylinder at Various Source to Receiver Distances

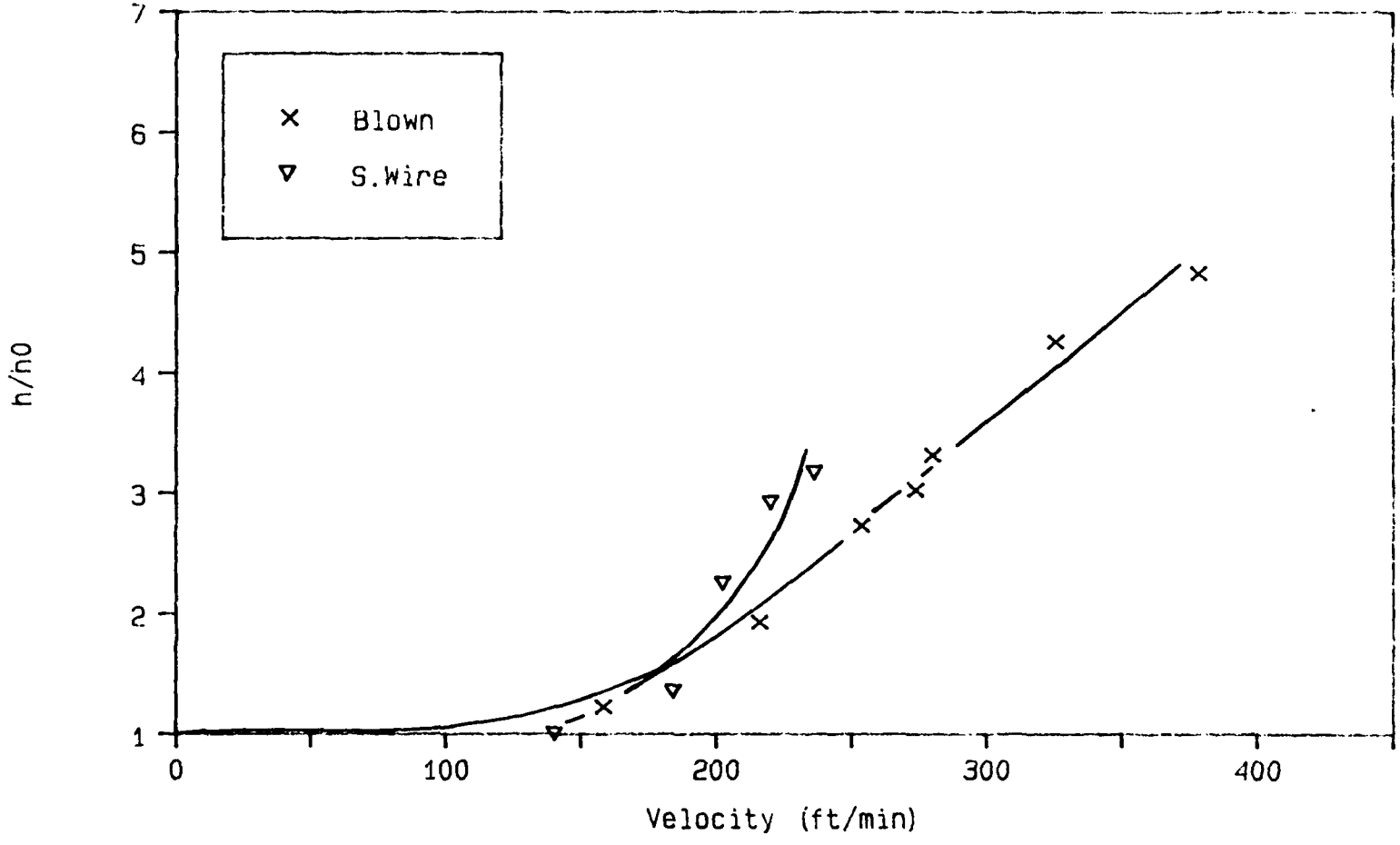

Figure 32. A Comparison of the Blown Air and Stretched Wire Ratios of h/h0 for the 1-in Diameter Cylinder at 3/4-in Source to Receiver Distance

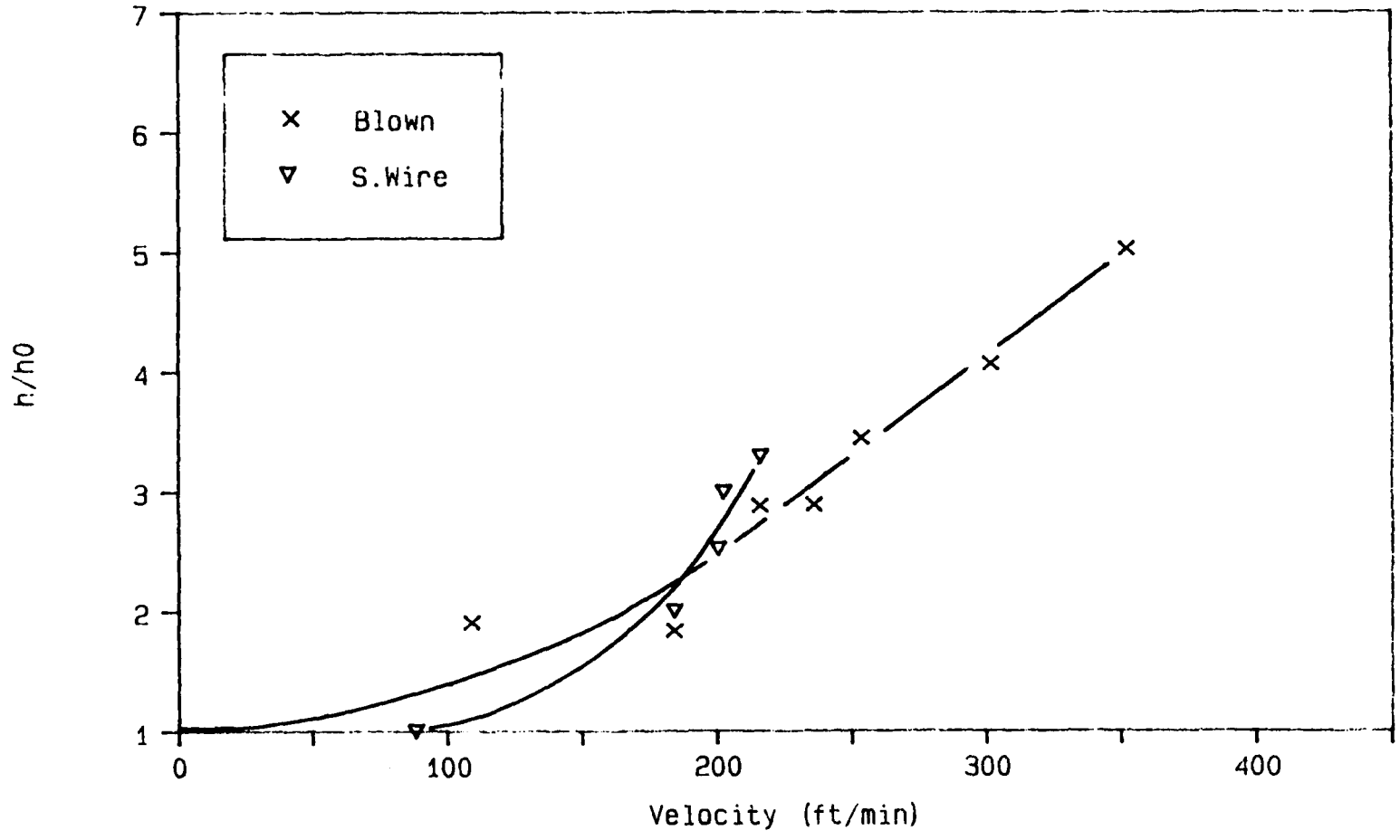

Figure 33. A Comparison of the Blown Air and Stretched Wire Ratios of h/h0 for the 1-in Diameter Cylinder at 1/2-in Source to Receiver Distance

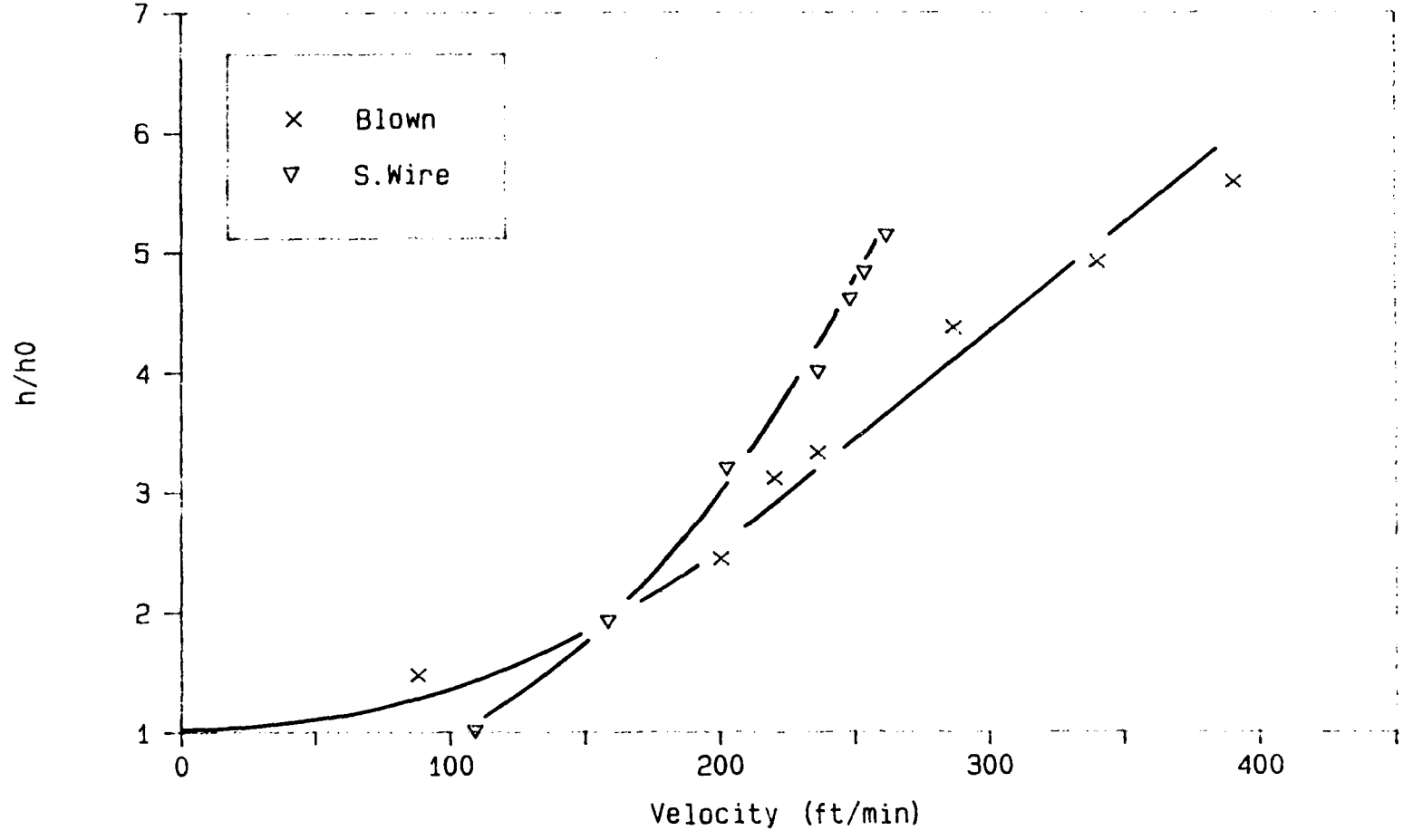

Figure 34. A Comparison of the Blown Air and Stretched Wire Ratios of h/h0 for the 1-in Diameter Cylinder at 1/4-in Source to Receiver Distance

yielded blown air h/h_o versus velocity plots slightly higher than the corona wind plot at 1/2-in d_e, and virtually overlapping plots at 3/4-in d_e. This difference of experimental results at equivalent d_e settings was most probably due to the differences in breakdown voltages explained above.

The interferometer photograph (Figure 35) of the test cylinder in blown air showed that the boundary layers of the blown air and corona wind (Figure 19) were markedly different despite the fact that the blown air plenum was designed to simulate the corona stretched wire emitter device. Flow separation occurred almost immediately in the blown air; the corona flow separated at about 90° from the bottom of the test cylinder.

1/4 Inch Diameter Test Cylinder

The 1/4-in cylinder was tested at nine configurations identical to those used during testing of the 1-in cylinder.

The average total heat transfer coefficient, h_{to}, for the free convection test runs on the 1/4-in diameter cylinder was 1.57 Btu/hr-ft^2-$^{\circ}$F; equivalent to the value for the 1-in-diameter test cylinder.

Stretched Wire Emitter. The data collected with the stretched wire emitter device are plotted in Figures 36 and 37 for field voltage and power, respectively. The interferometer photograph (Figure 38) for stretched wire corona cooling of the 1/4-in-diameter test cylinder showed the

Velocity

184 ft/min 209 ft/min 254 ft/min

Figure 35. Interferometer Photographs Showing the Effect of a Jet of Uncharged Air on the Thermal Boundary Layer of the One-Inch-Diameter Test Cylinder with the Plenum at 1/2-Inch Source to Receiver Distance

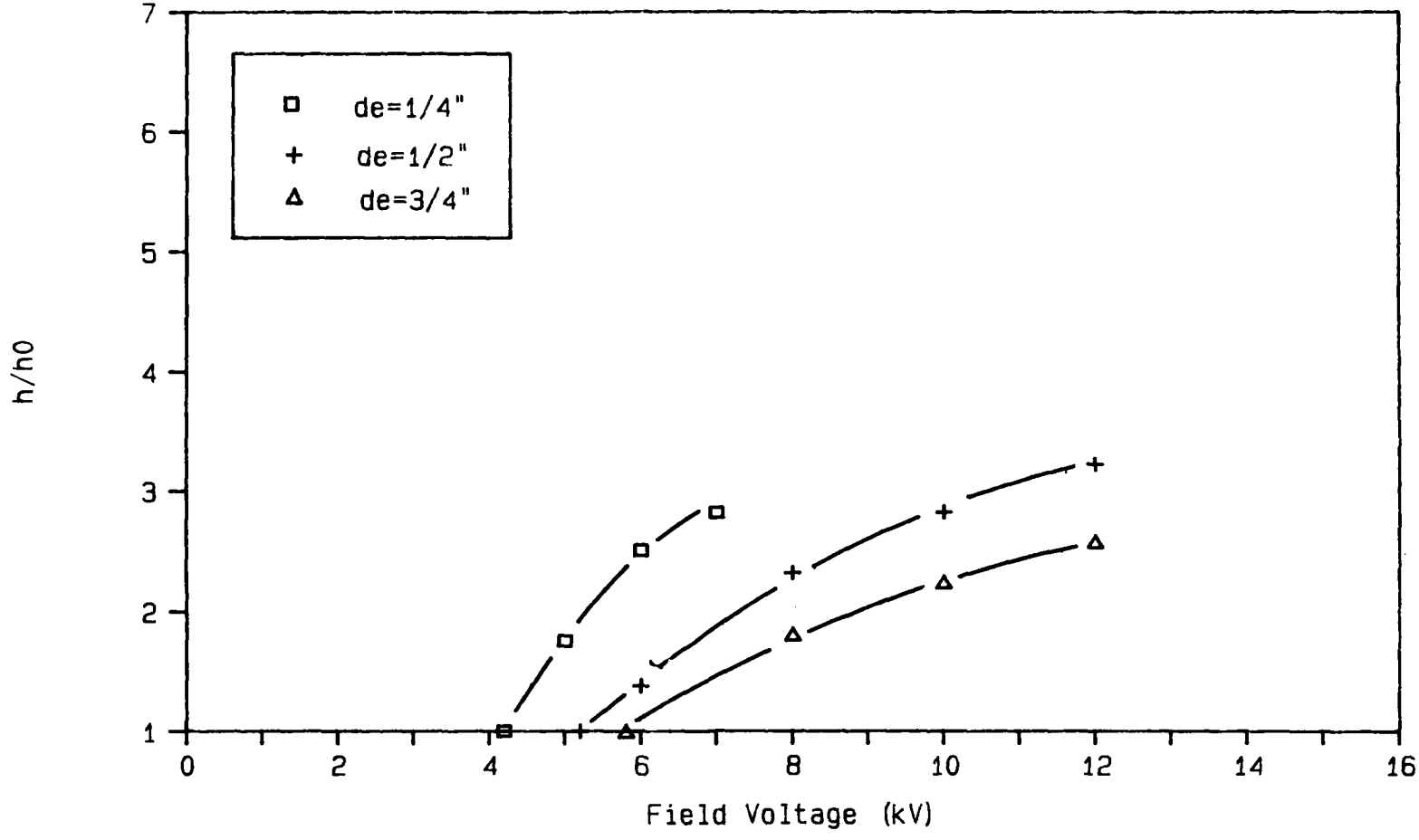

Figure 36. Effect of Corona Wind on the Ratio h/h0 for the 1/4-in Diameter Test Cylinder at Various Source to Receiver Distances with a Stretched Wire Emitter

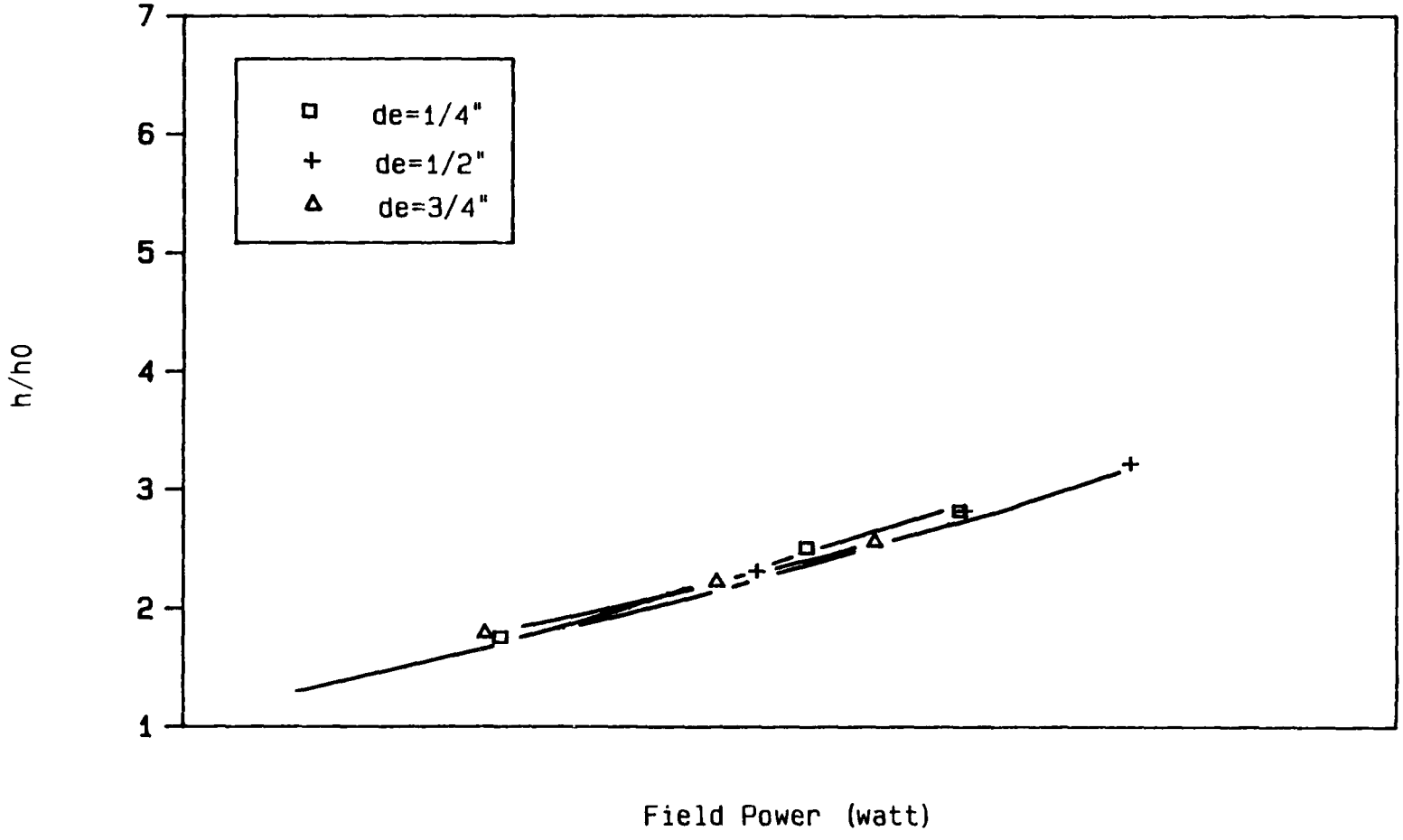

Figure 37. Effect of Field Power on the Ratio h/h0 for the 1/4-in Diameter Test Cylinder at Various Source to Receiver Distances with a Stretched Wire Emitter

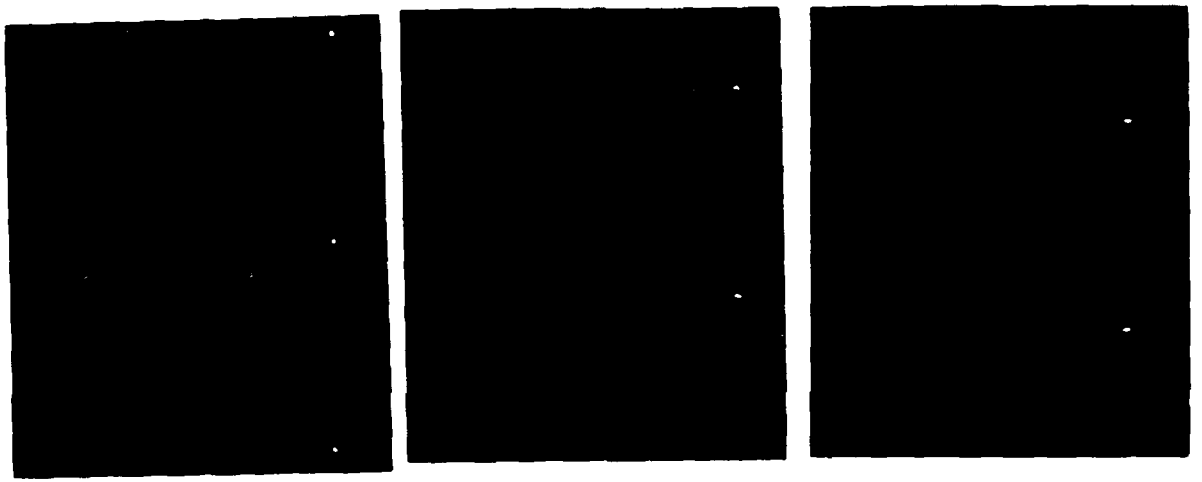

Field Voltage

0 kV 8 kV 12 kV

Figure 38. Interferometer Photograph Showing the Effect of the Corona Wind on the Thermal Boundary Layer of the 1/4-Inch-Diameter Test Cylinder with the Stretched Wire Emitter at 1/2-Inch Source to Receiver Distance

same pattern of flow separation as the 1-in-diameter test cylinder (Figure 19).

Multipoint Emitter. The data collected with the multipoint emitter device are plotted in Figure 39 and 40 for field voltage and power, respectively. Stretched wire versus multipoint comparison plots for the 1/4-in test cylinder are in Figures 41, 42, and 43 for field voltage and Figures 44, 45, and 46 for field power. At each of the three d_e settings, the multipoint emitter device produced higher h/h_o ratios and used power more efficiently than the stretched wire emitter device. These results exhibited the same trends as the results obtained with the 1-in cylinder with the exception of the 1/4-in d_e case.

Blown Air Plenum. Data collected with the blown air device are plotted in Figure 47. The 1/4-in-diameter test cylinder (Figure 48) had less turbulent flow than the 1-in-diameter test cylinder (Figure 35) in blown air at high velocities.

Comparison plots of the blown air and stretched wire results are in Figures 49, 50, and 51. As with the 1-in cylinder, the h/h_o ratios for the 1/4-in cylinder were first higher for blown air at low velocities, and then higher for corona wind at higher velocities. The velocities at which the plots crossed were higher for the 1/4-in cylinder than for the 1-in cylinder, and showed the same trend of becoming higher as the d_e spacing decreased.

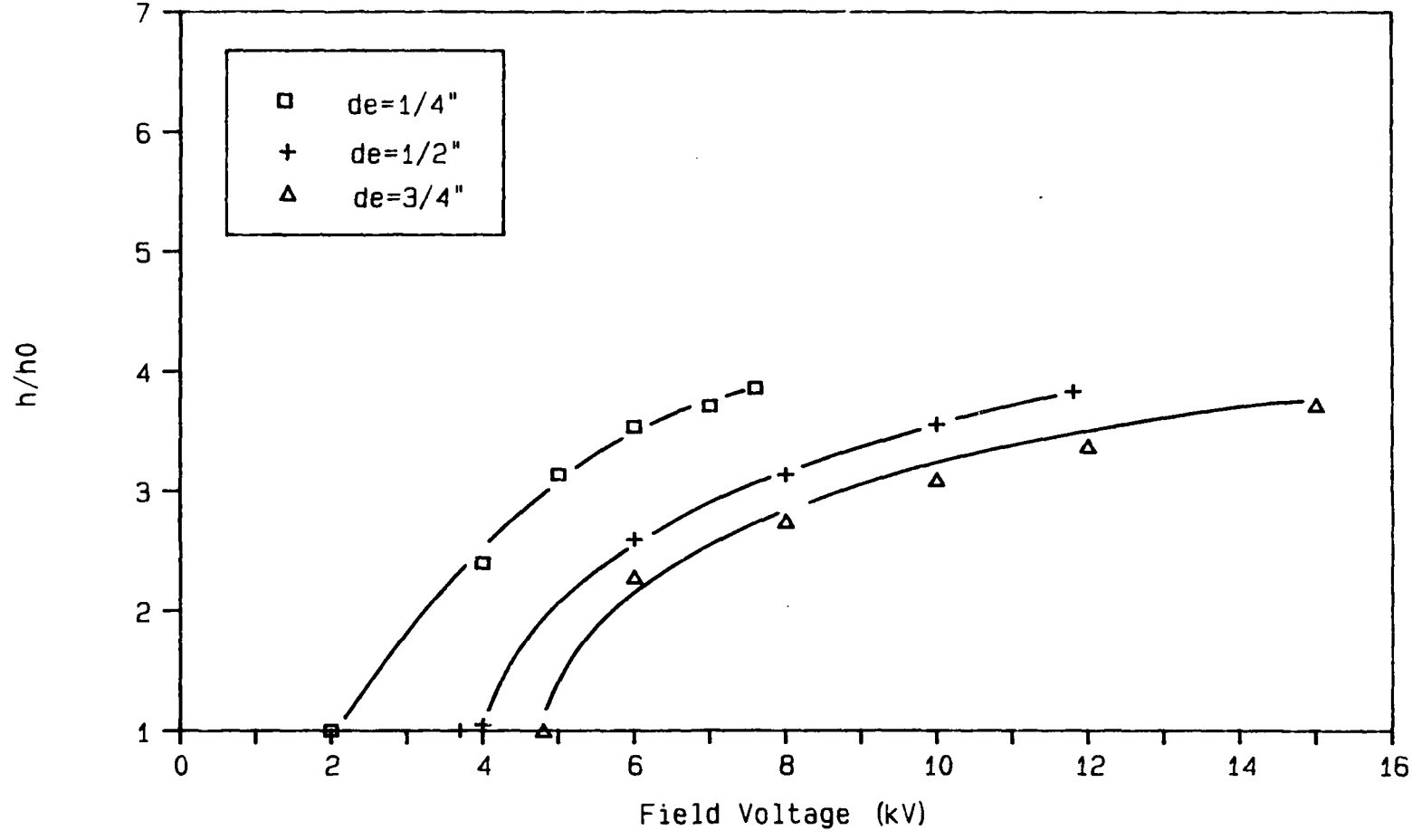

Figure 39. Effect of Corona Wind on the Ratio h/h0 for the 1/4-in Diameter Test Cylinder at Various Source to Receiver Distances with a Multipoint Emitter

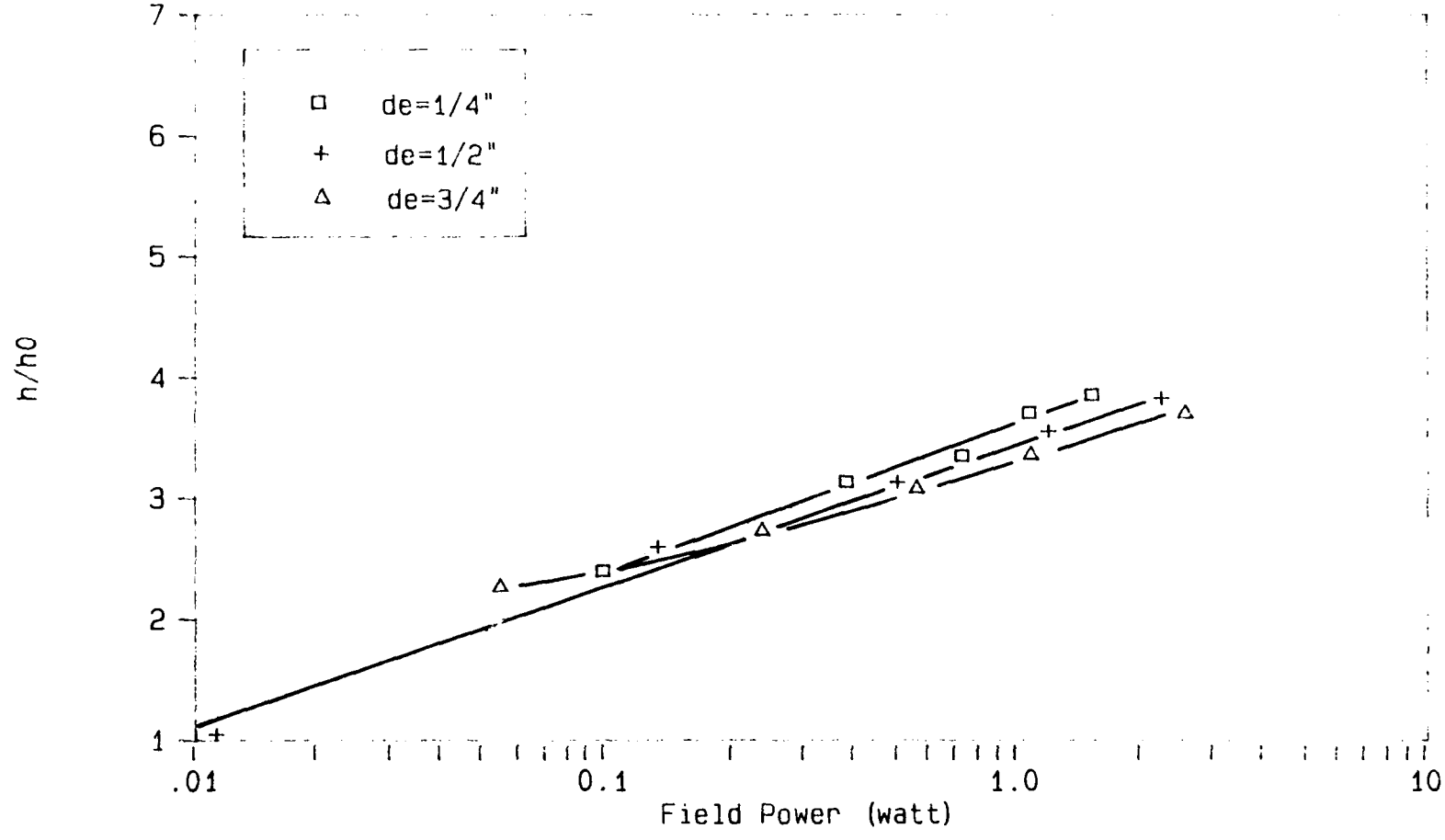

Figure 40. Effect of Field Power on the Ratio h/h0 for the 1/4-in Diameter Test Cylinder at Various Source to Receiver Distances with a Multipoint Emitter

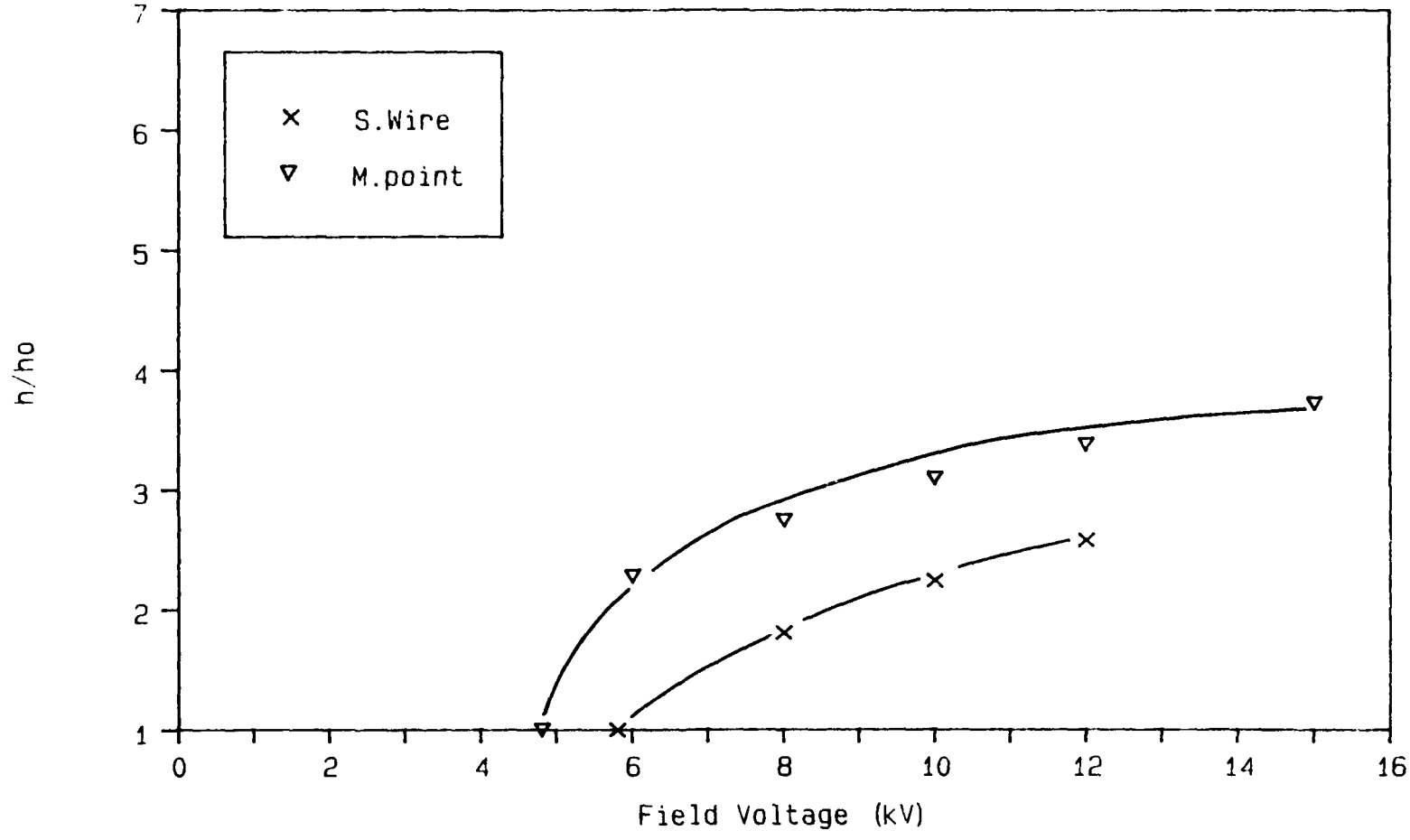

Figure 41. A Comparison of the Stretched Wire and Multipoint Emitter Ratios of h/h0 for the 1/4-in Diameter Cylinder at 3/4-in Source to Receiver Distance

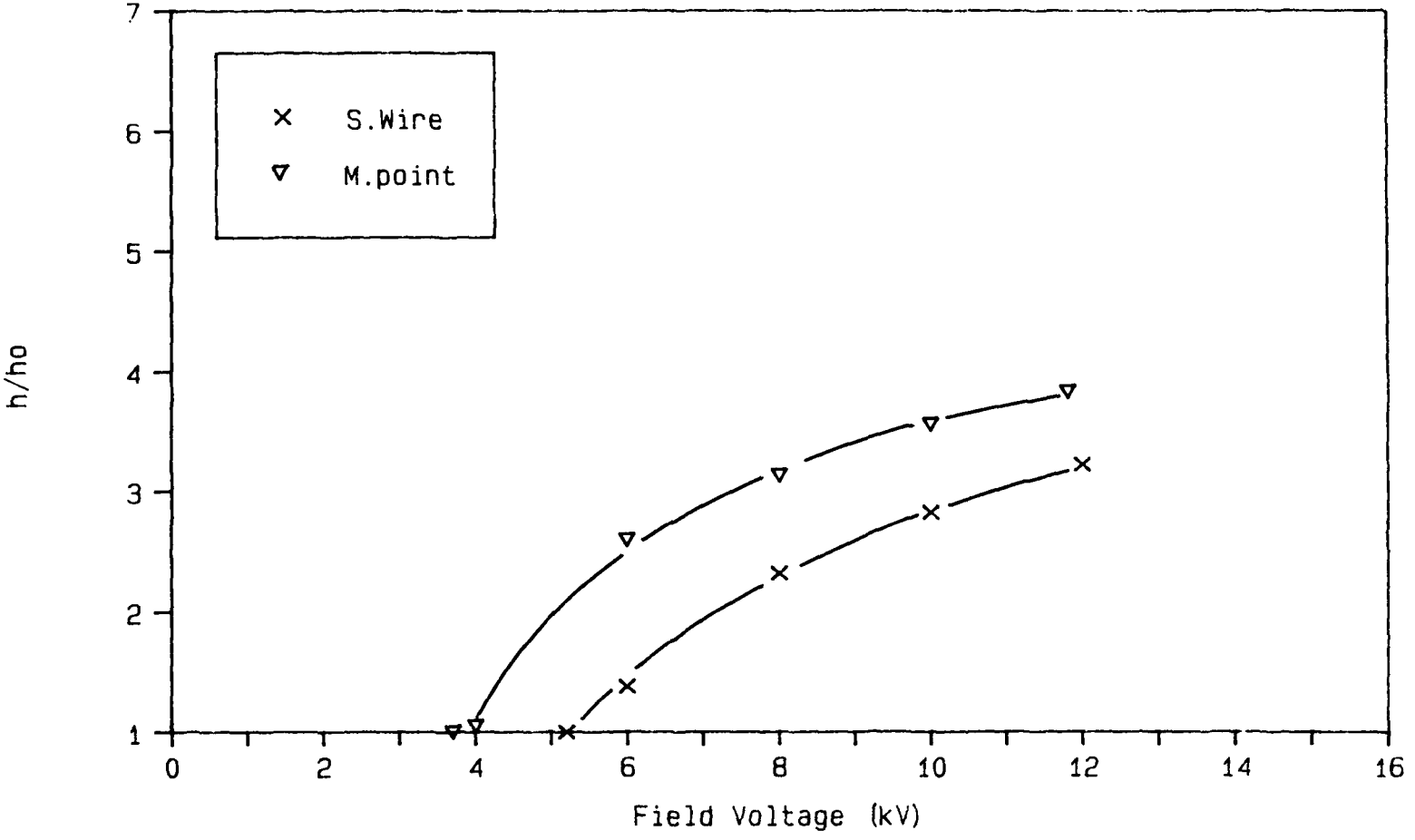

Figure 42. A Comparison of the Stretched Wire and Multipoint Emitter Ratios of h/h0 for the 1/4-in Diameter Cylinder at 1/2-in Source to Receiver Distance

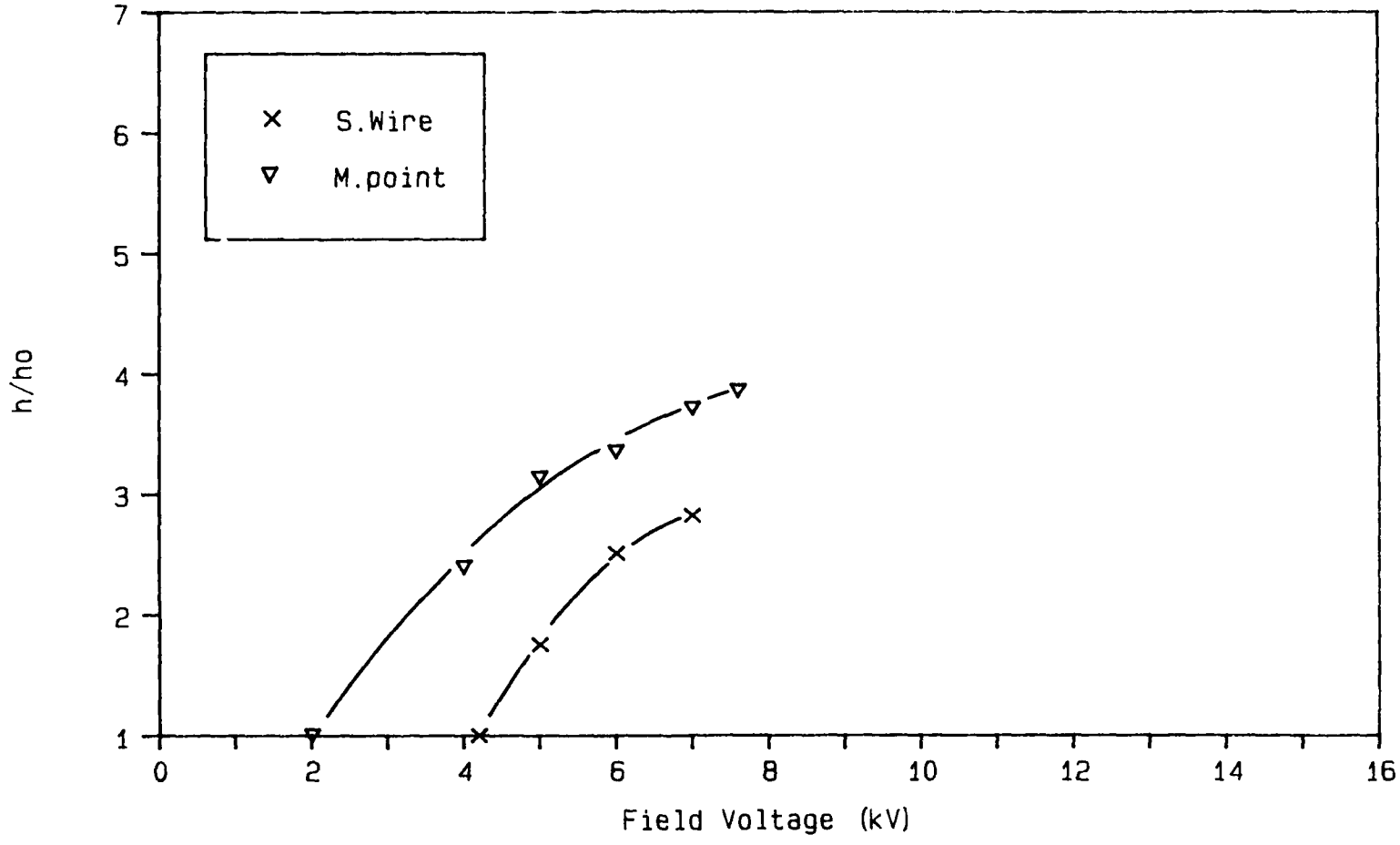

Figure 43. A Comparison of the Stretched Wire and Multipoint Emitter Ratios of h/h0 for the 1/4-in Diameter Cylinder at 1/4-in Source to Receiver Distance

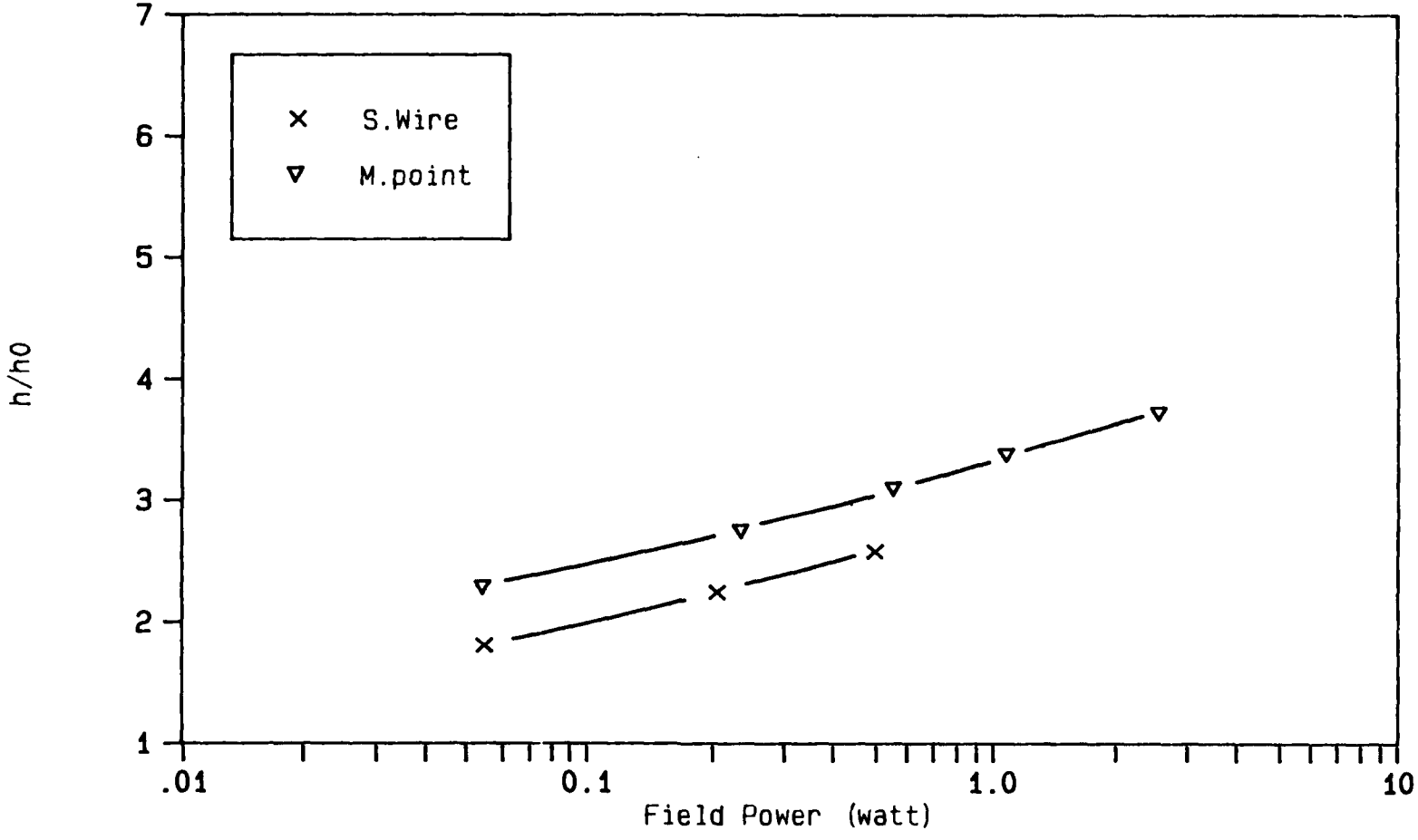

Figure 44. A Comparison of the Effect of Field Power on h/h0 for the 1/4-in Diameter Cylinder at 3/4-in Source to Receiver Distance with Stretched Wire and Multipoint Emitters

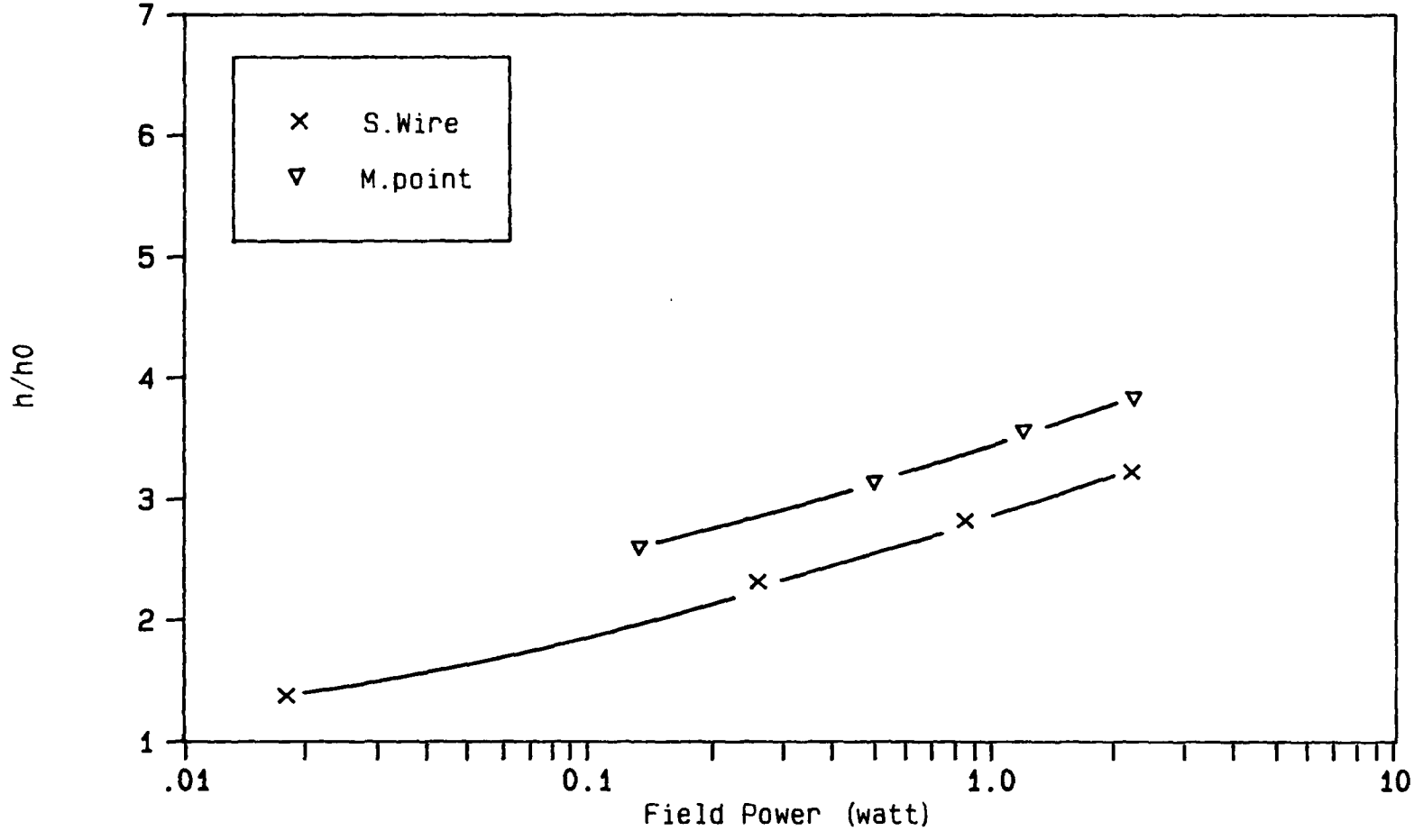

Figure 45. A Comparison of the Effect of Field Power on h/h0 for the 1/4-in Diameter Cylinder at 1/2-in Source to Receiver Distance with Stretched Wire and Multipoint Emitters

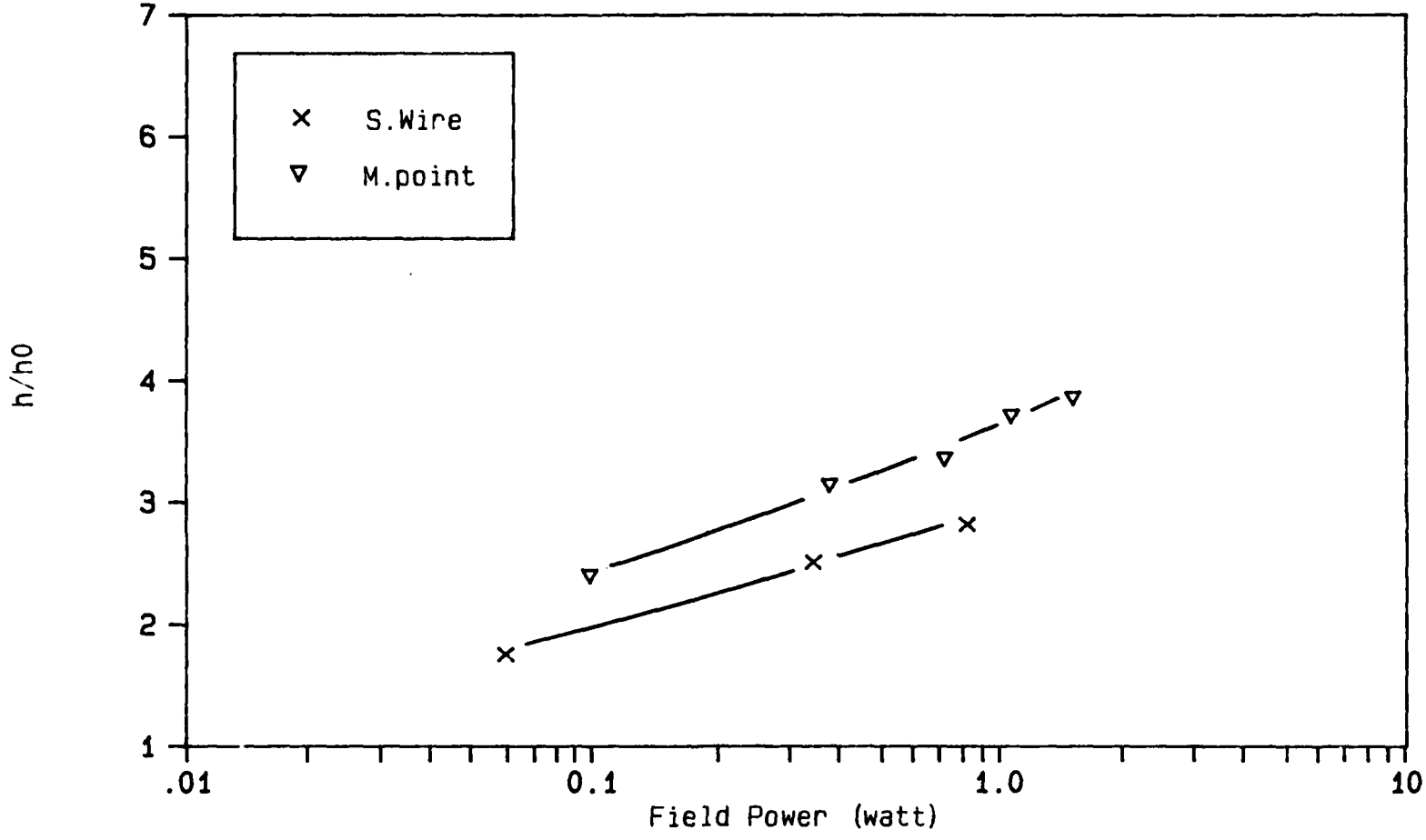

Figure 46. A Comparison of the Effect of Field Power on h/h0 for the 1/4-in Diameter Cylinder at 1/4-in Source to Receiver Distance with Stretched Wire and Multipoint Emitters

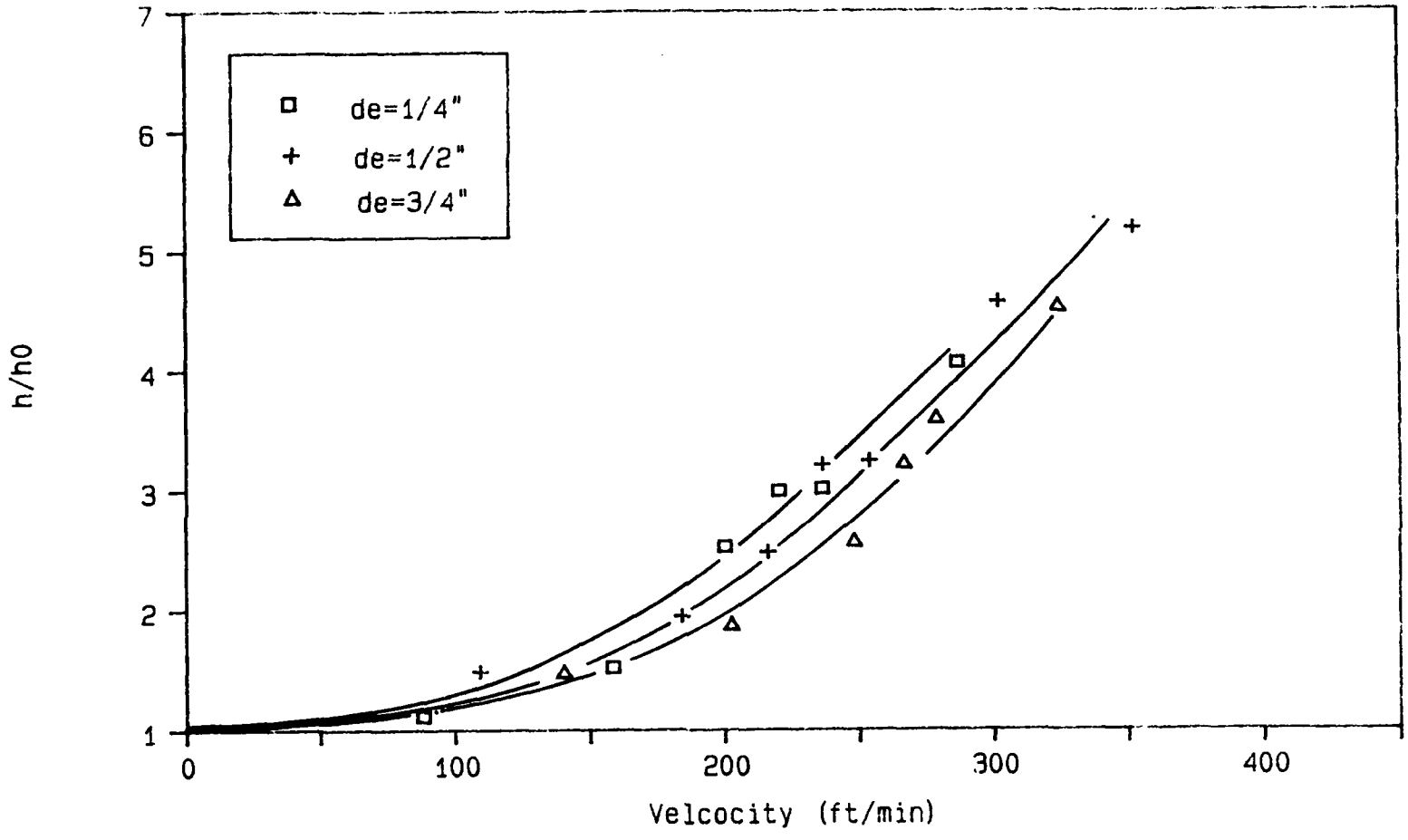

Figure 47. Effect of Blown Air on the Ratio h/h0 for the 1/4-in Diameter Test Cylinder at Various Source to Receiver Distances

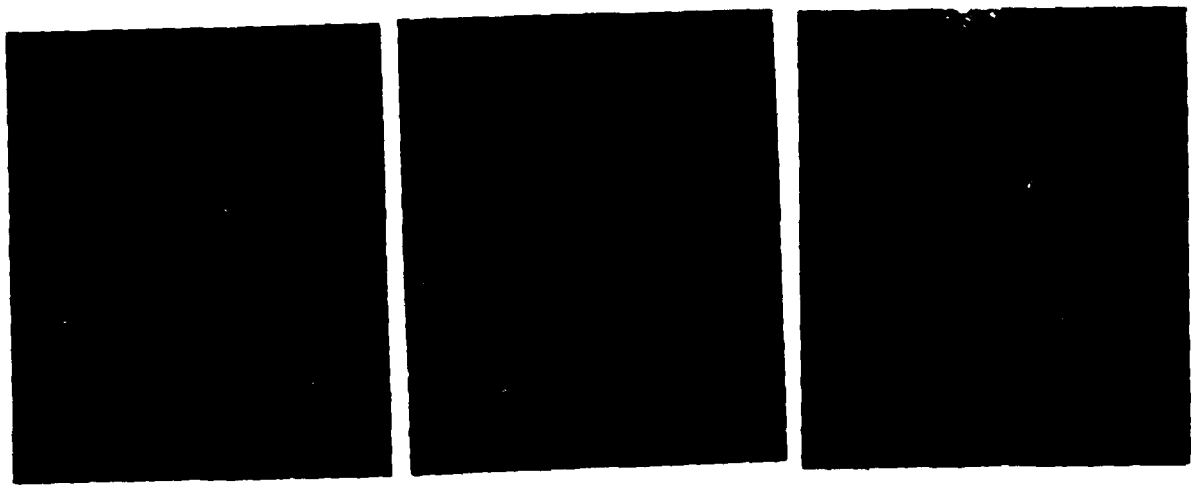

Velocity

0 ft/min | 164 ft/min | 254 ft/min

Figure 48. Interferometer Photographs Showing the Effect of a Jet of Uncharged Air on the Thermal Boundary Layer of the 1/4-Inch-Diameter Test Cylinder with the Plenum at 1/2-Inch Source to Receiver Distance

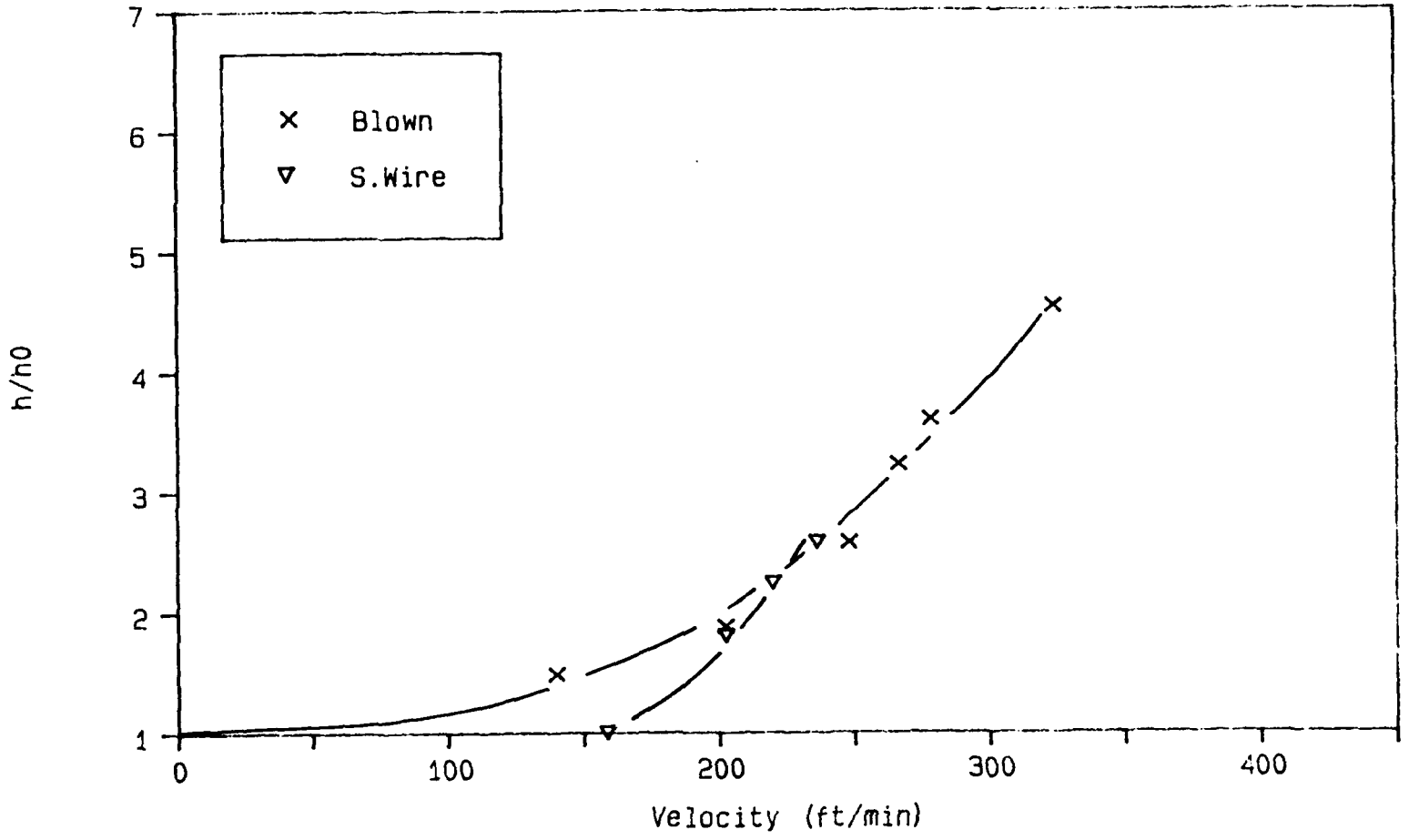

Figure 49. A Comparison of the Blown Air and Stretched Wire Ratios of h/h0 for the 1/4-in Diameter Cylinder at 3/4-in Source to Receiver Distance

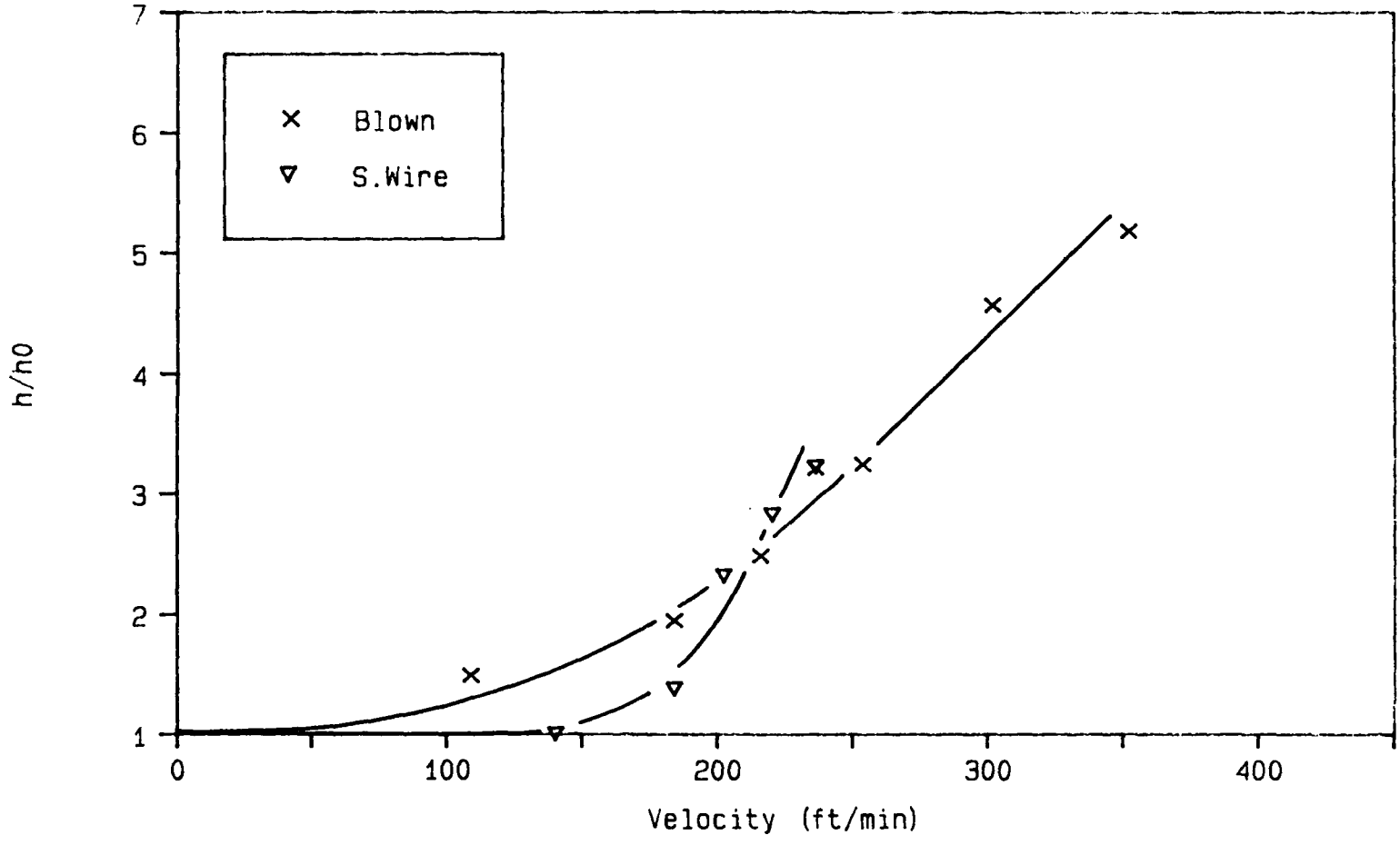

Figure 50. A Comparison of the Blown Air and Stretched Wire Ratios of h/h0 for the 1/4-in Diameter Cylinder at 1/2-in Source to Receiver Distance

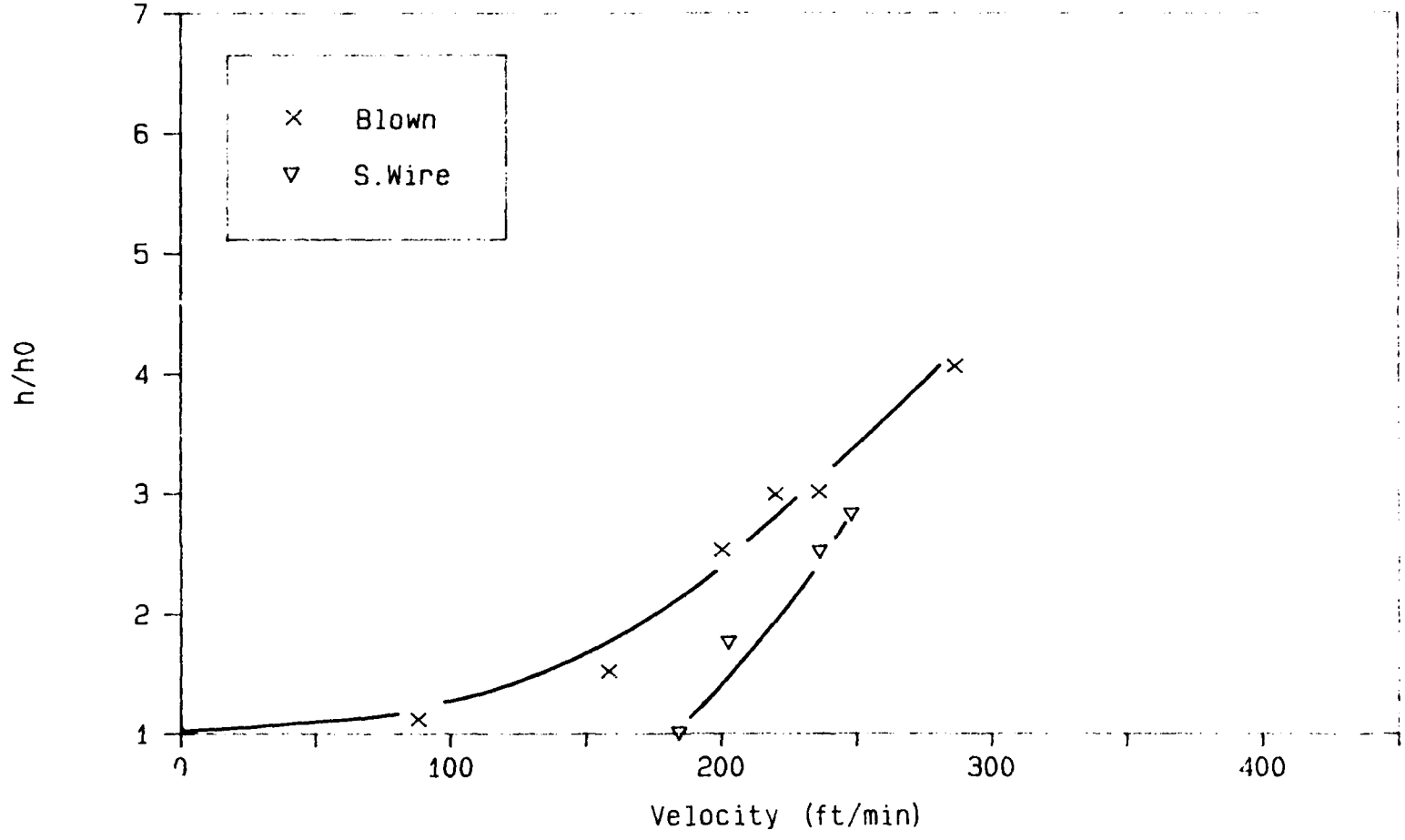

Figure 51. A Comparison of the Blown Air and Stretched Wire Ratios of h/h0 for the 1/4-in Diameter Cylinder at 1/4-in Source to Receiver Distance

2 Inch Diameter Test Cylinder

Test configurations for the 2-in cylinder matched those for the 1-in and 1/4-in cylinders. The average total free convection heat transfer coefficient was approximately 1.55 Btu/hr-ft^2-^{o}F; very close to the value for the 1-in and 1/4-in cylinders.

Stretched Wire Emitter. The data collected with the stretchedwire emitter device are plotted in Figures 52 and 53 for field voltage and power, respectively. As with the 1-in-diameter test cylinder (Figure 19), flow separation occurred at about 90^o from the bottom of the 2-in-diameter test cylinder (Figure 54).

The plots of the stretched wire data for all three test cylinders in Figures 55, 56, and 57 showed the 2-in cylinder to have higher h/h_o ratios than the 1/4-in cylinder. The h/h_o plot for the 2-in cylinder was approximately equal the h/h_o plot for the 1-in cylinder at d_e's of 3/4 in and 1/2 in, and lower than the 1-in cylinder h/h_o plot at 1/4-in d_e.

Multipoint Emitter. Figures 58 and 59 contain plots of the data collected with the multipoint emitter. As with the stretched wire emitter, Figures 60, 61, and 62 showed the 2-in cylinder to also have higher multipoint h/h_o ratios than the 1/4-in cylinder. At 3/4-in d_e the 2-in and 1-in cylinder h/h_o data plotted as approximately one curve. The data for the 2-in cylinder plotted lower than the data for the 1-in cylinder at d_e's of 1/2 and 1/4 in.

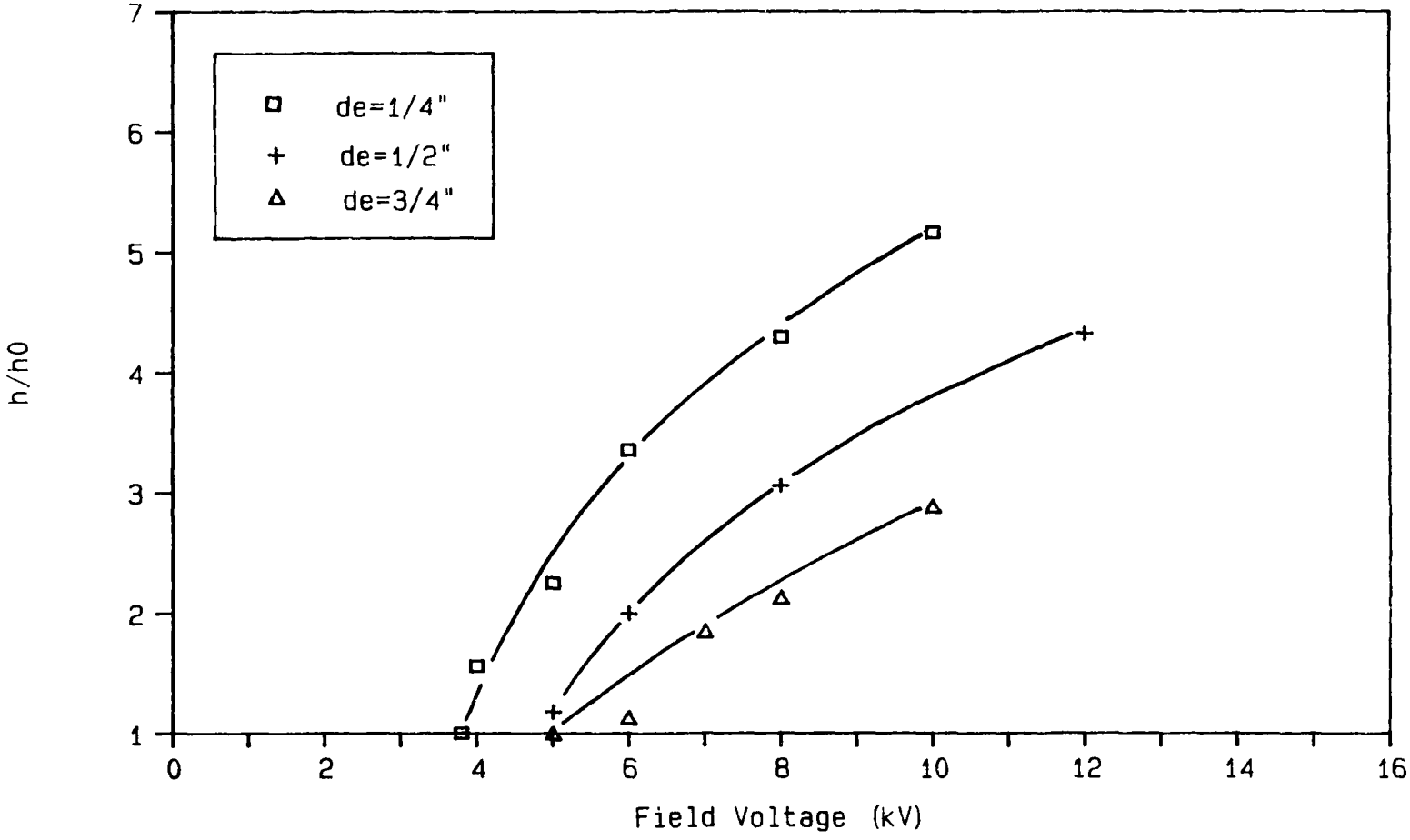

Figure 52. Effect of Corona Wind on the Ratio h/h0 for the 2-in Diameter Test Cylinder at Various Source to Receiver Distances with a Stretched Wire Emitter

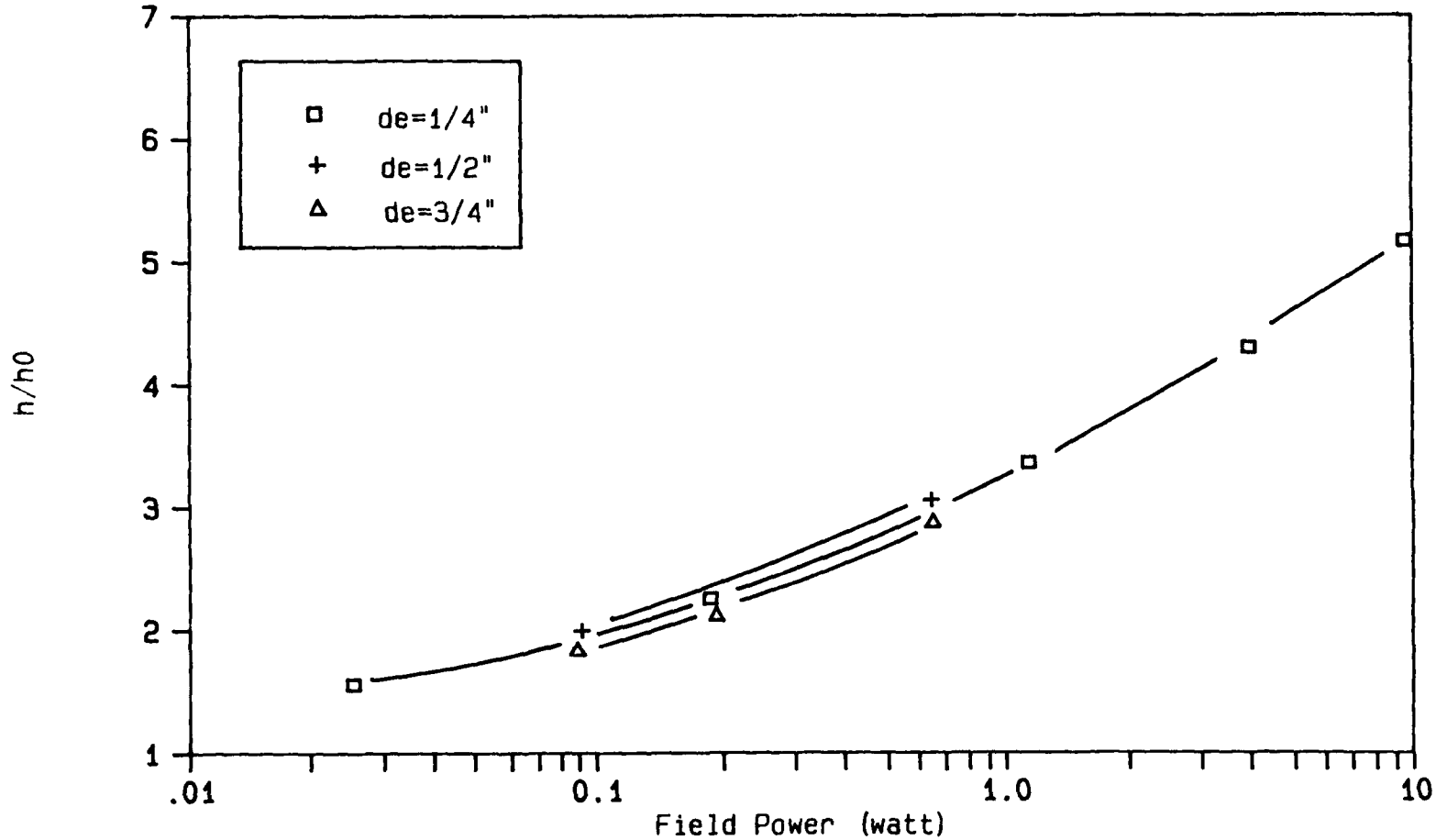

Figure 53. Effect of Corona Wind on the Ratio h/h0 for the 1/4-in Diameter Test Cylinder at Various Source to Receiver Distances with a Stretched Wire Emitter

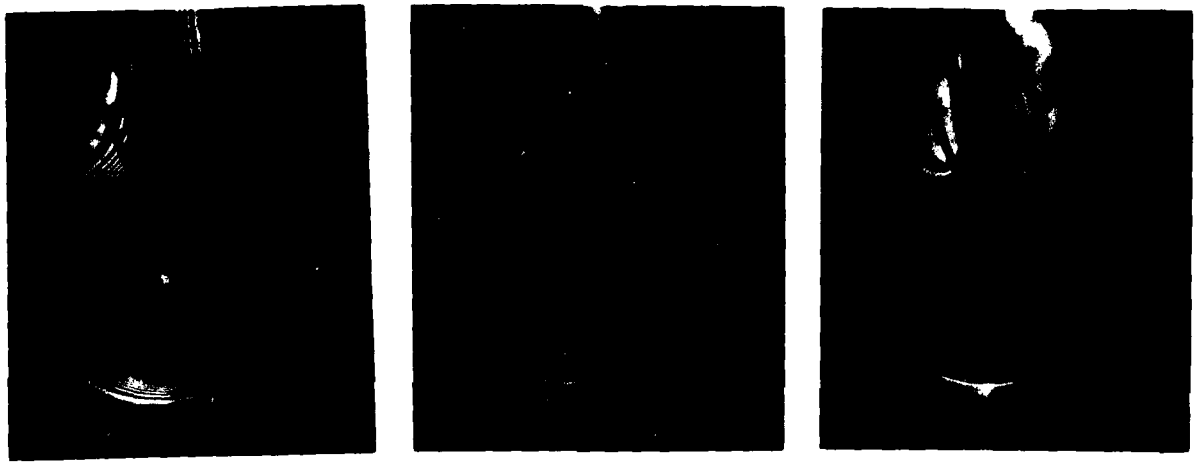

Field Voltage

0 kV 6 kV 10 kV

Figure 54. Interferometer Photograph Showing the Effect of the Corona Wind on the Thermal Boundary Layer of the Two-Inch-Diameter Test Cylinder with the Stretched Wire Emitter at 1/2-Inch Source to Receiver Distance

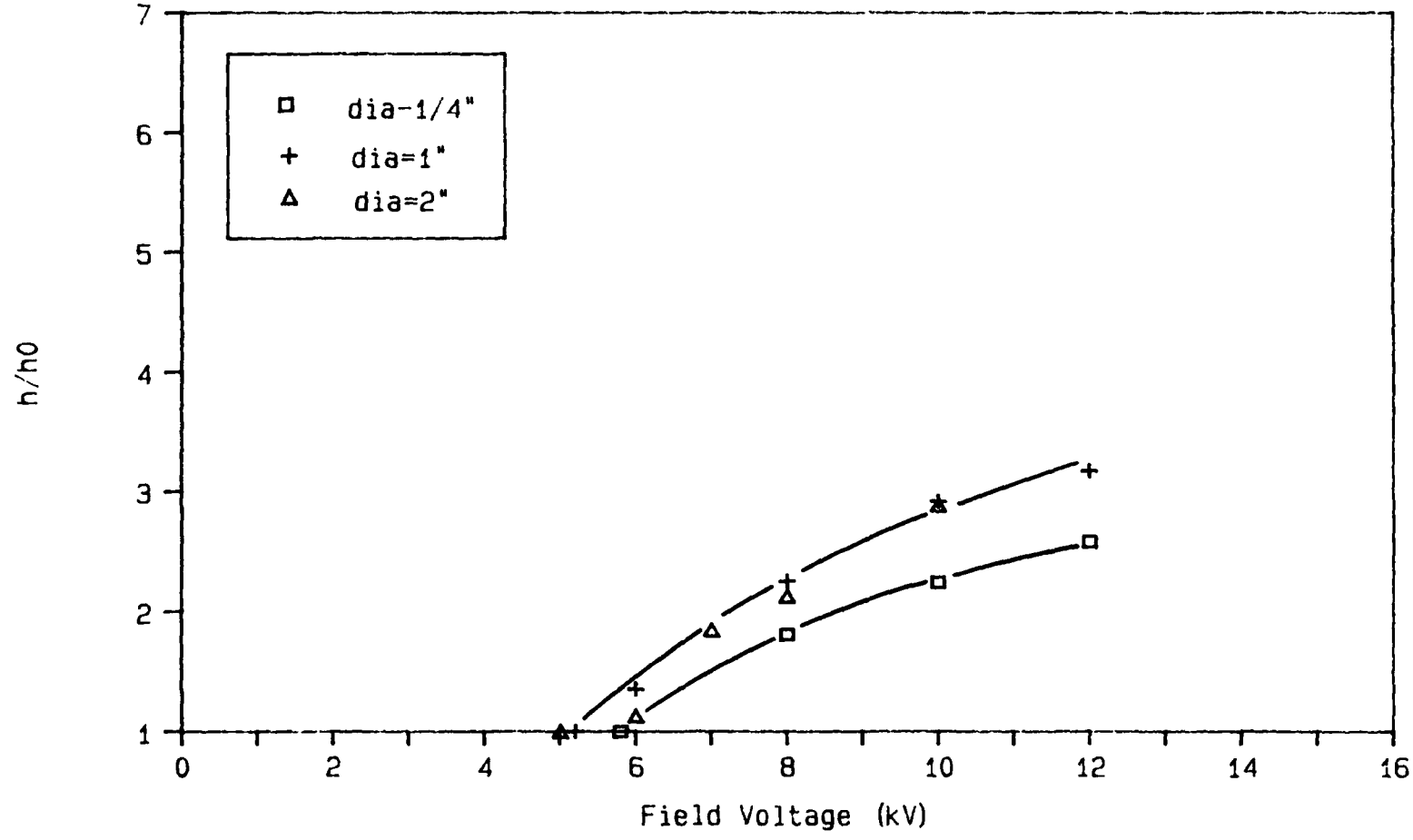

Figure 55. A Comparison of the Stretched Wire Ratios of h/ho for the 1/4-in, 1-in and 2-in Diameter Test Cylinders at 3/4-in Source to Receiver Distance

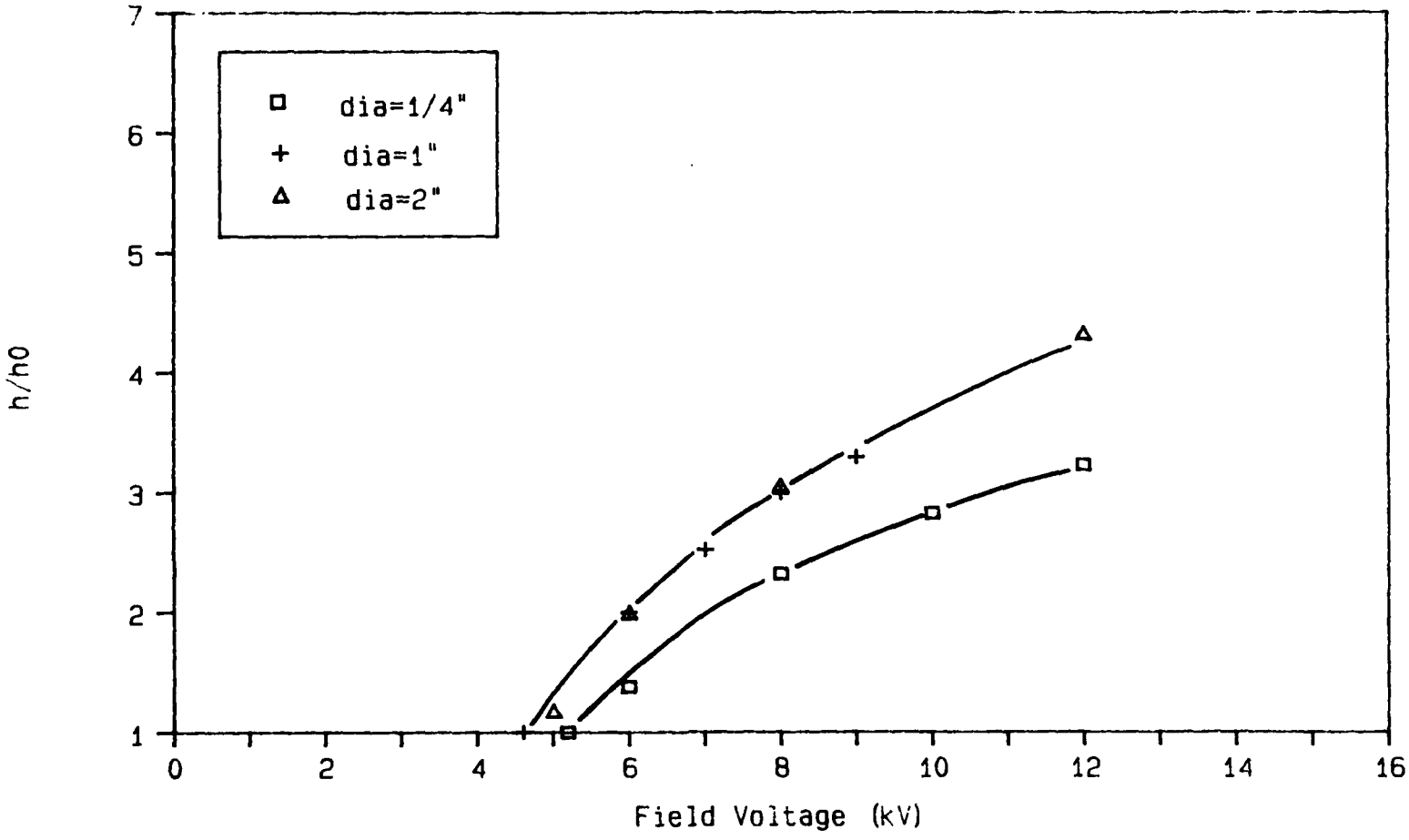

Figure 56. A Comparison of the Stretched Wire Ratios of h/ho for the 1/4-in, 1-in and 2-in Diameter Test Cylinders at 1/2-in Source to Receiver Distance

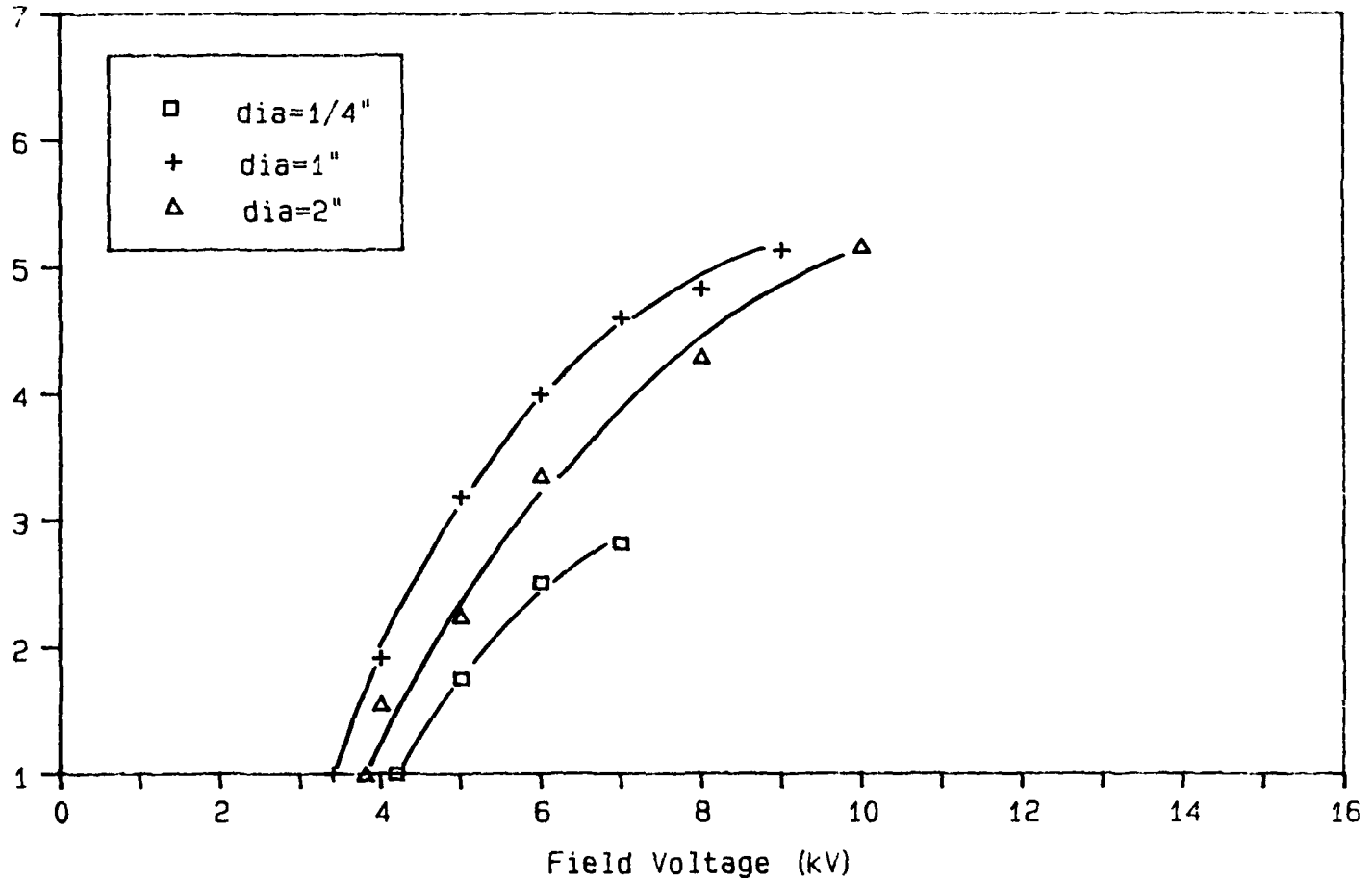

Figure 57. A Comparison of the Stretched Wire Ratios of h/ho for the 1/4-in, 1-in and 2-in Diameter Test Cylinders at 1/4-in Source to Receiver Distance

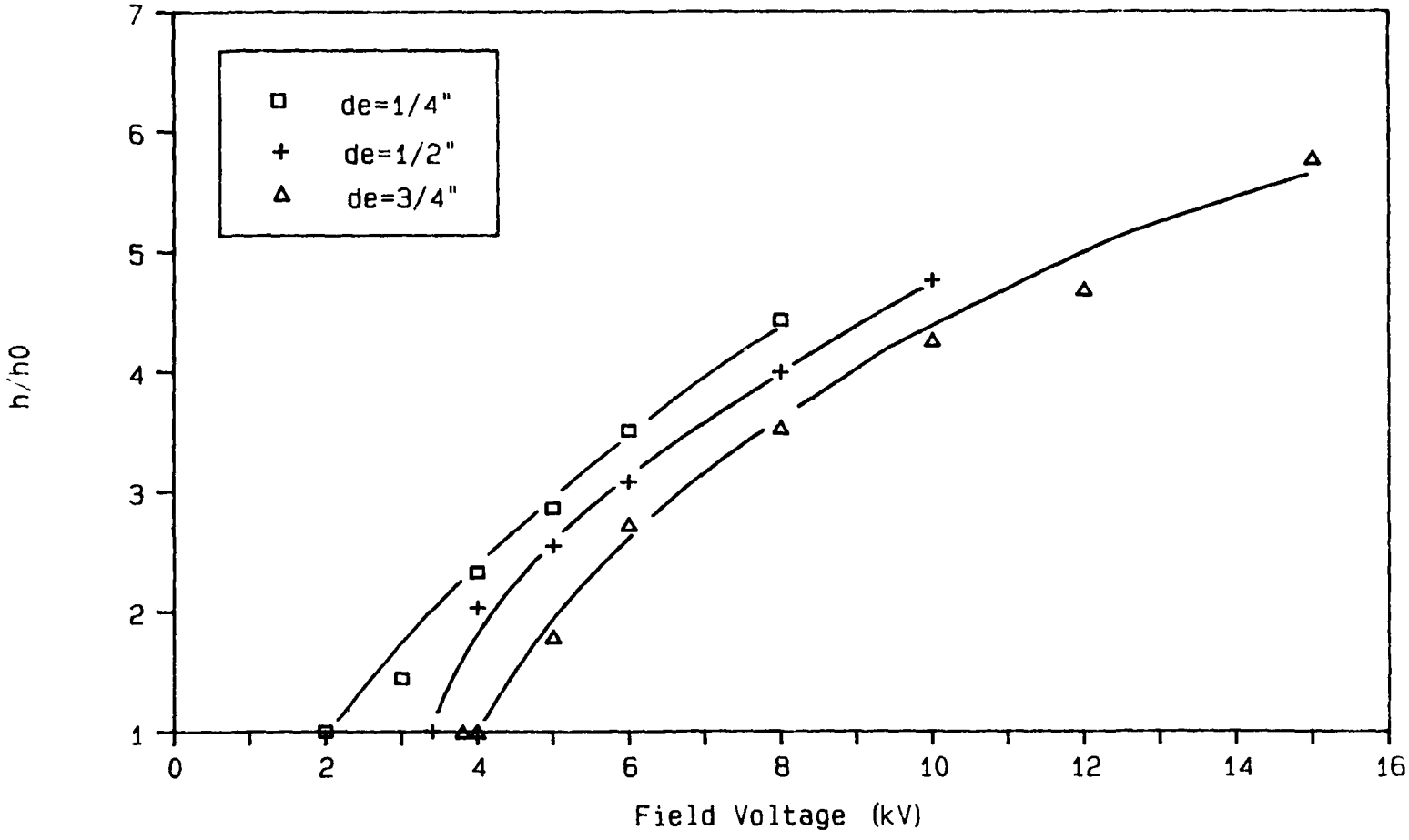

Figure 58. Effect of Corona Wind on the Ratio h/h0 for the 2-in Diameter Test Cylinder at Various Source to Receiver Distances with a Multipoint Emitter

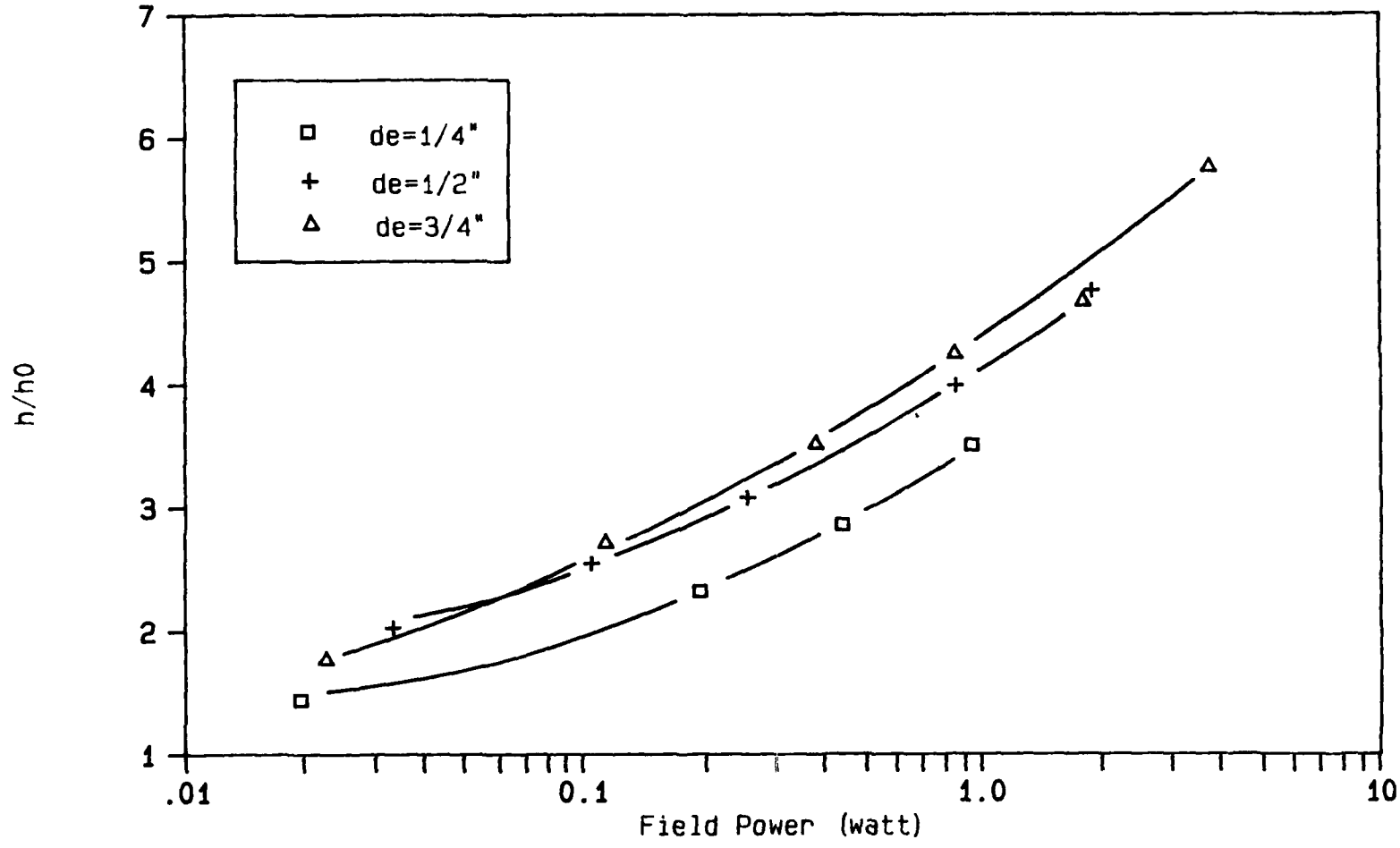

Figure 59. Effect of Field Power on the Ratio h/h0 for the 2-in Diameter Test Cylinder at Various Source to Receiver Distances with a Multipoint Emitter

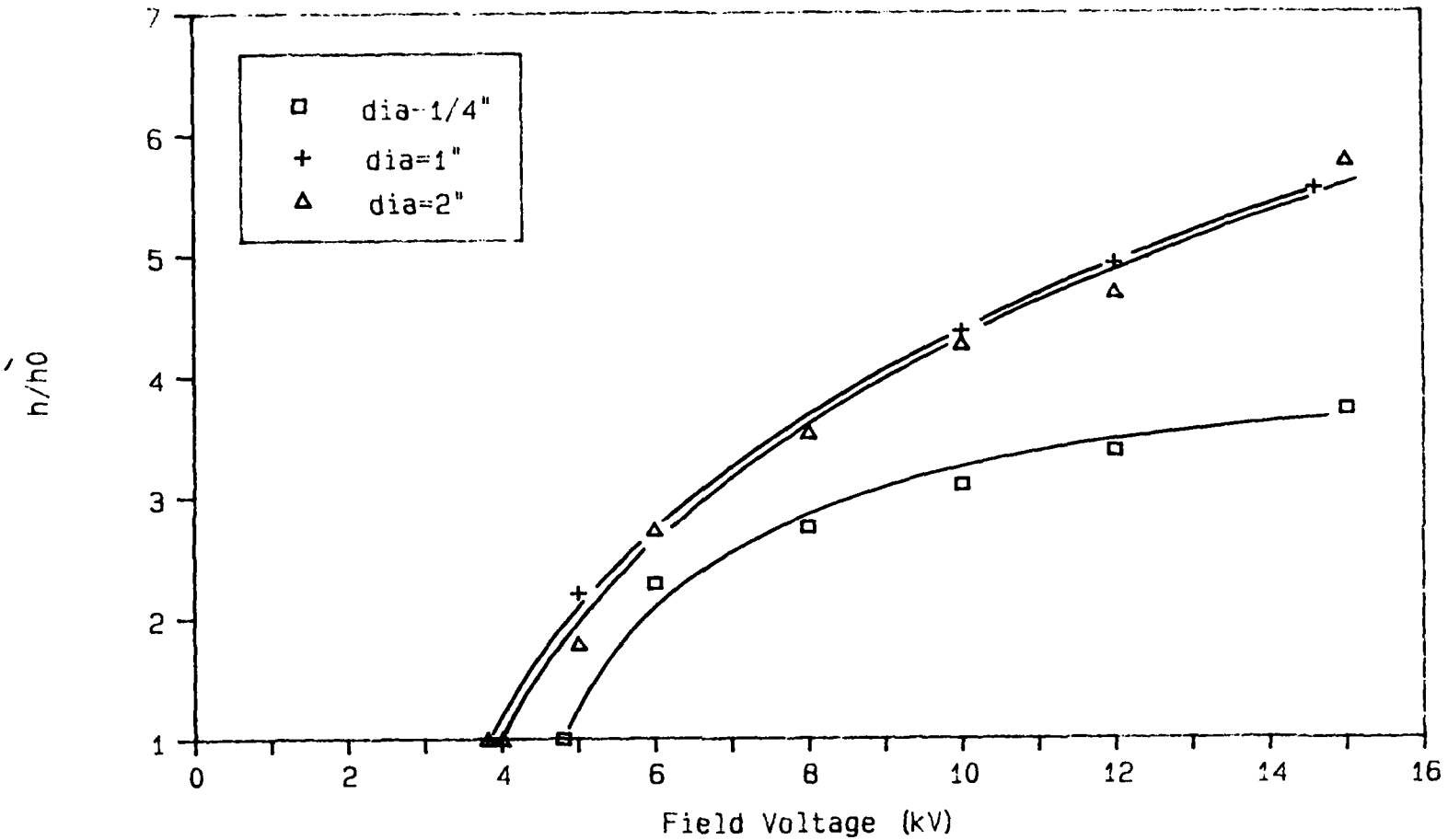

Figure 60. A Comparison of the Multipoint Ratios of h/ho for the 1/4-in, 1-in and 2-in Diameter Test Cylinders at 3/4-in Source to Receiver Distance

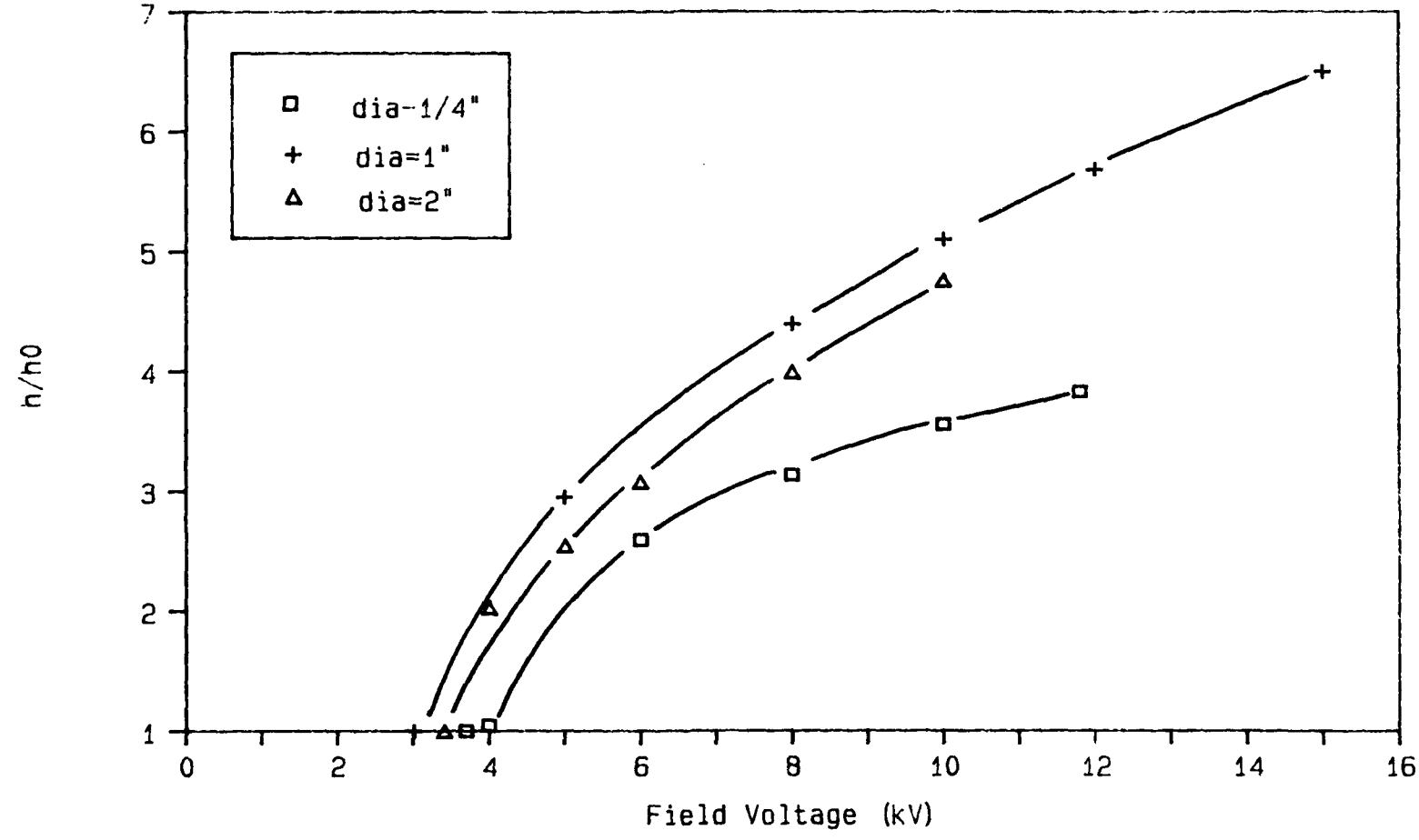

Figure 61. A Comparison of the Multipoint Ratios of h/ho for the 1/4-in, 1-in and 2-in Diameter Test Cylinders at 1/2-in Source to Receiver Distance

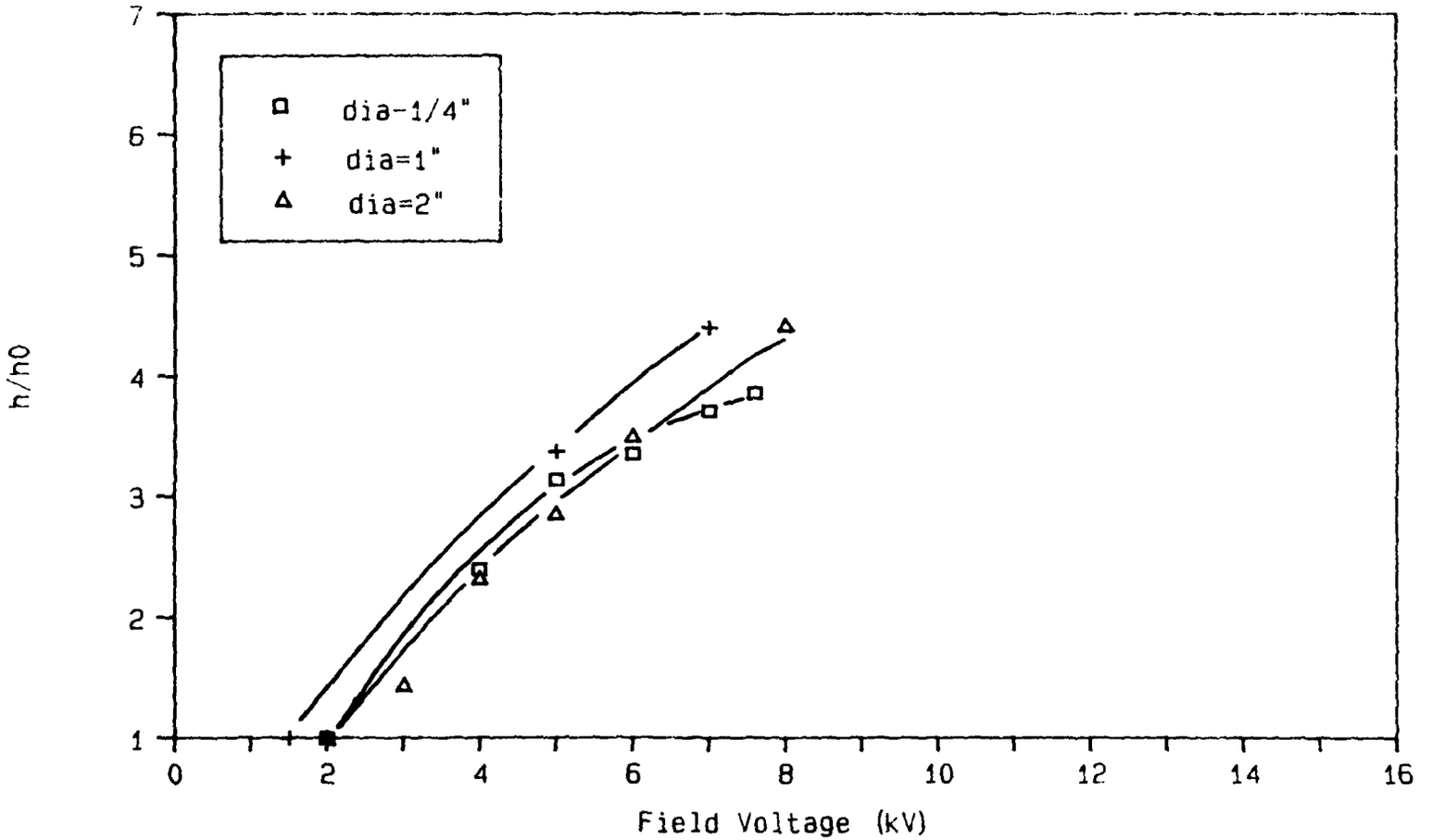

Figure 62. A Comparison of the Multipoint Ratios of h/ho for the 1/4-in, 1-in and 2-in Diameter Test Cylinders at 1/4-in Source to Receiver Distance

Multipoint and stretched wire h/h_o data collected with the 2-in cylinder were compared in Figures 63, 64, and 65 for field voltage and Figures 66, 67, and 68 for field power. These plots exhibit the same trends as the plots for the 1-in cylinder. The multipoint emitter produced higher h/h_o ratios and used power more efficiently than the stretched wire emitter at d_e settings of 3/4 in and 1/2 in, and the two curves converged rapidly into a single curve at 1/4-in d_e.

Blown Air Plenum. The blown air data in Figure 69 are plotted with the blown air data for the 1-in and 1/4-in cylinders in Figures 70, 71, and 72. The interferometer photograph (Figure 73) shows the same immediate flow separation that occurred with the 1-in-diameter test cylinder (Figure 35).

Comparison plots of the blown air and stretched wire test results for the 2-in cylinder are in Figures 74, 75, and 76. Again the h/h_o ratios for the 2-in cylinder were largest for blown air at low velocities and then larger for corona wind at higher velocities. The trend of higher crossover velocities for smaller d_e spacing was also repeated.

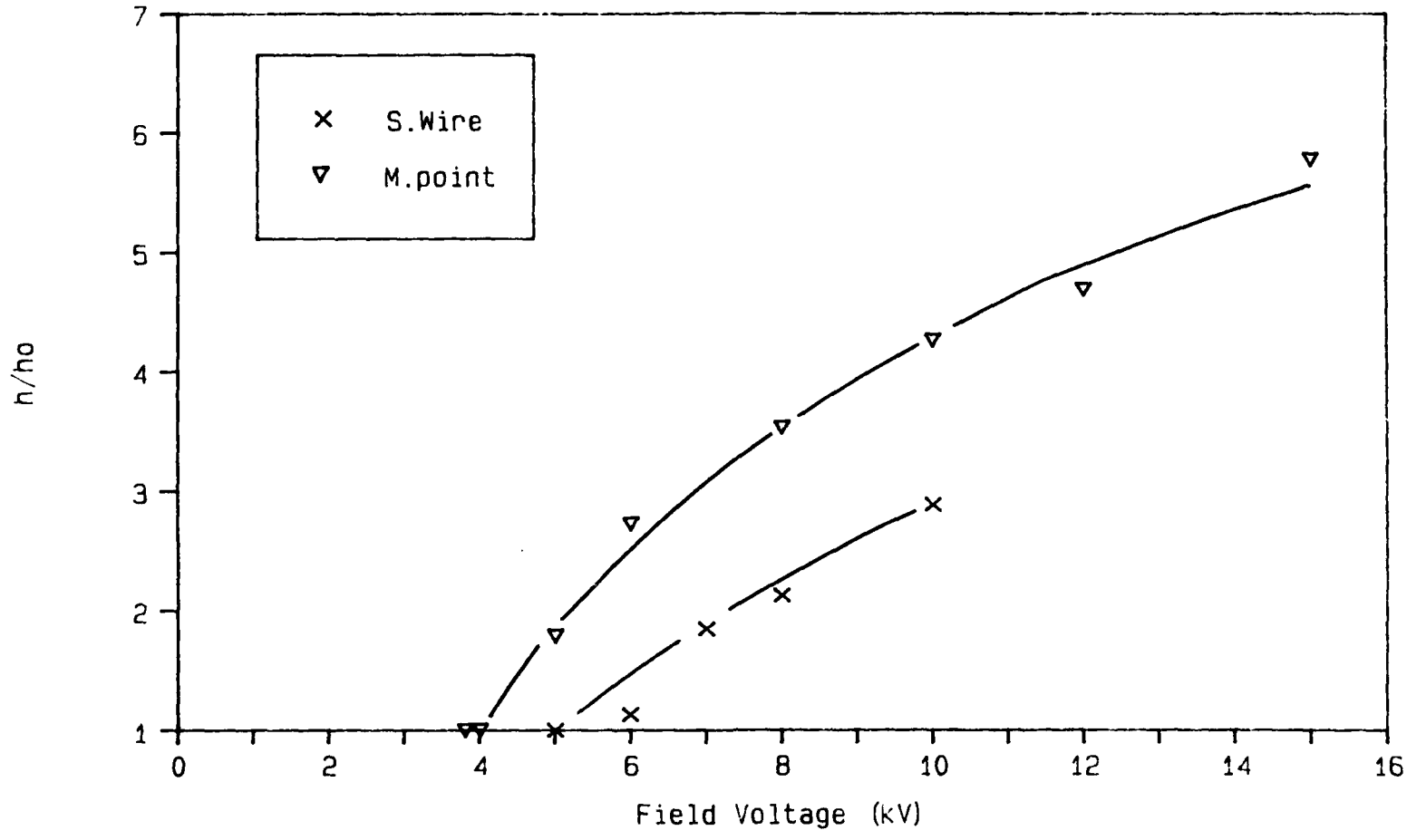

Figure 63. A Comparison of the Stretched Wire and Multipoint Emitter Ratios of h/h0 for the 2-in Diameter Cylinder at 3/4-in Source to Receiver Distance

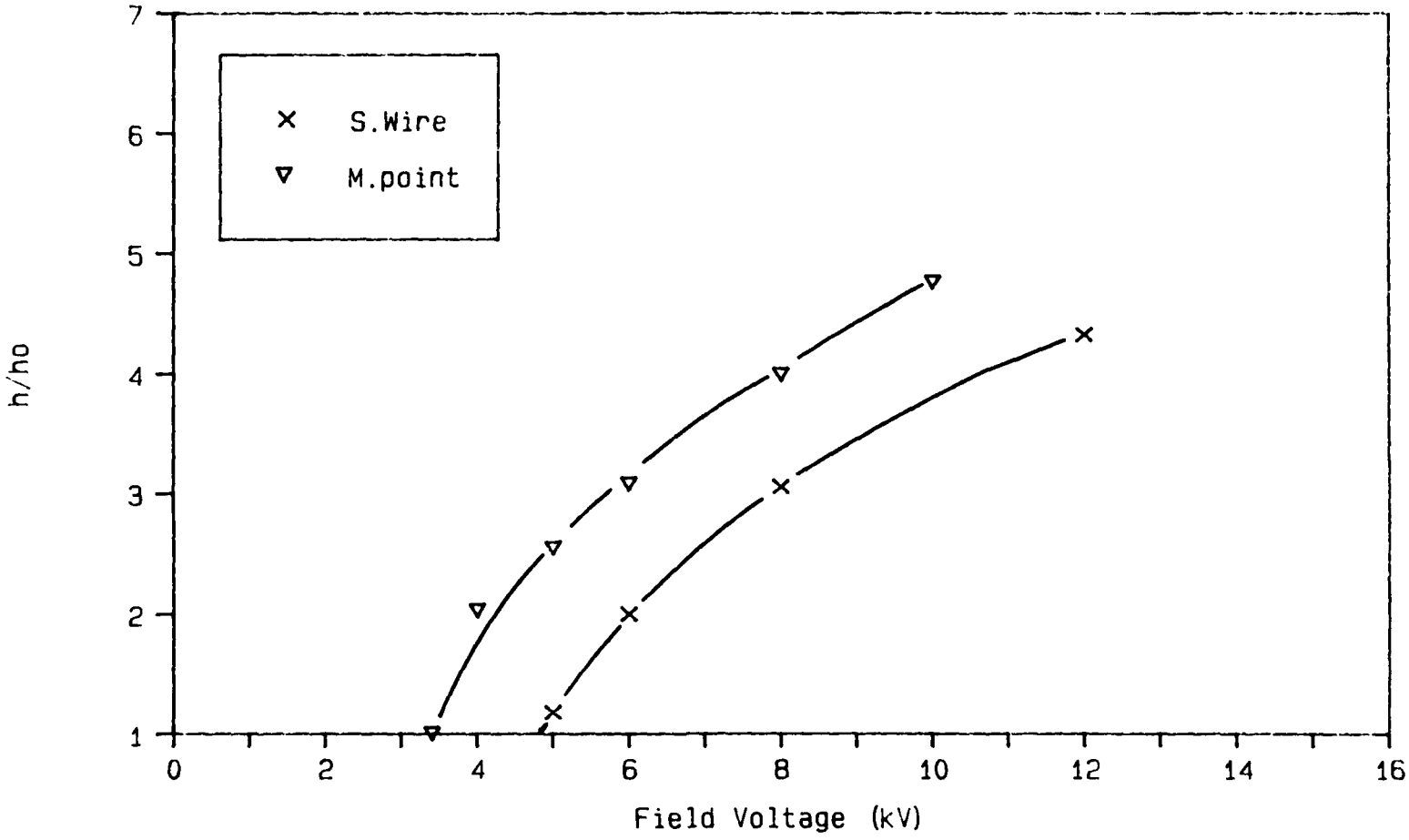

Figure 64. A Comparison of the Stretched Wire and Multipoint Emitter Ratios of h/h0 for the 2-in Diameter Cylinder at 1/2-in Source to Receiver Distance

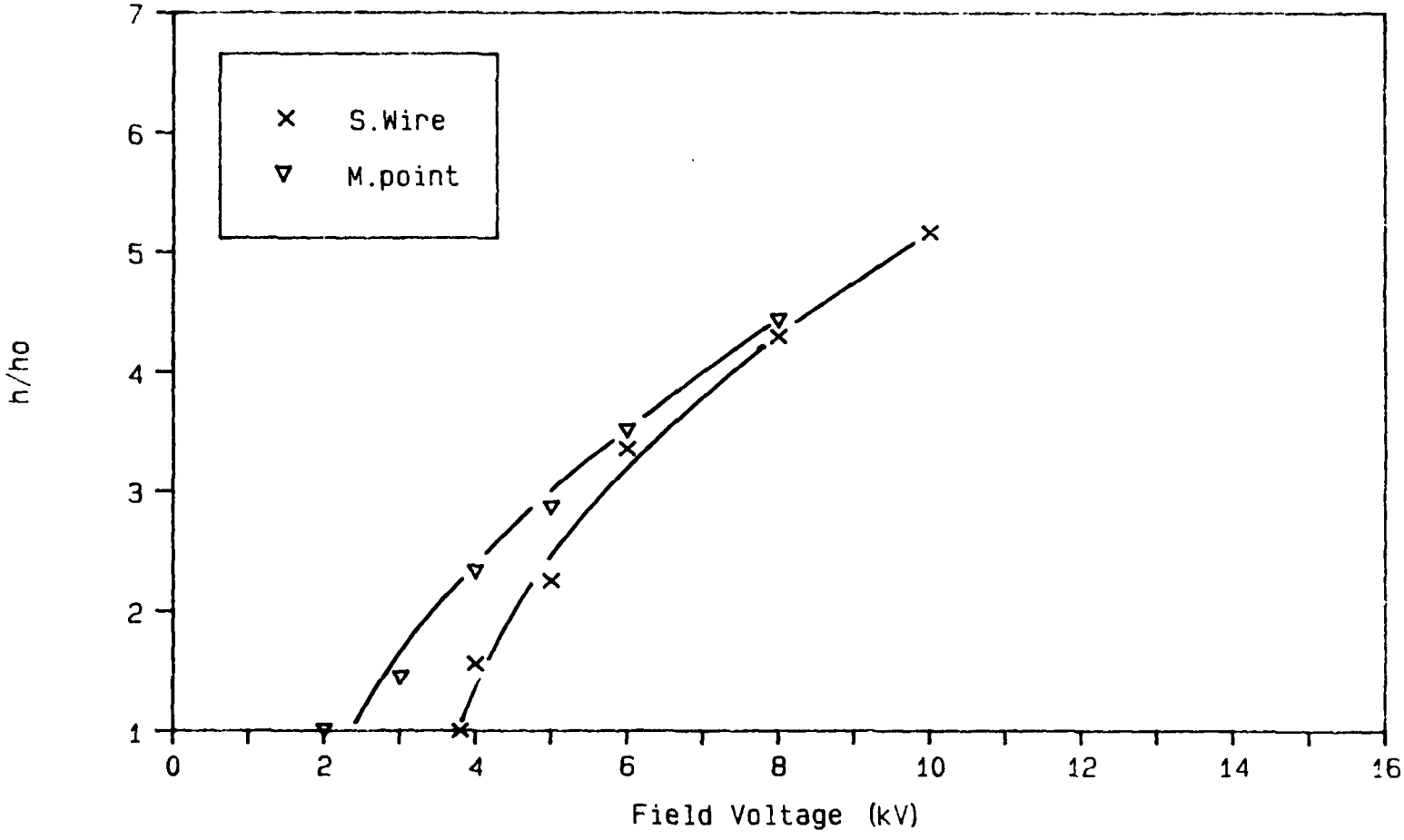

Figure 65. A Comparison of the Stretched Wire and Multipoint Emitter Ratios of h/h0 for the 2-in Diameter Cylinder at 1/4-in Source to Receiver Distance

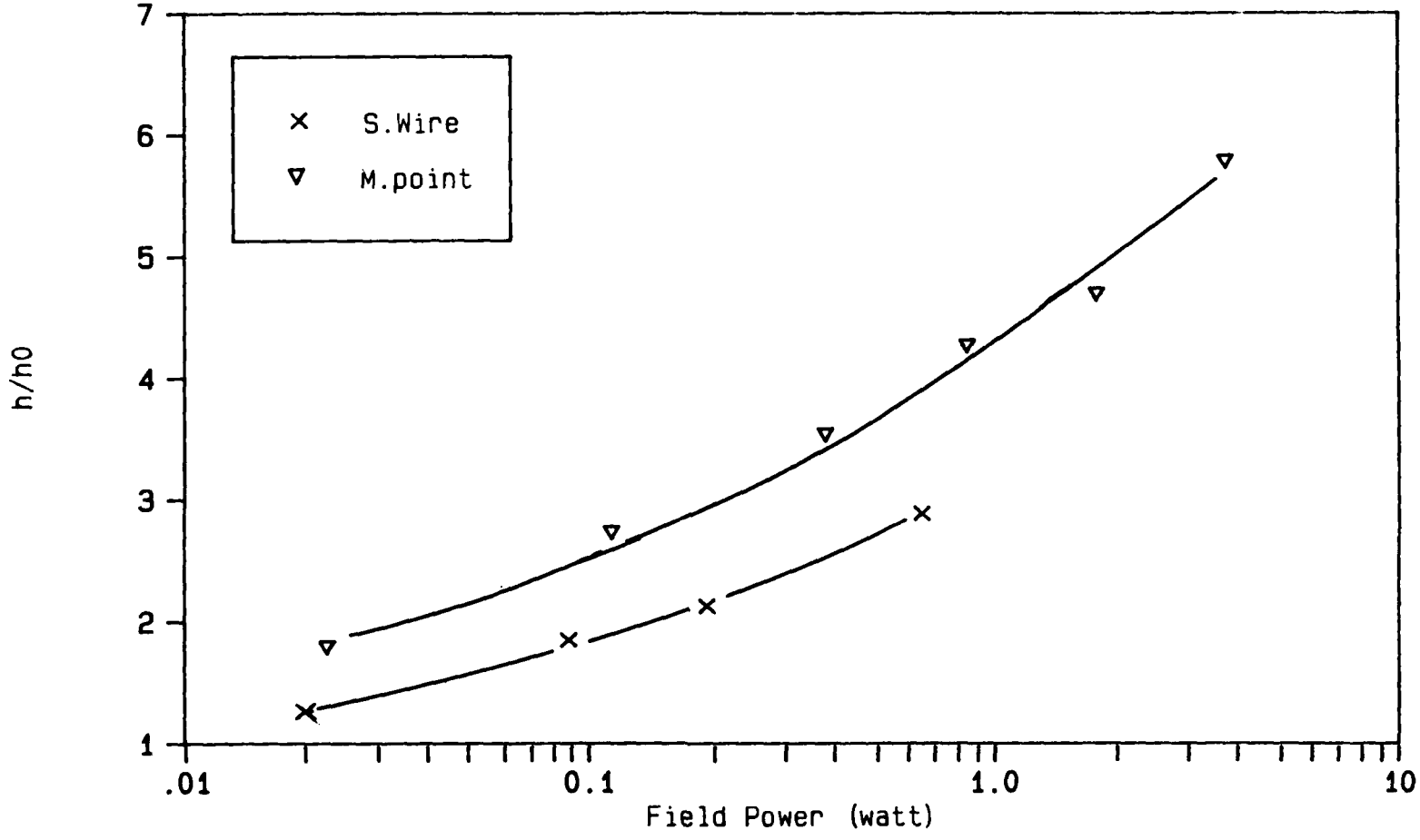

Figure 66. A Comparison of the Effect of Field Power on h/h0 for the 2-in Diameter Cylinder at 3/4-in Source to Receiver Distance with Stretched Wire and Multipoint Emitters

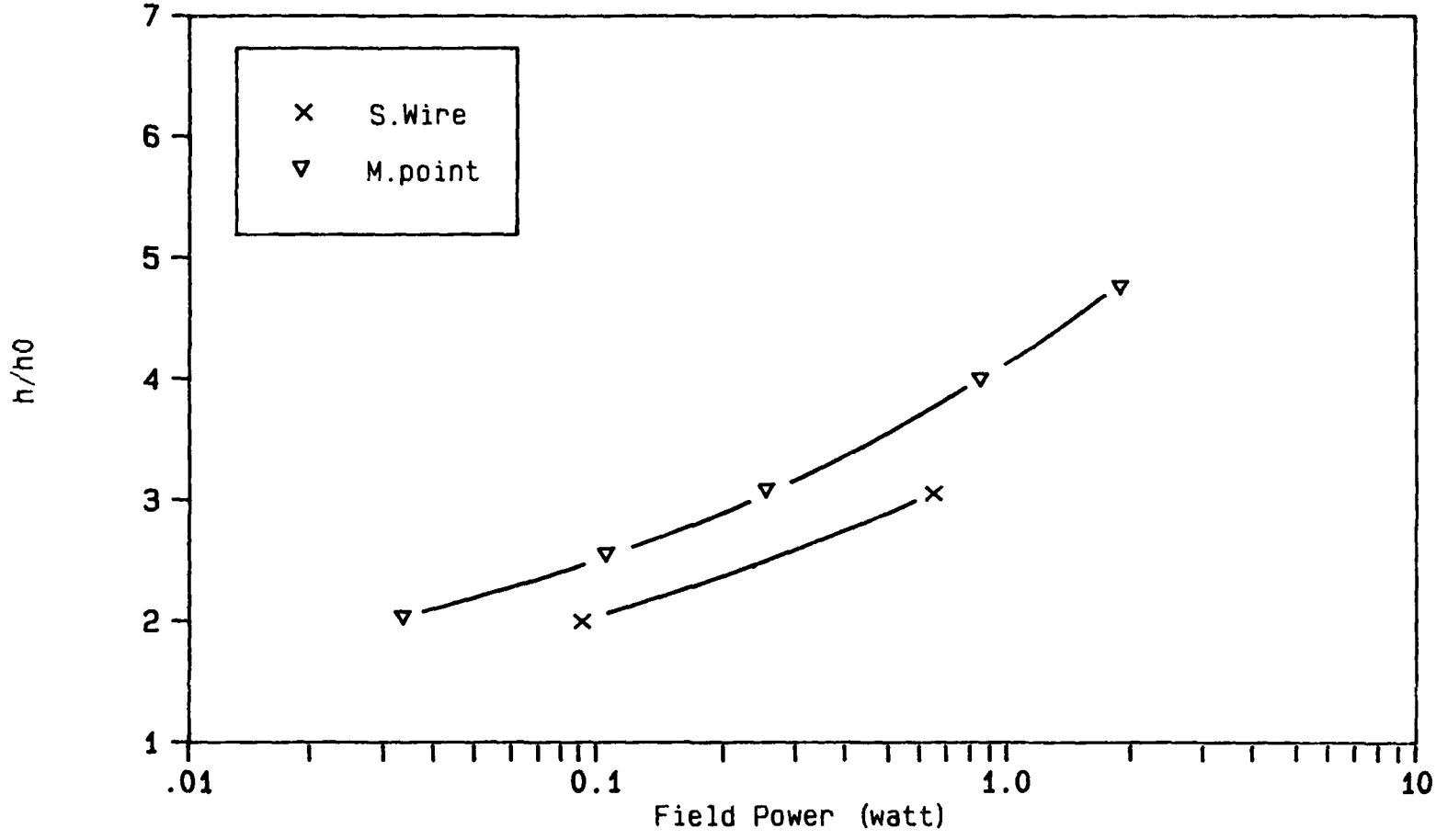

Figure 67. A Comparison of the Effect of Field Power on h/h0 for the 2-in Diameter Cylinder at 1/2-in Source to Receiver Distance with Stretched Wire and Multipoint Emitters

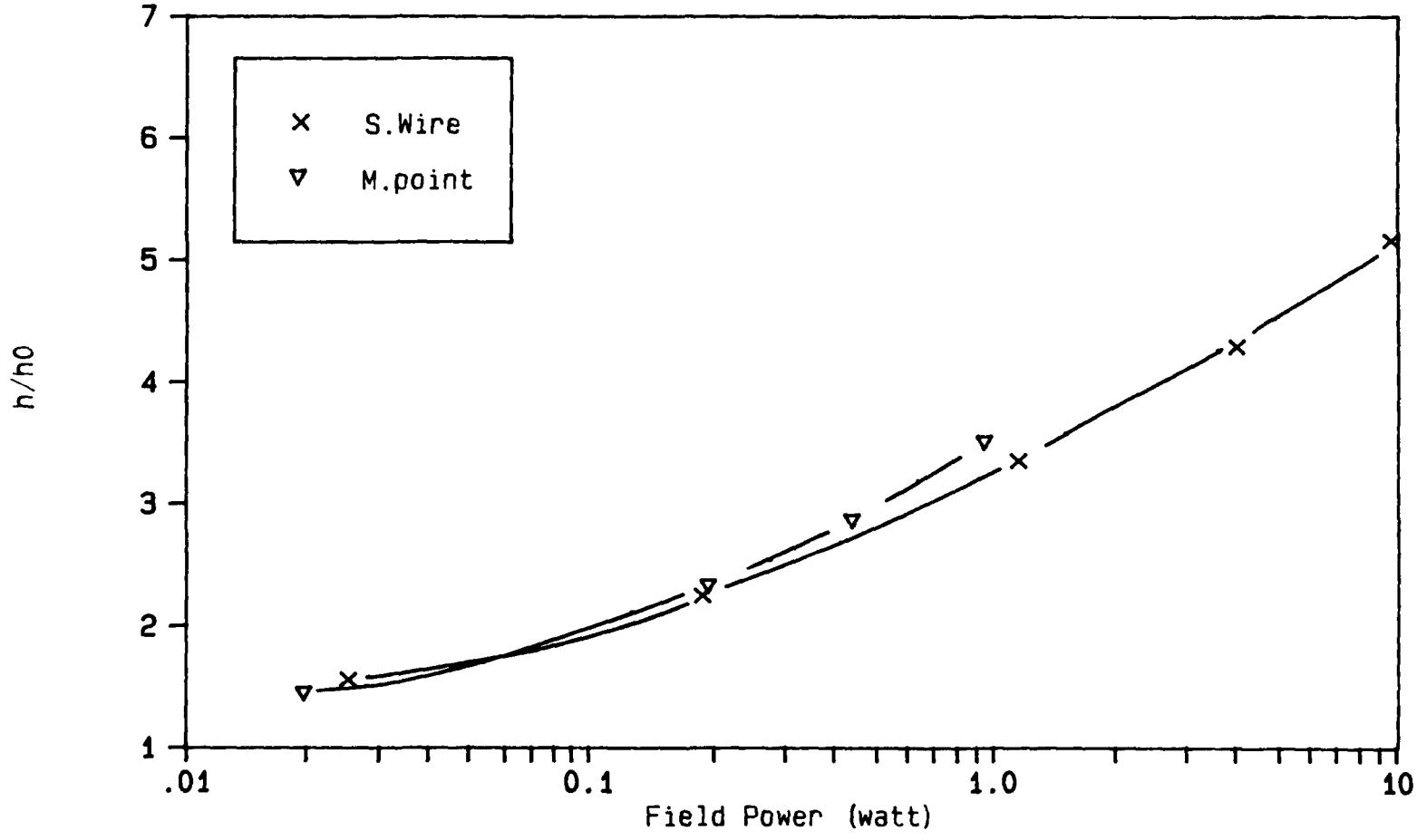

Figure 68. A Comparison of the Effect of Field Power on h/h0 for the 2-in Diameter Cylinder at 1/4-in Source to Receiver Distance with Stretched Wire and Multipoint Emitters

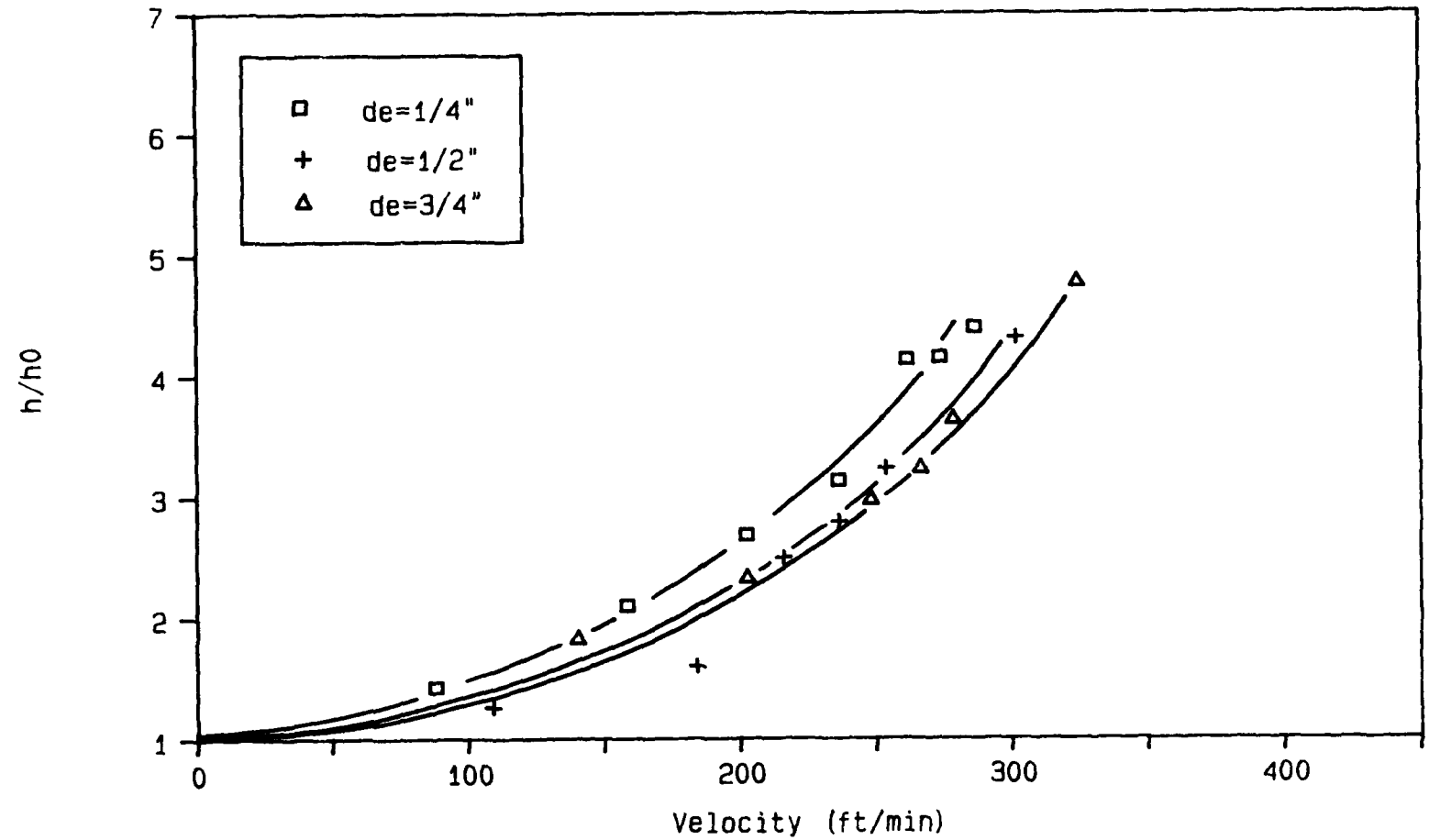

Figure 69. Effect of Blown Air on the Ratio h/h0 for the 2-in Diameter Test Cylinder at Various Source to Receiver Distances

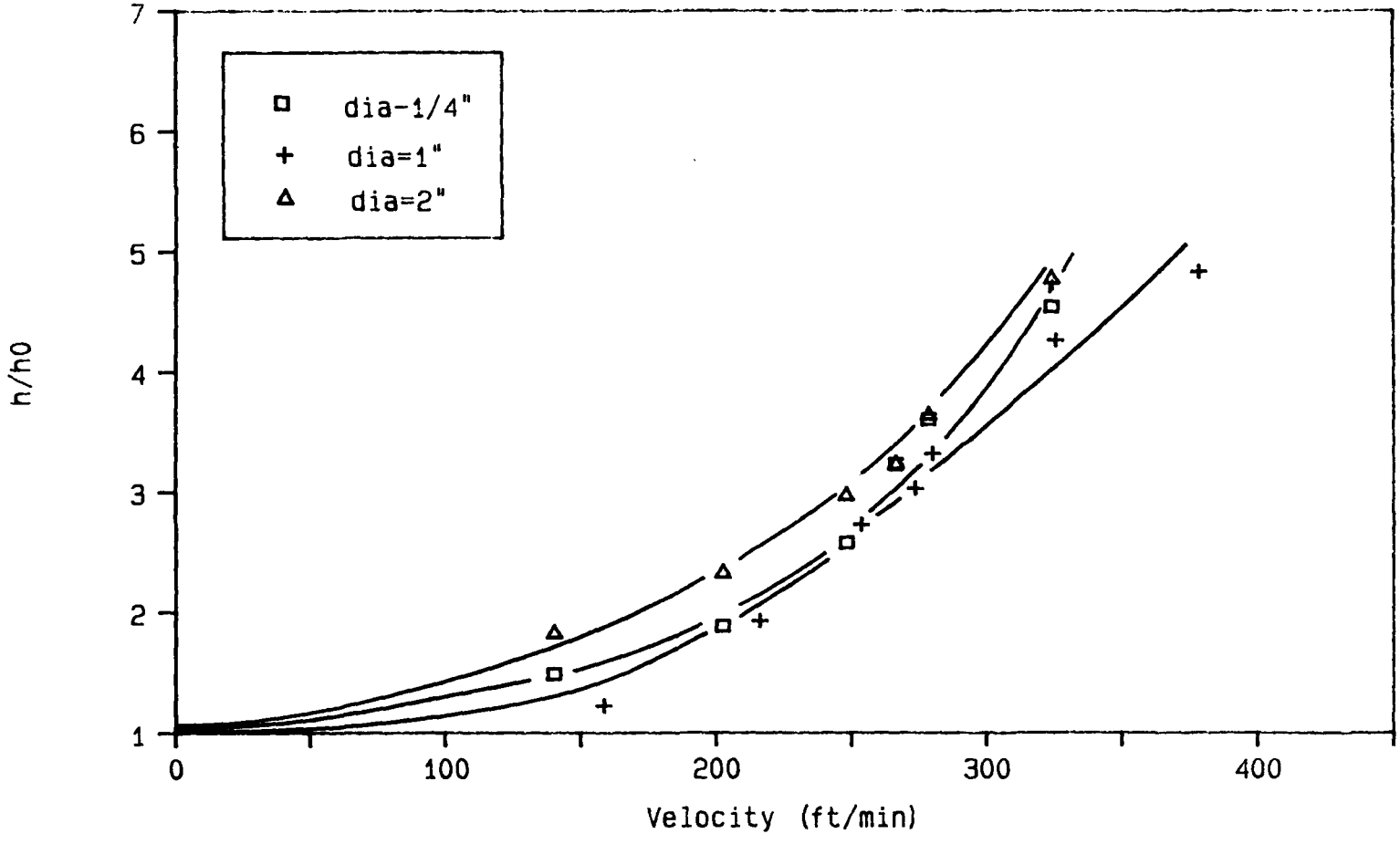

Figure 70. A Comparison of the Blown Air Ratios of h/ho for the 1/4-in, 1-in and 2-in Diameter Test Cylinders at 3/4-in Source to Receiver Distance

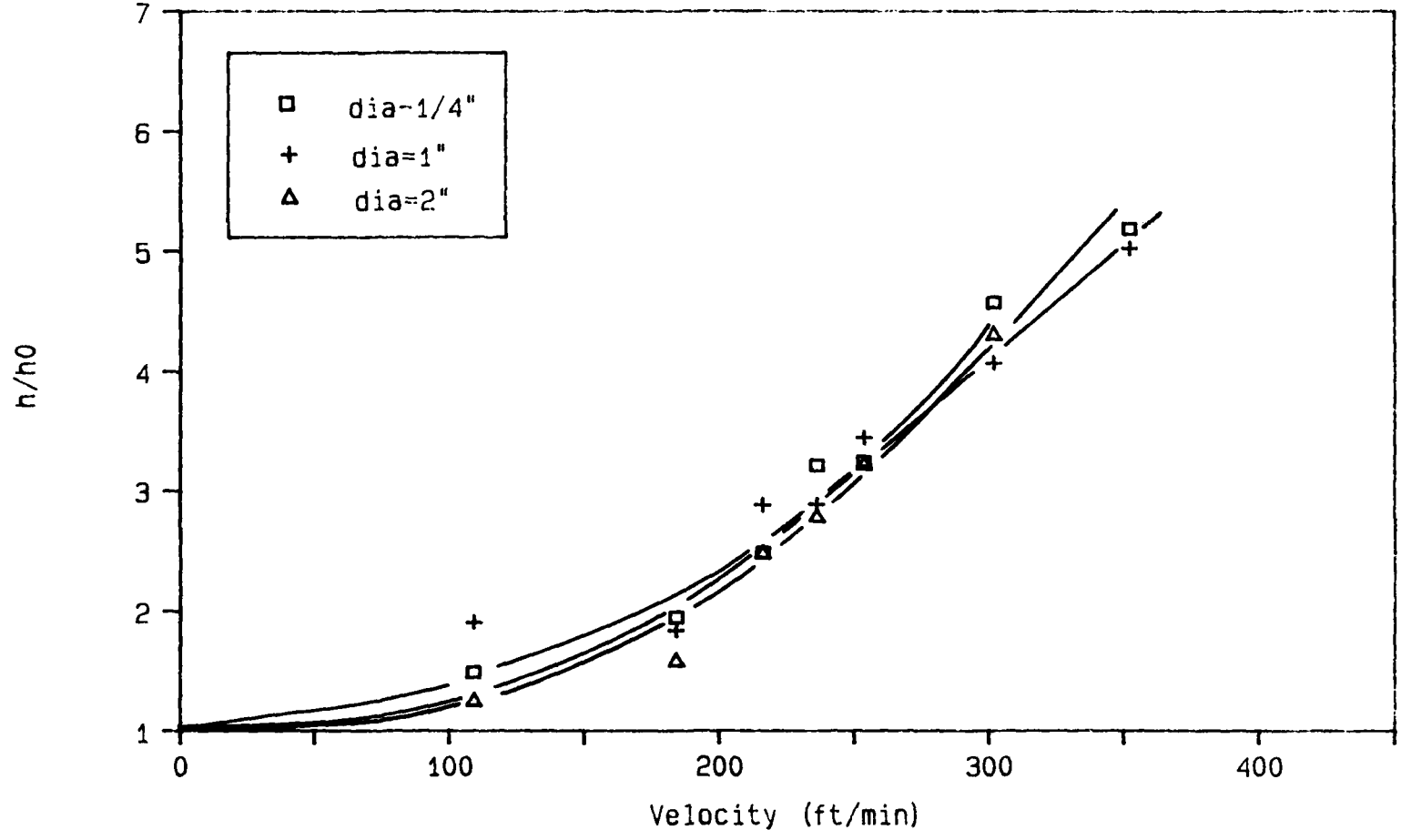

Figure 71. A Comparison of the Blown Air Ratios of h/ho for the 1/4-in, 1-in and 2-in Diameter Test Cylinders at 1/2-in Source to Receiver Distance

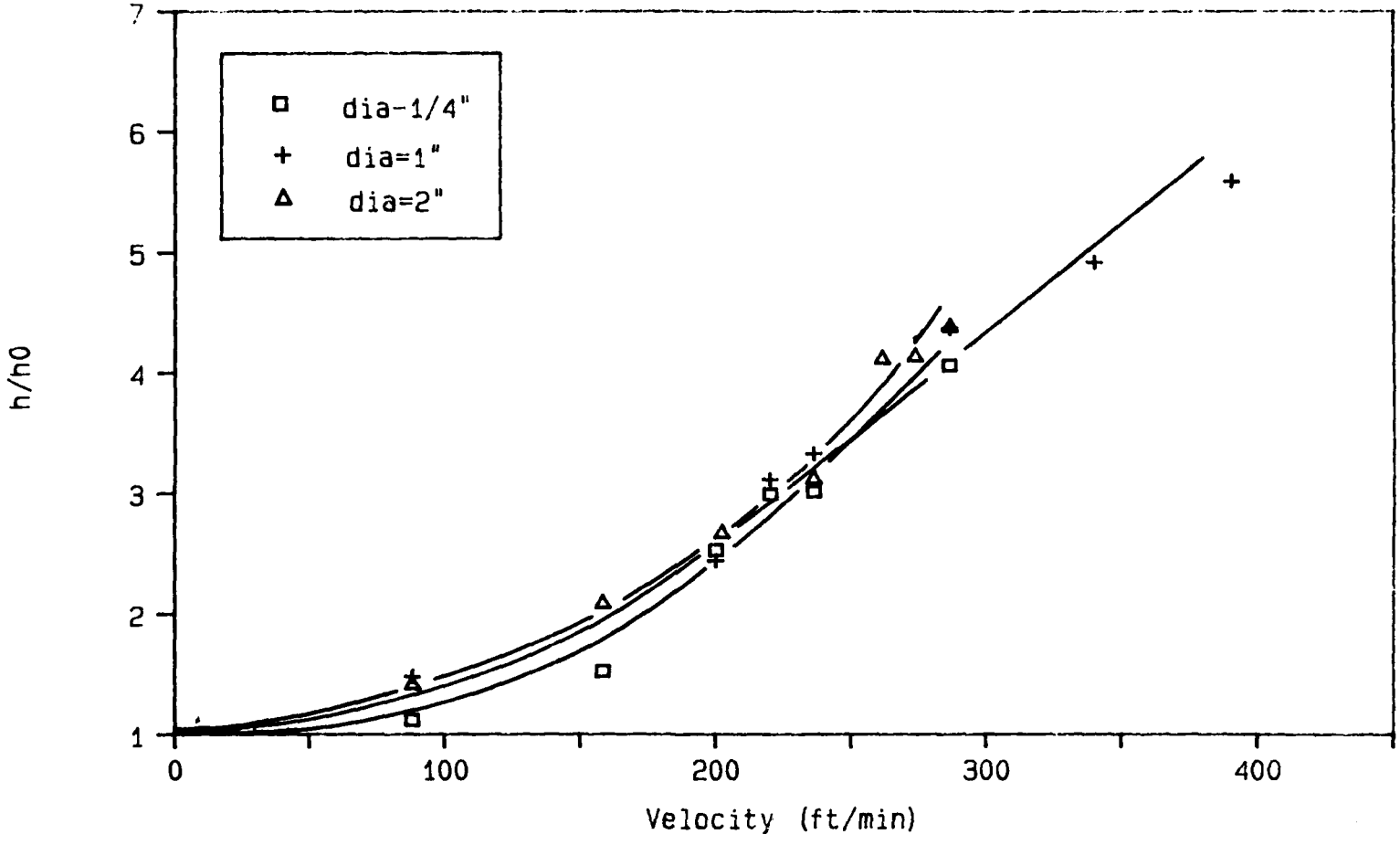

Figure 72. A Comparison of the Blown Air Ratios of h/ho for the 1/4-in, 1-in and 2-in Diameter Test Cylinders at 1/4-in Source to Receiver Distance

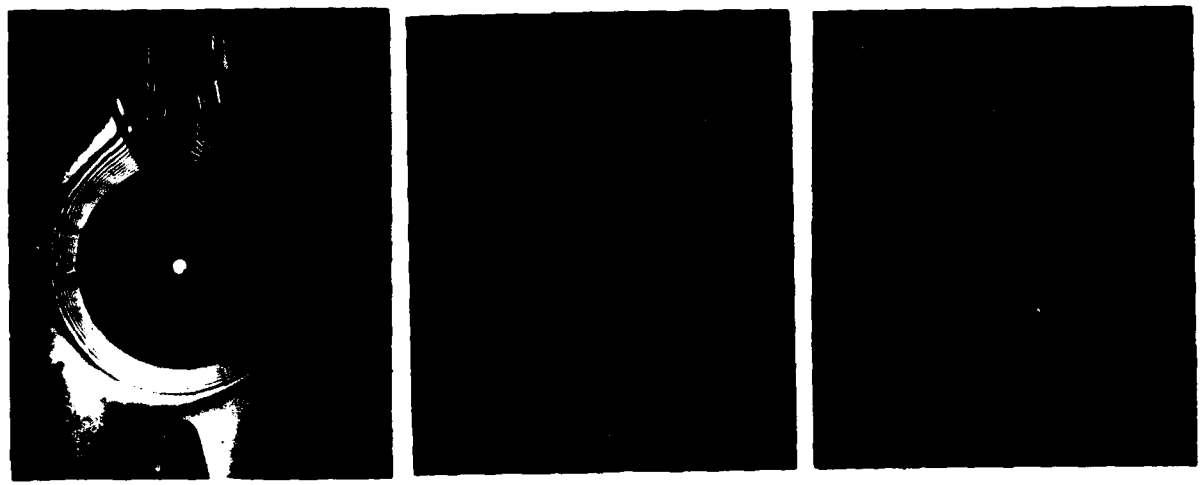

Velocity

0 ft/min | 184 ft/min | 302 ft/min

Figure 73. Interferometer Photographs Showing the Effect of a Jet of Uncharged Air on the Thermal Boundary Layer of the Two-Inch-Diameter Test Cylinder with the Plenum at 1/2-Inch Source to Receiver Distance

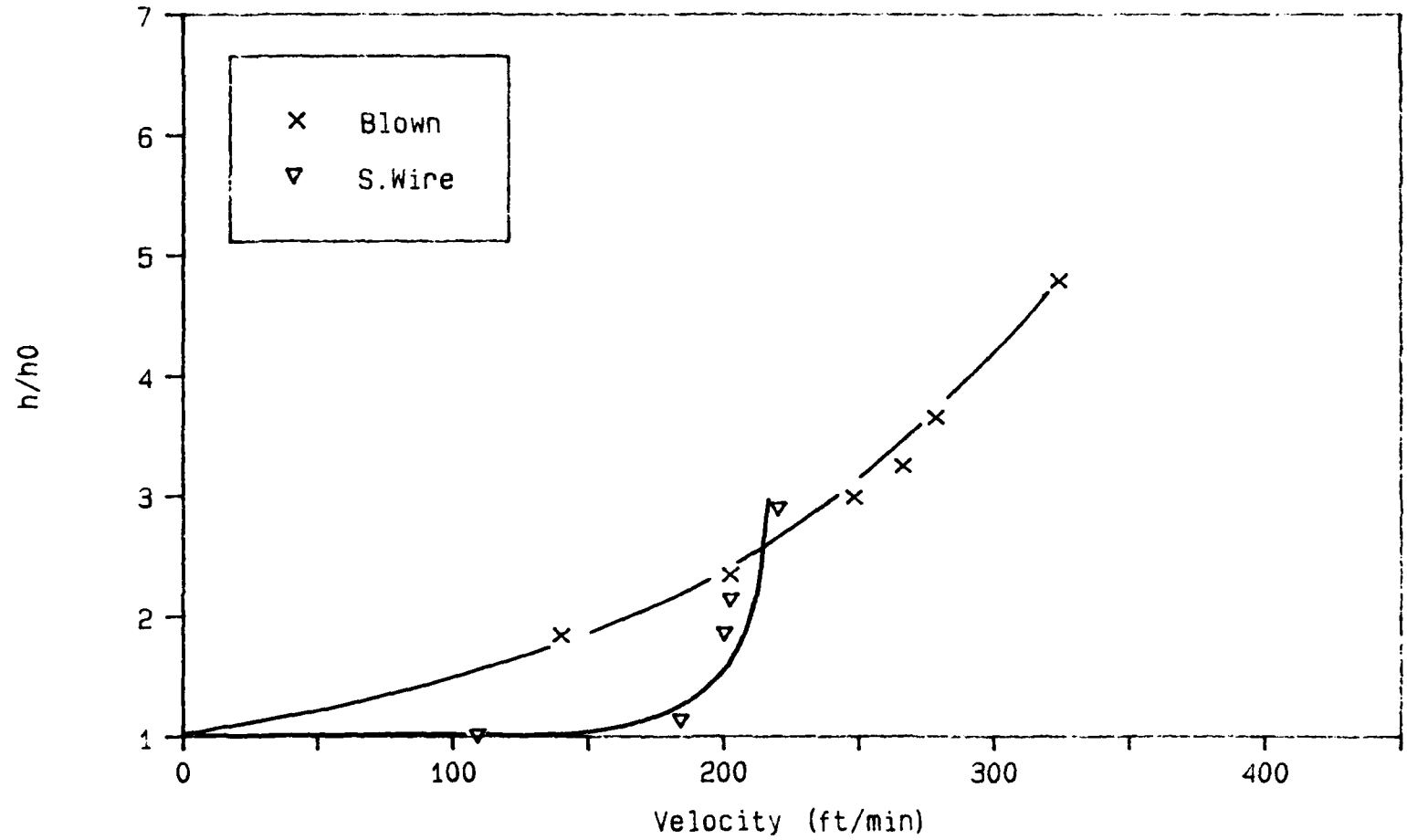

Figure 74. A Comparison of the Blown Air and Stretched Wire Ratios of h/h0 for the 2-in Diameter Cylinder at 3/4-in Source to Receiver Distance

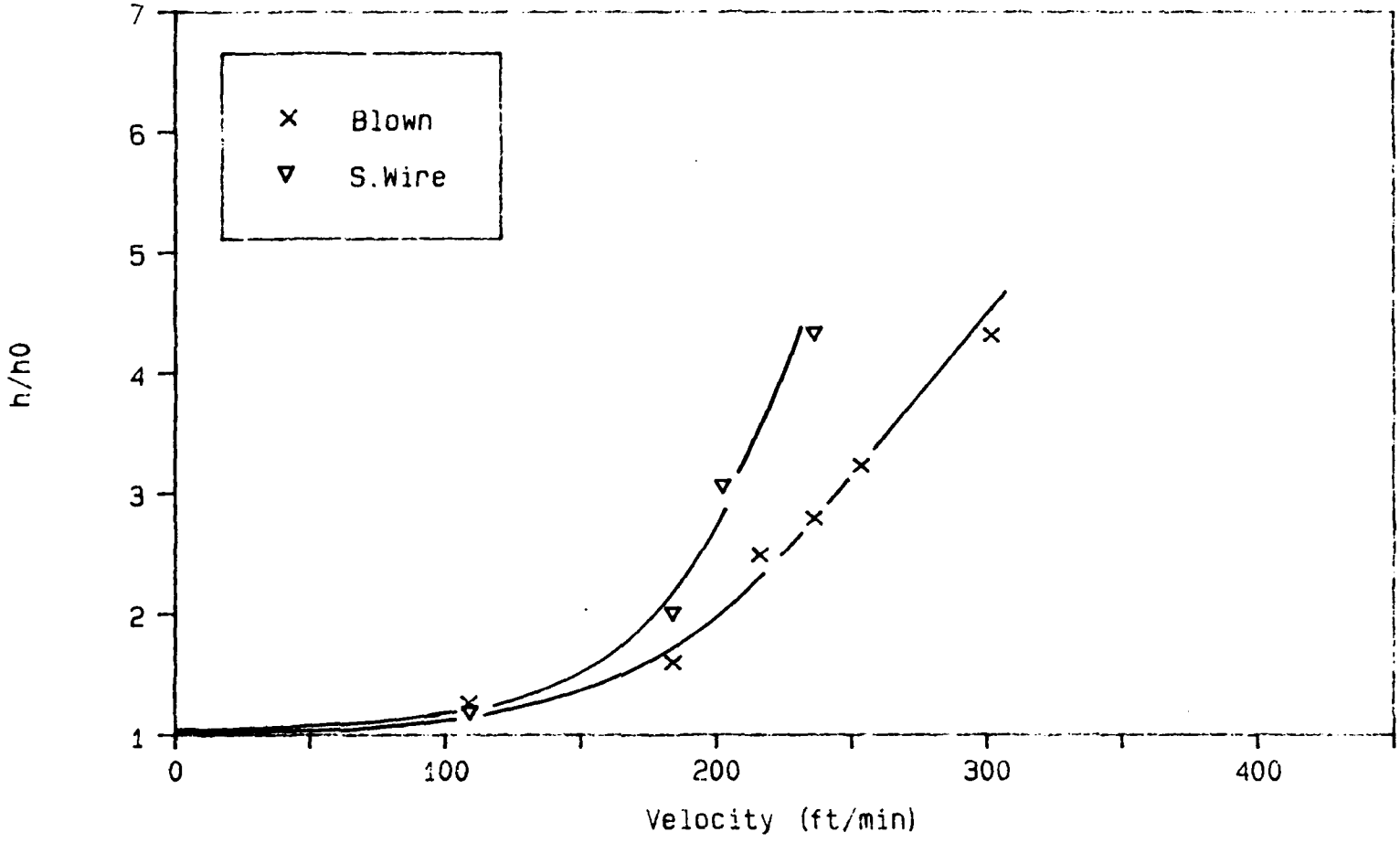

Figure 75. A Comparison of the Blown Air and Stretched Wire Ratios of h/h0 for the 2-in Diameter Cylinder at 1/2-in Source to Receiver Distance

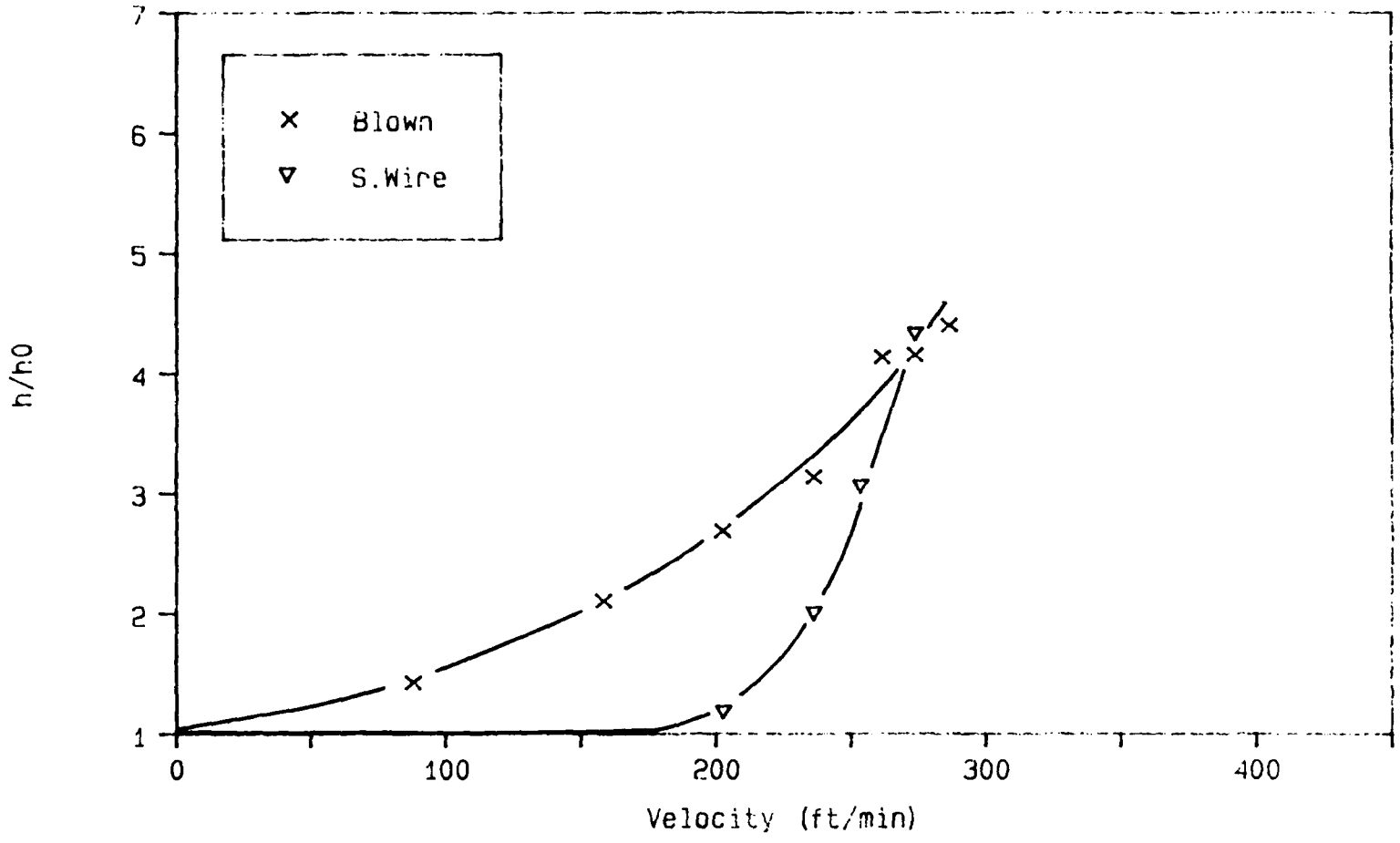

Figure 76. A Comparison of the Blown Air and Stretched Wire Ratios of h/h0 for the 2-in Diameter Cylinder at 1/4-in Source to Receiver Distance

VI. Conclusions

Based on the results of this study the following conclusions are drawn:

1. The convective heat transfer from a horizontal cylinder produced by corona wind was up to 6.5 times the free convection heat transfer rate.

2. Smaller source to receiver distances produced greater corona cooling effects.

3. The field voltage level required to produce ion flow, termed the breakdown voltage level, decreased as source to receiver distance decreased.

4. Convective heat transfer from horizontal cylinders produced by corona wind exhibited practically a step function increase at the breakdown voltage.

5. The multipoint emitter produced greater ion flow than a stretched wire emitter, and thus greater ion induced convection cooling. Exceptions were noted at a source to receiver distance of 1/4-inch, where the multipoint and stretched wire emitter cooling of the 1 and 2-in diameter cylinders was equal at field voltage levels above 6 kV. Corona cooling for the 1/4-in diameter test cylinder was greater for the mulitpoint emitter. This suggests that the relationship between cylinder size and d_e can be optimized to maximize corona cooling.

6. The multipoint emitter used power more efficiently than the stretched wire emitter.

7. Corona cooling was dependent on cylinder size.

8. The total heat transfer coefficient for free convection was independent of diameter.

9. Increases in relative humidity of the ambient air produced an increase in convective heat transfer. Relative humidity did however remain basically constant during and experimental test run, the ratio of h/h_o used for data analysis was therefore unaffected.

10. The stretched wire emitter produced greater convective cooling than the blown air plenum at velocities below 150 to 250 ft/min. Above those velocities, blown air cooling was greater than corona cooling.

VII. Recommendations

An analytical model of ion acceleration of air should be developed. The ability to model this phenomenon could then be extended to model corona wind in other atmospheres besides air. This may be particularly useful for study of corona cooling enhancements for weld processes, which are routinely performed in alternate atmospheres.

New multiple emitter designs should be studied. Multiple emitter devices produce greater ion flow. Emitter device design for maximizing cooling should be studied.

The relationship of cylinder diameter to multiple emitter cooling performance should be explored more extensively.

BIBLIOGRAPHY

1. Beal, J. B. and M. A. Badinger "Electrostatic Cooling (ESC) Applications," Second Annual AIAA/GNOS Aerospace Technology Symposium (October 25-26, 1984), GNOS 84-044.

2. Cross, J. A. "Electrostatically Assisted Heat Transfer, Inst. Phys. Conf. Ser. No. 48 (1979)

3. Didkovsky, A. B. and M. K. Bologa, "Vapor Film Condensation Heat Transfer and Hydrodynamics Under the Influence of an Electric Field," Int. J. Heat Mass Transfer, 24: 811-819 (1981)

4. Franke, M. E. and K. E. Hutson "Effects of Corona Discharge on Free Convection Heat Transfer Inside a Vertical Hollow Cylinder", Journal of Heat Transfer, 106:346-351 (May 1984).

5. Hogue, L. E. Effects of Corona Wind Cooling on the Cooling of a Horizontal Cylinder, MS Thesis GAE/AA/84D-4, School of Engineering, Air Force Institute of Technology (AU), Wright-Patterson AFB, OH, December 1984.

6. Hrycak, Peter "Heat Transfer From Round Impinging Jets to a Flat Plate," Int. J. Heat Mass Transfer 26: 1857-1865 (1983).

7. Kern, Donald Q. Process Heat Transfer (First Edition). New York: McGraw-Hill Book Company, 1950.

8. McAdams, William H. Heat Transmission, New York: McGraw-Hill Book Company, 1954.

9. Mitchell, A. S., "Heat Transfer by a Corona Wind Heat Exchanger," ASME, 78-WA/HT-43.

10. Reynolds, B. L. and R. E. Holmes, "Heat Transfer in a Corona Discharge," Mechanical Engineering, 7: 44-49 (October 1976).

11. Robinson, M. "Movement of Air in the Electric Wind of the Corona Discharge" AIEE Transactions,25:143-150 (May 1961).

12. Shannon, R. L., "Heat Transfer Augmentation Using a Corona Discharge Air Jet,"ASME Paper 78-ENAs-8, Intersociety Conference on Environmental Systems, San Diego, Calif, July 1978.

13. Sigmond, R. S. and M. Goldman "Corona Discharge Physics and Applications", Electrical Breakdown and Discharges in Gases, Series B: Physics, Vol 89b, edited by E. E. Kunhart and L. H. Luessen, New York and London: Plenus Press, 1983.

14. Stefkovich, M. E. Effects of Nozzle and Grid Accelerations of Corona Wind on Cooling of a Vertical Flat Plate, MS Thesis GAE/AA/83D-22, School of Engineering, Air Force Institute of Technology (AU), Wright-Patterson, AFB, OH, December 1983 (AD-A141-224).

15. Strock, Clifford. Heating and Ventilating's Engineering Databook (First Edition). New York: The Industrial Press, 1948.

16. Velkoff, H. R. and R. Godfrey "Low-Velocity Heat Transfer to a Flat Plate in The Presence of a Corona Discharge in Air," Journal of Heat Transfer, 101: 157-162 (February 1979).

17. -----. Inter-Probe Modular Energy Transfer Catalyzer. Product Brochure. Inter-Probe, Inc., North Chicago, Ill, 1980.

18. -----. Aluminum Vol II Design Application, edited by Kent R. Van Horn, American Society of Metals (1967).

19. -----. Heat Transfer Data Book, edited by Deborah A. Kaminski, Roy H. Roecker, Nancy D. Fitzroy, Florence F. Buckland, and R. Hosmer Norris: General Electric Company, Schenectady, N.Y., 1975.

20. -----. Thermocouples: How They Work and How to Use Them. Reprints from Instrumentation Magazine, Minneapolis-Honeywell Requlator Company, 1957.

21. -----. Physical and Electrical Properties of Fine Resistive Wire Bright and Enameled. Product Brochure. Driver-Harris Company, Harrison, New Jersey, 1958.

Appendix A

The Energy Balance Method (5)

The dimensionless ratio h/h_o was used to compare test results for the various experimental configurations. This h/h_o ratio is the average heat transfer coefficient for the cylinder with an applied high voltage field divided by the average heat transfer coefficient for the cylinder without an applied high voltage field. Stefkovich's (14) modification of Franke's (4) method for calculation h/h_o was extracted from Hogue's (5) work and is repeated below.

The expression for the heat transfer rate by convection from a horizontal cylinder is

$$Q_c = hA\Delta T \tag{1}$$

And similarly, for the free convection case

$$Q_{oc} = h_o A\Delta T \tag{9}$$

By using equations (1) and (9), the ratio Q_c/Q_{oc} is

$$\frac{Q_c}{Q_{oc}} = \frac{hA\Delta T}{h_o A\Delta T} \tag{10}$$

Then if the area A and temperature difference ΔT are held constant,

$$\frac{h}{h_o} = \frac{Q_c}{Q_{oc}} \tag{11}$$

The heat transfer rate at any time can be written as

$$Q_c = Q_{oc} + \Delta Q_c \tag{12}$$

Substituting equation (12) into equation (11) gives

$$\frac{h}{h_o} = 1 + \frac{\Delta Q_c}{Q_{oc}} \tag{13}$$

An expression for ΔQ_c which can be evaluated from experimental data is developed from the equation for ΔQ_t, the difference between the total heat transfer rate with a high voltage field applied and the free convection heat transfer rate.

$$\Delta Q_t = \Delta Q_c + \Delta Q_r + \Delta Q_{cd} \tag{14}$$

where

$$\Delta Q_c = \Delta Q_{c1} + \Delta Q_{c2} \tag{15}$$

For small changes in radiation, conduction, and end plate convection heat transfer rates, ΔQ_r, ΔQ_{cd}, and ΔQ_{c2} respectively,

$$\Delta Q_t = \Delta Q_c = \Delta Q_{c1} \tag{16}$$

Under steady state conditions, the total heat transfer rate from the cylinder is equal to the electrical power input by the heater coil.

$$Q_t = P_h = I_h^2 R \tag{17}$$

where

I_h = measured heater coil current

R = known heater coil resistance

The change in the total heat transfer rate is therefore

$$\Delta Q_t = \Delta P_h \tag{18}$$

Substituting equation (18) into equation (16) yields

$$\Delta P_h = \Delta Q_c \tag{19}$$

A further substitution of equations (9) and (19) into equation (13) yields

$$\frac{h}{h_o} = 1 + \frac{\Delta P_h}{h_o A \Delta T} \qquad (20)$$

Appendix B

Listing of the System Controller Program Code

```
10  REM      THIS PROGRAM SCANS CHANNELS WITH COPPER-CONSTANTAN
20  REM      THERMOCOUPLES AND GIVES THE TEMPERATURE READING ON EACH
30  REM      CHANNEL IN BOTH DEGREES C AND F.  IT ALSO GIVES AVERAGE
40  REM      TEMPERATURE AND THE DELTA FROM AMBIENT
50  REM
60  REM
70  REAL REFJUNCT,TEMPF,TEMPC,VOLTAGE,AVGC,AVGF,AMBC,DELTC,DELTF
80  INTEGER X,Y,CHAN,COUNT
90  INPUT "ENTER RUN NUMBER", X
100 INPUT "ENTER DATE (DAY/MO)", Y
110 DATA 7,709,701
120 READ BUS,SCN,DVM
130 COM SCN,DVM,BUS
140 PRINTER IS 16
150 INPUT "ANOTHER PASS? (YES=1, NO=2) ", R
160 ON R GOTO 170,600
170 INPUT "FULL PRINTOUT? (YES=1, NO=2) ", S
180 ABORTIO BUS
190 REMOTE BUS
200 RESET BUS
210 OUTPUT DVM USING "K";"F1R7T2T3"
220 AVGC=0
230 AVGF=0
240 IMAGE /, "RUN NO.: ", DD, /,"DATE: ", DDDD,//
250 PRINT USING 240; X,Y
260 FOR CHANNEL=0 TO 13
270 REFJUNCT=0
280 OUTPUT SCN USING "F";VOLTAGE
290 TRIGGER DVM
300 ENTER DVM USING "F";VOLTAGE
310 TEMPC=FNTEMP(VOLTAGE,REFJUNCT)
320 TEMPF=TEMPC*1.8+32.0
330 REM
340 REM      HERE WANT TO CALCULATE THE AVERAGE CYLINDER TEMP USING A
350 REM      WEIGHTED AVERAGE WHERE THE CENTER OF THE CYLINDER IS GIVEN
360 REM      44% WEIGHTING AND THE ENDS ARE EACH GIVEN 28% WEIGHTING
370 REM
380 CHAN=CHANNEL+1
390 COUNT=CHANNEL DIV 4+1
400 ON COUNT GOTO 410,440,410,480
410 AVGC=AVGC+.07*TEMPC
420 AVGF=AVGF+.07*TEMPF
430 GOTO 510
440 AVGC=AVGC+.11*TEMPC
450 AVGF=AVGF+.11*TEMPF
460 GOTO 510
470 IMAGE "CHANNEL ", DD, ":",/, MDDD.D, "C", 2X, MDDD.D, "F", /
480 IF CHANNEL()13 THEN 520
490 AMBC=TEMPC
500 AMBF=TEMPF
510 ON S GOTO 520,530
520 PRINT USING 470;CHAN,TEMPC,TEMPF
```

```
530 NEXT CHANNEL
540 DELTC=AVGC-AMBC
550 DELTF=AVGF-AMBF
560 IMAGE "AVG CYL TEMP:", /, MDDD.D, "C", 2X, MDDD.D, "F", //, "DELTA
          TEMP", /, MDDD.D, "C", 2X, MDDD.D, "F", //
570 PRINT USING 560; AVGC,AVGF,DELTC,DELTF
580 OUTPUT DVM; "A1"
590 GOTO 150
600 END
610 DEFFNTEMP(VOLTAGE,RJUNCT)
620 COM SCN,DVM,BUS
630 DIM JUNCT(2),COEFF(8)
640 JUNCT(1)=3.6880238E1
650 JUNCT(2)=41277001E-2
660 COEFF(0)=.10086091
670 COEFF(1)=25727.94369
680 COEFF(2)=-767345.8295
690 COEFF(3)=78025595.81
700 COEFF(4)=-9247486589
710 COEFF(5)=6.97688E11
720 COEFF(6)=-2.66192E13
730 COEFF(7)=3.94078E14
740 COEFF(8)=1.00E13
750 TEMP=FNPOLY(COEFF(*),VOLTAGE+1E-6*((JUNCT(2)*RJUNCT+JUNCT(1))*
          RJUNCT))
760 RETURN TEMP
770 DEF FNPOLY(CO(*),VAL)=(((((((CO(8)*VAL+CO(7))*VAL+CO(6))*VAL+CO(5))
          *VAL+CO(4))*VAL+CO(3))*VAL+CO(2))*VAL+CO(1))*VAL+CO(0)
780 FNEND
```

VITA

Captain Pamela Renee Cleaver Hodge was born [redacted] After graduation from Lincoln High School in Port Arthur, Texas, she enrolled at Prairie View A&M University. She graduated with honors May 1977 with the degree of Bachelor of Science in Mechanical Engineering. After graduation she was employed as a design engineer at Exxon Pipeline Company, Houston, Texas. She joined the United States Air Force in 1980 and was commissioned in 1981 through Officer Training School. She served as a project engineer for the F100 engine on the F16 aircraft while stationed at Kelly Air Force Base, Texas, until entering the School of Engineering, Air Force Institute of Technology, in May 1984.

UNCLASSIFIED
SECURITY CLASSIFICATION OF THIS PAGE

ADA202714

REPORT DOCUMENTATION PAGE

1a. REPORT SECURITY CLASSIFICATION: unclassified	1b. RESTRICTIVE MARKINGS
2a. SECURITY CLASSIFICATION AUTHORITY	3. DISTRIBUTION/AVAILABILITY OF REPORT
2b. DECLASSIFICATION/DOWNGRADING SCHEDULE	
4. PERFORMING ORGANIZATION REPORT NUMBER(S): AFIT/GE/AA/86J-1	5. MONITORING ORGANIZATION REPORT NUMBER(S)
6a. NAME OF PERFORMING ORGANIZATION: School of Engineering; 6b. OFFICE SYMBOL (If applicable): AFIT/EN	7a. NAME OF MONITORING ORGANIZATION
6c. ADDRESS (City, State, and ZIP Code): Air Force Institute of Technology, Wright-Patterson AFB, OH 45433	7b. ADDRESS (City, State, and ZIP Code)
8a. NAME OF FUNDING/SPONSORING ORGANIZATION; 8b. OFFICE SYMBOL (If applicable)	9. PROCUREMENT INSTRUMENT IDENTIFICATION NUMBER
8c. ADDRESS (City, State, and ZIP Code)	10. SOURCE OF FUNDING NUMBERS: PROGRAM ELEMENT NO. / PROJECT NO. / TASK NO. / WORK UNIT ACCESSION NO.

Approved for public release IAW AFR 190-1
12 Jan 1989

11. TITLE (Include Security Classification): (see item 19)

12. PERSONAL AUTHOR(S): Pamela R. C. Hodge, B.S., M.S., Capt, USAF

13a. TYPE OF REPORT	13b. TIME COVERED	14. DATE OF REPORT (Year, Month, Day)	15. PAGE COUNT
MS Thesis	FROM ____ TO ____	1988 August	

16. SUPPLEMENTARY NOTATION

17. COSATI CODES			18. SUBJECT TERMS (Continue on reverse if necessary and identify by block number)
FIELD	GROUP	SUB-GROUP	
20	13		CoronaWind;Electrostatic Cooling;

19. ABSTRACT (Continue on reverse if necessary and identify by block number)

Title: CORONA WIND COOLING COMPARISONS FOR HORIZONTAL CYLINDERS

Thesis Advisor: Milton E. Franke, PhD

Experiments were conducted to determine the effect of the corona wind on the convective heat transfer rate from each of three horizontally mounted, heated aluminum cylinders. The cylinder was maintained at ground potential and an emitter was connected to a high voltage source. Two emitter devices were used, stretched wire and multipoint. Emitter to cylinder spacing and field voltage were parameters.

An energy balance method was used for data analysis. Free convection heat transfer rates were used as a baseline. The results of all experiments were compared. The results of all experiments were compared and contrasted. The multipoint emitter was a more efficient emitter device. than the stretched wire emitter. The corona wind increased free convection cooling by a factor of as much as 6.5.

20. DISTRIBUTION/AVAILABILITY OF ABSTRACT	21. ABSTRACT SECURITY CLASSIFICATION
☐ UNCLASSIFIED/UNLIMITED ☐ SAME AS RPT. ☐ DTIC USERS	Unclassified

22a. NAME OF RESPONSIBLE INDIVIDUAL	22b. TELEPHONE (Include Area Code)	22c. OFFICE SYMBOL
Milton Franke, PhD	(503)255-2362	AFIT/ENY

DD FORM 1473, 84 MAR — 83 APR edition may be used until exhausted. All other editions are obsolete.

SECURITY CLASSIFICATION OF THIS PAGE
UNCLASSIFIED